COMMUNICATIONS

Dear reader,

Current modern civil engineering structures need new scientific results in theoretical, simulation, and experimental areas more than ever before. Traditional problems of engineering construction proposals are complemented with new urgent issues of safety and reliability, energy saving, environmental protection and structure diagnostics. It is the impressive appeal to design constructions of such high quality. Special requirements are placed on traffic structures – railway and road engineering structures, bridges, tunnels and, especially, on their dynamic loading and interaction problems of the system vehicle – construction – environment components.

The eight papers in this Volume were written by the authors from the Faculty of Civil Engineering of the University of Žilina and two papers were written by the authors from other work places. The major topics of this Volume are from the areas of Structural Engineering and Constructions. I am convinced that papers included in this Volume adequately reflect recent scientific efforts and results achieved by the authors in the field of Civil Engineering Structures.

Milan Moravčík

COMMUNICATIONS

Jozef Melcer *

A VEHICLE – BRIDGE INTERACTION

The problem of a vehicle – bridge interaction can be followed in the literature since the year 1849. At the early state the analytical methods were applied. The development of computers brings the change in the approach to the used methods of solution. The Finite Element Method and Component Element Method represent the revolution and qualitative jump in the development. They enable to solve very truthful space computing models numerically. The results of numerical computation must by verified by the in situ experimental measurements. Mutual interconnection of numerical and experimental techniques represents the most effective way in the process of uncovering of objective reality concerning of real action of bridge structure under the passing of vehicles.

1. Introduction

The solution of problems of a vehicle – bridge interaction belongs to the oldest solved problems of structural dynamics. The works of the civil engineer Willis [1] and mathematician Stokes [2] in which they tried to clarify the breakdown of Chester Rail Bridge in England in 1847 are not only considered the first attempts to solve the problems of a vehicle – bridge interaction but also the first works in the field of structural dynamics. The works of Krilov [3] and Timosenko [4] concerning mass less force movement along mass beam started a series of approximate solutions of the problem with various types of boundary conditions and load. Inglis monograph [5] brings a survey of these early studies. A more serious attention to the dynamic of highway bridges starts to be paid in 20th century. The 1st important report on this topic was published in 1931 by the Special Committee on Highway Bridges of the American Society of Civil Engineers [6]. The year 1950 can be considered a fault in the development by the use of digital and analog computers and measuring technique. A detailed and systematic research into the vehicle – bridge interaction problems was carried out at the University of Illinois, Urbana, USA from 1950 to 1960. The results of this research were published by the Committee on Deflections Limitations of Bridges of the Structural Division of the ASCE in [7]. The complete survey of advances used till 1959 was published by Wright and Green in [8]. The total review of the world development till 1975 of the vehicle – highway bridge interaction problems was published by Tseng Huang in [9]. This period is characterized by using the plane computing models of vehicles and bridges with a finite number of degrees of freedom. Equations of motion are derived in the form of differential equations and are solved numerically by some step-by-step integration methods. Revolution in the solution of vehicle – bridge interaction problems represents the invasion of finite methods especially the Finite Element Method and Finite Strip Methods [10]. This enables to analyse the space computing models of bridges and vehicles. Computing models of vehicles are usually created by the use of the Component Element Methods [11]. Development of statistical methods initiated the modelling of surface unevenness by power spectral densities of unevenness and application of numerical simulation methods in the modelling of fatigue processes and lifetime of structures. The Monte Carlo Method is currently used at the modelling of stochastic processes. Possibilities of personal computers and software in the area of user environment orientate the progress to assurance the maximal user comfort and obtaining the effective graphical outputs. Display of graphical outputs is connected with picture animation.

Bridge engineering in the Slovak and Czech Republic has rich tradition, high technical level and positive response all over the world. The works of professor Koloušek in the theoretical and experimental fields laid the foundation of a new branch of science – Dynamic of Structure an especially Dynamic of Bridges in our country [12]. Problems of a vehicle – railway bridge interactions are solved in the Railway Research Institute (VÚŽ) and in the Institute of Theoretical and Applied Mechanics of the Czech Academy of Sciences (ÚTAM AV ČR) in Prague. Research in the field of a vehicle – highway bridge interaction was formed step by step following the road network infrastructure construction. The Department of Structural Mechanics of the University of Zilina and the Department of Structural Mechanics of the Czech Technical University in Prague contributed substantially to the mentioned research. Besides theoretical research the systematic attention was paid to the development of experimental methods on the Civil Engineering Research Institute (VÚIS), the Institute of Construction and Architecture of the Slovak Academy of Sciences in Bratislava (ÚSTARCH SAV) and the Building Testing and Research Institute in Bratislava and Prague (TSÚS). The problems of vehicle – bridge interactions are solved in monographs [13], [14]. The present development aims at the solution of specific problems, e.g. optimal control of bridge – friendly vehicle [15].

* Jozef Melcer
   Department of Structural Mechanics, Faculty of Civil Engineering, University of Žilina, Slovakia, E-mail: melcer@fstav.utc.sk

2. Description of the problem

Real admission to the solution of the problem of a vehicle – bridge interaction comes out from the mutual combination of numerical and experimental approaches. Numerical methods in the present days offer an effective tool for the solution of this problem. If the entering values are put into calculation in regular magnitudes and verified on the basis of experimental measurements, the results of numerical calculations correspond to the results obtained experimentally. The contemporary state of computing technology enables to solve all the problems in real time. For the creation of computing programs it is suitable to use the high-level program languages. The results obtained from the numerical and experimental analyses are used in the process of construction of transport means and in the design of optimal parameters of bridges with respect to its lifetime and reliability. In the relation to the passengers the results pay attention to the ride comfort of passengers.

Numerical solution of the problem of a vehicle – bridge interaction requires to consider at least the following issues:
- creation of a vehicle computing model and its mathematical description,
- creation of a bridge computing model and its mathematical description,
- modelling and mathematical description of the surface unevenness,
- creation of a computer program for numerical solution of equations of motion,
- creation of a computer program for evaluation and display of the obtained data.

There are many concrete techniques how to create computing models of vehicles and bridges. Basically, they can be divided into two categories on the basis of a resulting type of equations of motion. Equations of motion can be formed as differential or integral equations. The possibilities of numerical solution of both types of equations of motion are in the present time very large. It is practically the question of individual approach of the author.

Computing models of vehicles are usually created as discrete models composed of systems of mass points or mass bodies, discrete springs and dampers, or they are created in the sense of Finite Element Methods. Such computing models are described by a system of ordinary differential equations. In the Department of Structural Mechanics, Faculty of Civil Engineering in Zilina the Component Element Methods is successfully used for creation of computing models of vehicles [11]. In compliance of this Method the equations of motion can be written in the form

$$[m_v] \cdot [\ddot{r}(t)] = [F_v(t)], \qquad (1)$$

where $[m_v]$ is the mass matrix of vehicle, $[\ddot{r}(t)]$ is the vector of second derivatives of displacement components corresponding to individual degrees of freedom and $[F_v(t)]$ vector is the complete vector of forces acting on a vehicle. The sample of 3D computing models of vehicle is plot in Fig. 1.
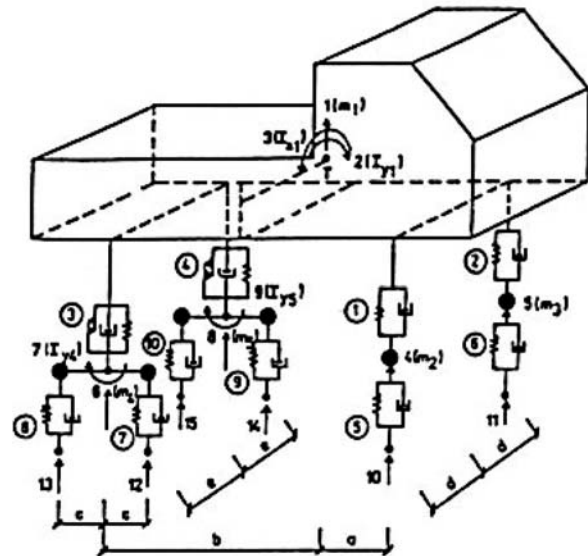

Fig. 1 3D computing model of vehicle.

The bridge structure can be modelled as a system with continuously distributed mass or as a system with a finite degree of freedoms. Nowadays, bridge structures are modelled in compliance with FEM where the computing model is created as an arbitrary combination of line 1D elements, slab – wall or shell 2D elements or 3D space elements. The equations of motion in a matrix form described in compliance with FEM forced vibration of a bridge can be written as

$$[M] \cdot [\ddot{u}] + [B] \cdot [\dot{u}] + [K] \cdot [u] = [F(t)] . \qquad (2)$$

$[M]$ is the global mass matrix, $[B]$ is the global damping matrix, $[K]$ is the global stiffness matrix, $[u]$ is the global vector of unknown nodal parameters of displacements (vector of generalized nodal displacements) and $[F(t)]$ is the vector of excitation forces transformed into nodal points in compliance with FEM. In Fig. 2 the FEM computing model of two span bridge structure is showen.
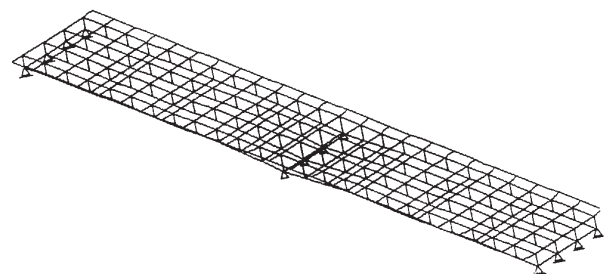

Fig. 2 Two span FEM computing model of a bridge.

A mathematical description of the road surface unevenness is also an integral part of the problem. The road surface unevenness can be defined as deterministic or stochastic. The local discrete

unevenness and periodically repeated unevenness are modeled as deterministic. A terrain step represents a specific case of deterministic unevenness. From a mathematical point of view it is a function with point singularity. For the purpose of numerical modeling of such unevenness it is better to substitute the real shape of the terrain step by an alternate function identical with the function describing the trajectory of the vehicle wheel hub. At present the randomly variable road profile is derived from power spectral densities of unevenness for a certain category or pavement and the quality of its surface on the basis of in situ experimental measurements in the form [16].

$$S(\Omega) = C \cdot \Omega^{-2}, \tag{3}$$

where C [rad.m] is a parameter describing the measure of unevenness and Ω is so called length angular frequency in [rad.m^{-1}]. When the coordinates on the vertical and horizontal axes are plotted in a logarithmical measure, the power spectral densities of unevenness can be very well approximated by a straight line, Fig. 3.
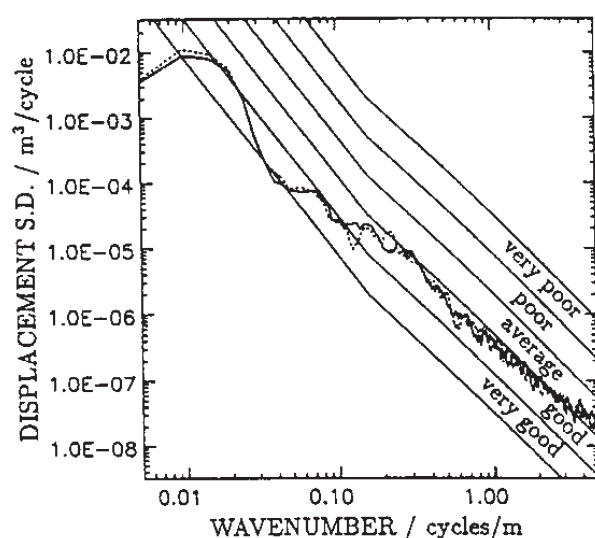

Fig. 3 Power spectral densities of road unevenness according to [16]

Equations of motion describing the vehicle and bridge vibration are solved numerically. For the solution a numerical integration method is applied. The whole calculation is realized in time domain with time step Δt. From surface unevenness and from bridge displacements the displacements of contact points of vehicle are determined. From equations of motions describing the vehicle vibration the contact forces corresponding to such kinematical excitation are calculated. The bridge response is calculated on the contact forces representing the excitation forces inducing the bridge vibration. After the calculation of the bridge response the vehicle is moved forward about the length corresponding to the time step Δt and the whole cycle is repeated.

In the Department of Structural Mechanics, Faculty of Civil Engineering in Zilina the equations of motion are usually com-

piled as differential equation and they are solved numerically. Various methods are used for numerical solution of differential equations. For example, the central difference method, Newmark's method, Wilson's method, predictor-corrector method. We have very good experience is with the use of Runge-Kutta 4th or 5th order method.

In the present time it is optimal to use a higher level programming language, for example MATLAB, to create a computing program. This programming language is matrix oriented, interactive and computing procedures are supported by effective graphics. The creation of a program is easier in comparison with classical program languages. For example, the program statement for a numerical integration of differential equations by the Runge-Kutta 4th order integration method can be written in one line

$$[t,y] = ode45('vozidlo',[t0,tfinal],[InKon]) \ . \tag{4}$$

The symbols in the former statement have the following meaning: $ode45$ is a matlab function for integration of differential equations by the Runge-Kutta 4th order integration method. In the parentheses behind this function in apostrophes is the name of functional file in which the system of solving equations is stored '$vozidlo$', in the 1st brackets [t0, tfinal] contain the initial and final values of the time interval in which the numerical integration is carried out and in the 2nd brackets [$InKon$] contains initial conditions (initial displacements and initial speeds of integrated functions). This statement recalls vector t time steps of numerical integration and column matrix y in which the functional values of wanted functions are stored.

In the past two program systems for analysis of the problems of a vehicle – bridge interaction and for the processing of obtained results were created. The 1st program system BRIDGEW2 was created in the program language FORTRAN. In this program the Runge-Kutta 5th order integration procedure was adopted. Some working windows of the program system are presented in Fig. 4 . The 2nd program system ISV was created in language C++ and for integration of differential equations the Central Difference Method was employed.

3. Application in practice

The Old Bridge in Bratislava was erected in the year 1945 as a temporary bridge of the Roth-Wanger system, but it serves for transport needs up to these days, Fig. 5. The 1st bridge span from Bratislava water side 75 m long acts as a single beam. This span has been strengthened and statically and dynamically tested many times. The simulation of a vehicle motion along the bridge span was carried out for the need of tuned vibration control of the bridge. Some comparison of the numerically and experimentally obtained results, corresponding to the speed of vehicle motion 42 km/h, is presented in the following text.

The planar computing model of a vehicle and bridge was adopted for numerical analysis. Equations of motions were derived in
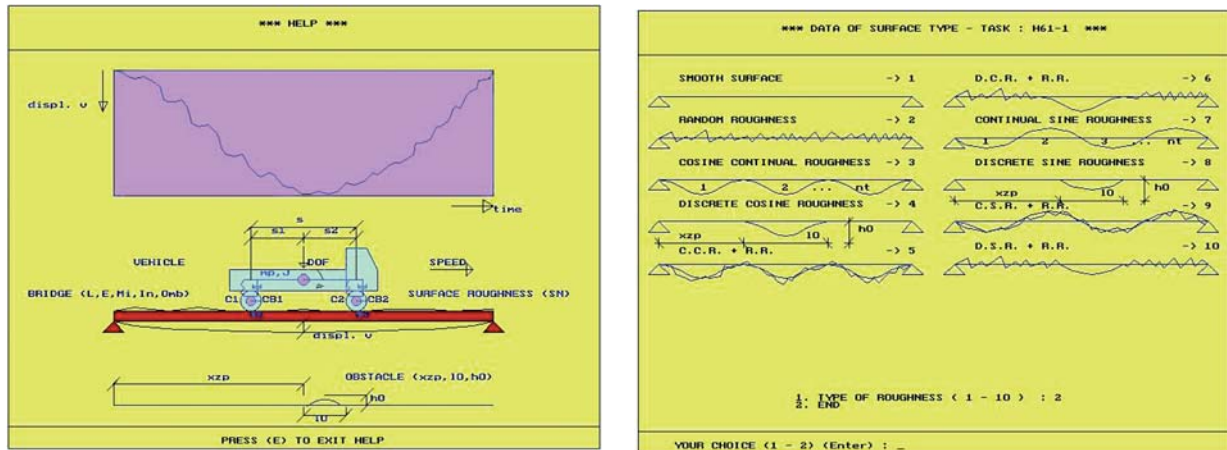
Fig. 4 Some working views of program system BRIDGEW2 according to [14]

Fig. 5 Old Bridge in Bratislava
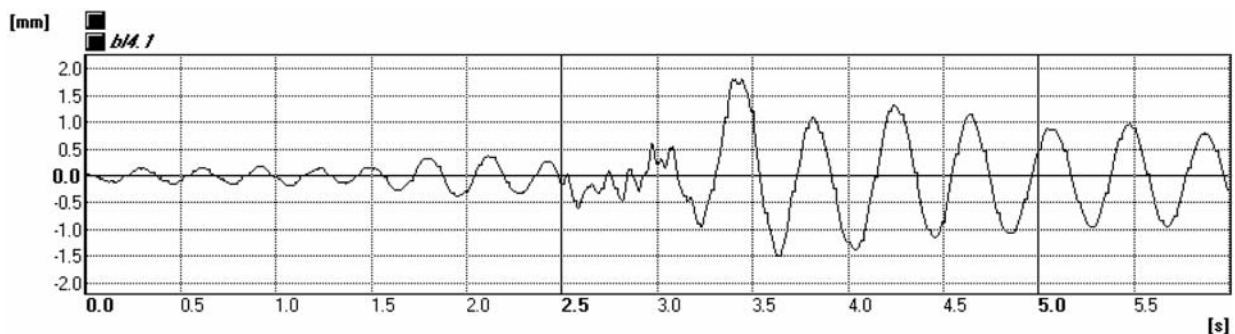
Fig. 6 Experimentally obtained time record of vertical mid span deflection

the form of differential equations and were solved numerically with the help of Runge-Kutta 5th order integration procedure. The vertical dynamic mid span deflections were numerically and experimentally tested under the vehicle passing over a standard obstacle. The results were mutually compared, Fig, 6 and Fig. 7.

As we can see the mutual agreement between the experimentally and numerically obtained results is very good, especially in the part of the record corresponding to the driving of the vehicle behind the obstacle. A very good agreement is also at a numerically modelled frequency composition of vibration and at experi-

Fig. 7 Numerically obtained time record of vertical mid span deflection

mentally obtained frequency composition of vibration. It is seen very well from the power spectral density functions (PSDF), Fig. 8 and Fig. 9.
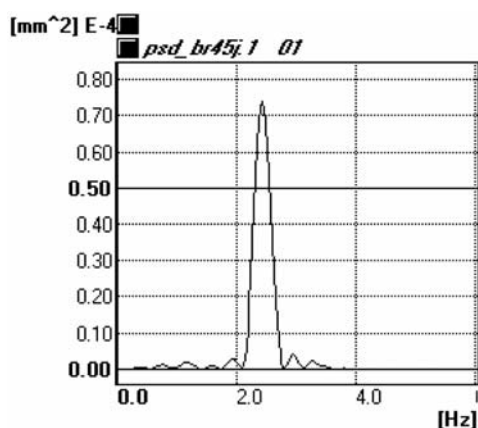
Fig. 8 Experimentally obtained PSDF

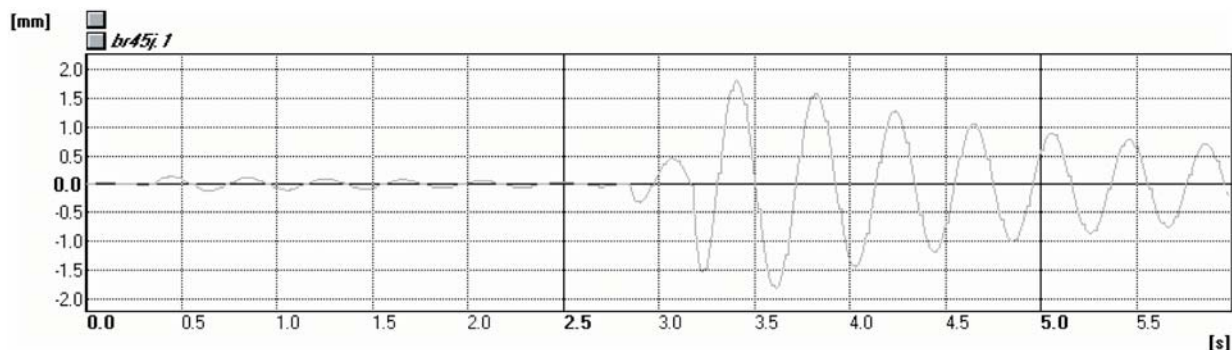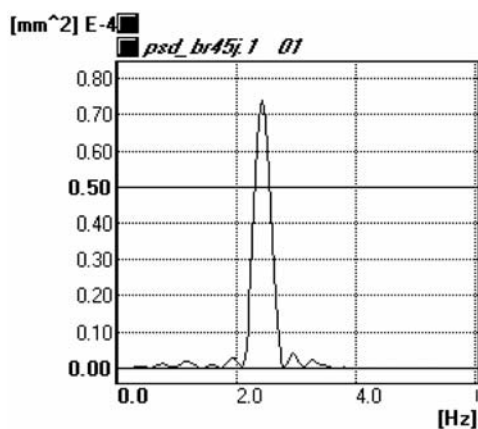

Fig. 9 Numerically obtained PSDF

The coherence function, Fig. 10, confirms practically 100% agreement of the experimentally and numerically obtained vibration records in the frequency range from 2 to 3 Hz, which is the area of maximal power.
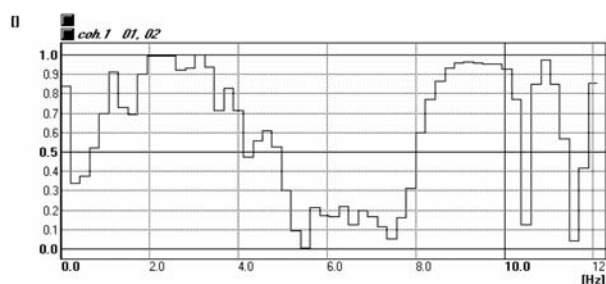
Fig. 10 Coherence function for experimentally and numerically obtained vibration records

4. Conclusions

The vehicle – bridge interaction problem represents the oldest problem of structural dynamic at all. Contemporary approach to the solution of this problem comes out from a mutual combination of numerical and experimental approaches. Numerical methods offer an effective tool for the solution of the problem in the present days. The contemporary state of computing technology enables to solve all the problems in real time. It is suitable to use the high-level program languages for the creation of computing programs. The results obtained from the numerical and experimental analyses are used for the design of optimal bridge parameters and for specification of lifetime and reliability recommendations.

References

[1] WILLIS, R.: *Appendix, Report of the Commissioners Appointed to Inquire into the Application of Iron to Railway Structures*, Stationary Office, London, 1849.

[2] STOKES, G. G.: *Discussion of a Differential Equation Relating to the Breaking of Railway Bridges,* Transactions Cambridge Philosophic Society, 8, 1849, p. 707.

[3] KRYLOV, A. N.: *Über die erzwungenen Schwingungen von gleichförmigen elastischen Stäben*, Mathematische Annalen, Jahrg.61, 1905, s.221. (From: Matematičeskij zbornik Akademii Nauk, Vyp. 61, Peterburg, 1905.)

[4] TIMOŠENKO, S. P.: *Forced vibration of prismatic bars (in Russian)*, Izvestija Kievskogo politechničeskogo instituta, 1908.

[5] INGLIS, C. E.: A *Mathematical Treatise on Vibrations in Railway Bridges,* Cambridge University Press, Cambridge, Mass., 1934.

[6] *Impact on Highway Bridges,* Final Report of the Special Committee on Highway Bridges, Transactions ASCE, Vol. 95, 1931, p. 1089-1117.

[7] *Deflection Limitations of Bridges,* Progress Report of the Committee on Deflection Limitations of Bridges of the Structural Division, Proc. ASCE, Vol. 84, No. ST3, May, 1958, p. 1633.

[8] WRIGHT, D. T., – GREEN, R.: *Highway Bridge Vibration, Review of Previous Studies.* Queen s University Kingston, Ontario, 1959.

[9] HUANG, T.: *Vibration of Bridges.* Shock and Vibration Digest, 3/1976, p. 61–76.

[10] BATHE, K. J.: *Finite Element Procedures in Engineering Analysis,* Prentice-Hall, New Jersey, 1982.

[11] LEVY, S., WILKINSON, J. P. D.: *The Component Element Method in Dynamics with Application to Earthquake and Vehicle Engineering,* McGraw-Hill, New York, 1976.

[12] KOLOUŠEK, V.: *Dynamics of Structures I, II, III. (in Czech)*, SNTL, Prague, 1954, 1956, 1961.

[13] FRÝBA, L.: *Dynamic of Railway Bridges (in Czech)*, ACADEMIA, Prague, 1992.

[14] MELCER, J.: *Dynamic Calculation of Highway Bridges (in Slovak)*, EDIS, University of Zilina, 1997.

[15] MÁCA, J., ŠMILAUER, V., VALÁŠEK, M.: *Optimal Control of Bridge – Friendly Trucks,* Proc. III International Conference on New Trends in Statics and Dynamics of Buildings, Slovak republic, Bratislava, Civil Engineering Faculty STU, October 21 – 22, 2004, STU Bratislava, p. 109 – 112.

[16] CEBON, D.: *Handbook of vehicle - road interaction,* Swets&Zeitlinger B.V. Publishers, Lisse, Netherlands, 1999.

Josef Vičan – Jozef Gocál – Branislav Meliš *

FATIGUE ASSESSMENT OF EXISTING BRIDGE MEMBERS

Correct consideration of the service load effects plays a very important role on assessment of railway bridges, especially on fatigue assessment. Eurocode EN 1991-2 introduces twelve types of service trains and prescribes their sequel in normal and heavy duty. The service trains, consisting of locomotive and defined number of wagons, are specified by amount of axle forces and distances between them. However, there is no commentary which would illuminate a background of the service trains technical data. Consequently, it is difficult to say how representative the service load models specified in this standard prescription are in comparison with the actual railway traffic effects, namely in conditions of the Slovak Railways. Therefore, the paper deals with confrontation of the actual railway traffic load effects and the effects of traffic load defined in EN 1991-2. The confrontation is based on fatigue assessment of existing railway bridge truss girder.

1. Introduction

At the present time, the design of structures is connected with consecutive implementing European standards (Eurocodes) into the national standardization. Eurocode EN 1991–2 [1] deals with traffic actions on bridges. For design of railway bridges, this standard introduces load model 71 (LM 71) that may be multiplied by the factor α to get so called classified vertical loads. The classified vertical loads shall be used for design of railway bridge members from the view point of ultimate limit state, especially strength resistance verification. In the case of fatigue resistance verification, the standard [1] establishes twelve types of service trains for modelling railway traffic service load and it also prescribes their sequel in normal and heavy duty. The service trains, consisting of locomotive and defined number of wagons, are specified by amount of axle forces and distances between them. However, there is no commentary that would illuminate a background of the service trains technical data. Consequently, it is difficult to say how representative the service load models specified in this standard are in comparison with the actual railway traffic, namely in conditions of the Slovak Railways.

This paper analyses the effects of service load specified in EN 1991–2 [1] for fatigue assessment of railway bridges in order to compare them with effects of actual service loads on Slovak Railways. The comparison is based on fatigue assessment of chosen fatigue prone bridge structural detail in accordance with the Eurocode 3 [2], [3], by means of linear fatigue-damage accumulation hypothesis according to Palmgren-Miner [4].

2. Analysis of service load response

Actual service load effects of railway bridges may be obtained either by experimental measurement or by numeric simulations. Usually, application of the first approach is financially and time demanding, and therefore it is mostly used for verification of accuracy and calibration of computational model for the second approach.

Such a combined approach was applied to determine actual service load effects on the steel truss riveted girder of the observed railway bridge, which is situated in km 309.309 of railway track
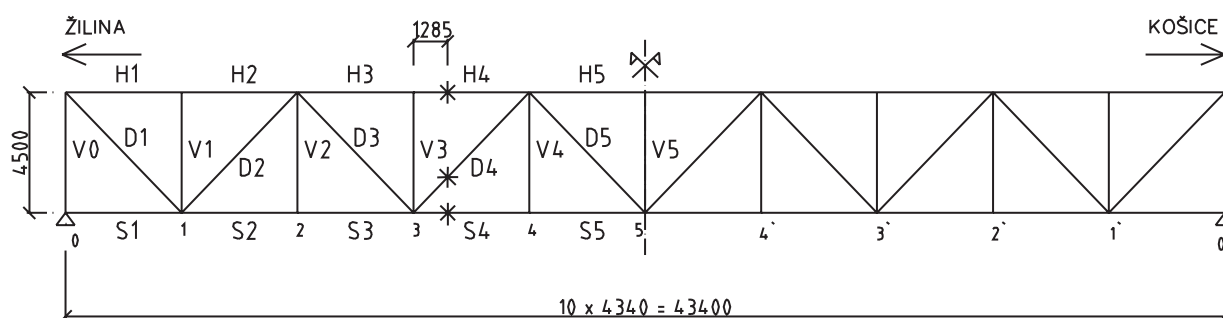

Fig. 1 Longitudinal arrangement of truss girder

* Josef Vičan, Jozef Gocál, Branislav Meliš
Department of Structures and Bridges, Faculty of Civil Engineering, University of Žilina, Slovakia, E-mail: Josef.Vican@fstav.utc.sk

Košice – Žilina. Fig. 1 shows longitudinal arrangement of the truss girder with designation of investigated cross sections of members determining the loading capacity of the girder. Fig. 2 shows a bridge computational spatial model, which was realised using the program IDA NEXIS.
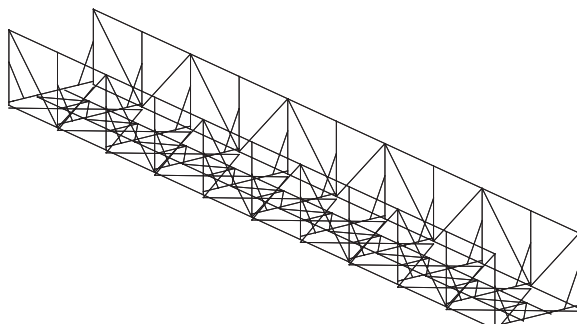

Fig. 2 Spatial computational model of the bridge

Effects of actual railway traffic service load were obtained by simulation of passing 204 freight trains corresponding to actual heavy traffic during one week. Small effects of passenger trains were neglected. Complete data of trains – their composition, frequency, weight and geometry of wagons were acquired from the information system ŽSR IRIS-N. The dynamic effects were taken into account by dynamic factor $\varphi = 1.08$ obtained within numerical simulations in accordance with approach defined in standard [1]. Histograms of stress ranges in the observed cross sections of upper chord, bottom chord and diagonal, respectively, are presented in Fig. 3. The number of single stress-range levels corresponds to considered service life of the bridge $T_d = 100$ years.

Similarly, the effects of heavy railway traffic according to EN 1991–2 [1] were obtained by simulation of passages of freight trains specified in this standard. The standard specifies amounts and spacing of axle-forces of single traffic load models as well as the number of passages per day. The number of passages corresponding to considered service life of 100 years might be obtained by simple multiplying. The histograms of stress ranges in the observed cross sections of upper and bottom chord are presented in Fig. 4.

3 Fatigue assessment of bridge members

The method of fatigue assessment is based on well-known Wöhler's curve of fatigue resistance, which relates the fatigue life to the cyclic-stress range and can be expressed in a logarithmic form as

$$\log N = \log C - m \cdot \log \Delta\sigma$$

where: N is a total number of constant-amplitude-stress cycles to failure, $\Delta\sigma$ is the constant amplitude tensile-stress range, m is the material parameter indicating the constant slope of Wöhler's curve in a logarithmic form and C is the material parameter dependent on the type of notch detail.

To consider the variable-stress range experienced by a fatigue-sensitive bridge component, the direct use of standard Wöhler's curves is not possible. Providing that the stress-range histogram is known, the linear fatigue damage accumulation model according to Miner [4] can be applied to consider the partial fatigue damage at the different stress-range levels. This linear damage accumulation hypothesis, generally known as Palmgren-Miner's hypothesis, can be expressed as follows:
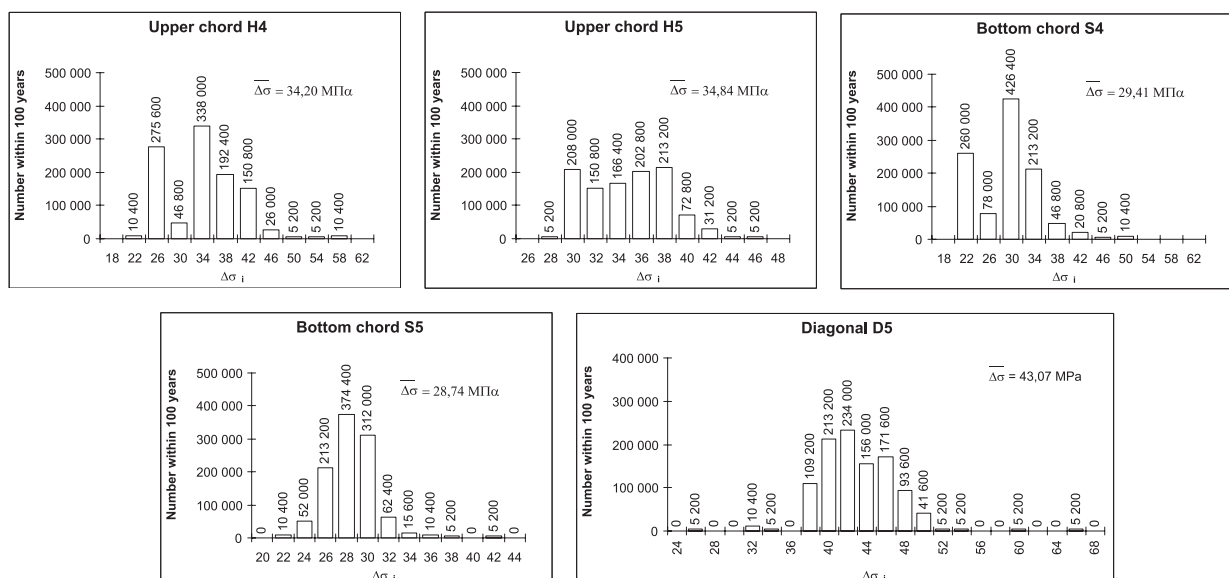

Fig. 3 Histograms of stress ranges due to effects of real heavy traffic within 100 years
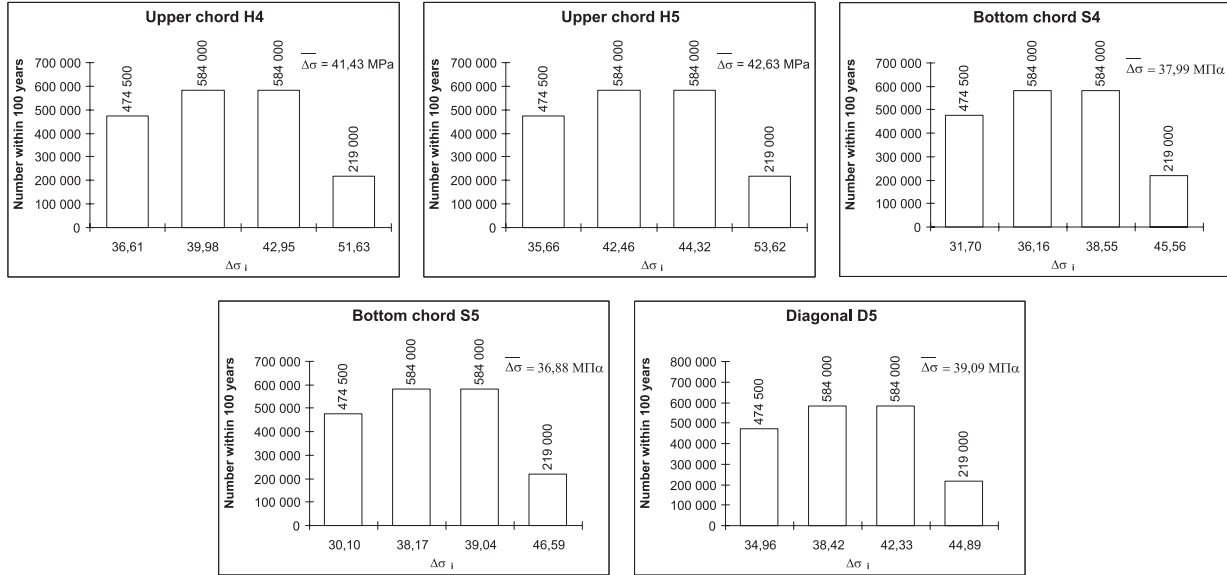
Upper chord H4

Number within 100 years

700 000 · 600 000 · 500 000 · 400 000 · 300 000 · 200 000 · 100 000 · 0

474 500 · 584 000 · 584 000 · 219 000

$\overline{\Delta\sigma}$ = 41,43 MPa

36,61 · 39,98 · 42,95 · 51,63

$\Delta\sigma_i$

Upper chord H5

Number within 100 years

700 000 · 600 000 · 500 000 · 400 000 · 300 000 · 200 000 · 100 000 · 0

474 500 · 584 000 · 584 000 · 219 000

$\overline{\Delta\sigma}$ = 42,63 MPa

35,66 · 42,46 · 44,32 · 53,62

$\Delta\sigma_i$

Bottom chord S4

Number within 100 years

700 000 · 600 000 · 500 000 · 400 000 · 300 000 · 200 000 · 100 000 · 0

474 500 · 584 000 · 584 000 · 219 000

$\overline{\Delta\sigma}$ = 37,99 МПα

31,70 · 36,16 · 38,55 · 45,56

$\Delta\sigma_i$

Bottom chord S5

Number within 100 years

700 000 · 600 000 · 500 000 · 400 000 · 300 000 · 200 000 · 100 000 · 0

474 500 · 584 000 · 584 000 · 219 000

$\overline{\Delta\sigma}$ = 36,88 МПα

30,10 · 38,17 · 39,04 · 46,59

$\Delta\sigma_i$

Diagonal D5

Number within 100 years

800 000 · 700 000 · 600 000 · 500 000 · 400 000 · 300 000 · 200 000 · 100 000 · 0

474 500 · 584 000 · 584 000 · 219 000

$\overline{\Delta\sigma}$ = 39,09 МПα

34,96 · 38,42 · 42,33 · 44,89

$\Delta\sigma_i$

Fig. 4 Histograms of stress ranges due to effects of heavy traffic according to EN 1991–2 within 100 years

$$D = \sum_i \frac{n_i}{N_i} \qquad (2)$$

where: n_i is the number of cycles associated with the stress range $\Delta\sigma_i$ for band "i" in the spectrum, N_i is the total number of cycles to failure under constant stress range $\Delta\sigma_i$ and D is the damage accumulation index. The stress ranges below the cut-off limit $\Delta\sigma_L$ (0) are neglected. The failure due to fatigue occurs when $D > 1.0$.

Another way, how the stress-range spectrum may be considered in fatigue assessment, is to replace them by an equivalent constant amplitude stress range spectrum that causes the same fatigue failure as the origin spectrum. It may be expressed again on the basis of Palmgren-Miner's hypothesis using Wöhler's curves. For the assessment purpose, it is useful to relate it to two million cycles, which is the number of cycles corresponding to the fatigue resistance defined in [2], [3]. Then, the equivalent stress range may be obtained from the equation

$$\Delta\sigma_{E,2} = \left(\frac{\Sigma n_i \Delta\sigma_i^{m_1} + \Delta\sigma_D^{(m_1 - m_2)} \cdot \Sigma n_j \Delta\sigma_j^{m_2}}{2 \cdot 10^6} \right)^{\frac{1}{m_1}} \qquad (3)$$

where: $m_1(m_2)$ is the slope of the first (second) part of the bili-near Wöhler's curve, $n_i(n_j)$ is the number of cycles associated with stress range level $\Delta\sigma_i(\Delta\sigma_j)$ – the index "i" corresponds to the slope m_1, the index "j" corresponds to the slope m_2. Stress ranges under the cut-off limit $\Delta\sigma_L$ (Fig. 5) are neglected.

The standard [2] provides a simplified method for determining the equivalent stress range related to two million cycles, which is defined by relation

$$\Delta\sigma_{E,2} = \lambda \cdot \Phi_2 \cdot \Delta\sigma_p , \qquad (4)$$

where: $\Delta\sigma_p = |\sigma_{p',\,max} - \sigma_{p,\,min}|$ is the stress range caused by LM 71, Φ_2 is the dynamic factor and $\lambda = \lambda_1 \cdot \lambda_2 \cdot \lambda_3 \cdot \lambda_4$ ($\lambda \le$

$\le \lambda_{max} = 1.4$) is the damage equivalence factor considering the damage effect of actual traffic load, the length of the member influence line or area, the traffic volume, the bridge design life, the number of tracks and the fatigue limit. Then, the fatigue assessment is given by relation

$$\gamma_{Ff} \cdot \Delta\sigma_{E2} \le \frac{\Delta\sigma_C}{\gamma_{Mf}} , \qquad (5)$$

where: $\Delta\sigma_C$ is the characteristic value of fatigue resistance corresponding to the chosen fatigue prone structural detail according to standard [3], γ_{Ff} is the partial safety factor for fatigue load (recommended value is $\gamma_{Ff} = 1.0$) and γ_{Mf} is the partial safety factor for fatigue resistance depending on the chosen design method (damage-tolerance or safe-life method) and on the consequences of failure according to standard [3].

4. Assessment of fatigue life

Fatigue assessment was realised for an element weakened by a rivet hole and subjected to axial force and bending moment. This detail is classified according to EN 1993-1-9 [3] as the fatigue detail of category 90. Considering the partial safety factor for fatigue resistance $\gamma_{Mf} = 1.15$, the design value of fatigue strength is $\Delta\sigma_C = 90/1.15 = 78.26$ MPa. The Wöhler's curve for the investigated fatigue detail is presented in Fig. 5. The fatigue assessment was realised in two ways:
- using Palmgren-Miner's linear damage accumulation hypothesis – for actual heavy traffic load and for the heavy traffic load according to standard [1],
- using a simplified method of determining the equivalent stress range $\Delta\sigma_{E2}$, to which the total number of cycles to failure N_E under constant stress range $\Delta\sigma_i$ and corresponding cumulated fatigue damage $D = 2 \cdot 10^6/N_E$ were determined.

The results of fatigue assessment of the observed details are presented in Fig. 6.
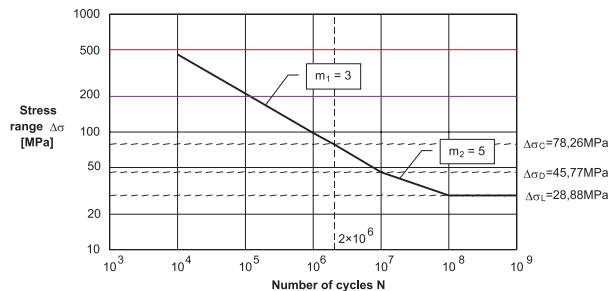

Fig. 5 Wöhler's curve for investigated fatigue detail

5 Conclusions

Based on the results of fatigue assessment it can be stated that all the observed bridge members satisfy the requirement for design fatigue life of 100 years, regardless of the type of service load under consideration. Both the standard approaches for considered railway service load – use of fatigue service trains according to [1] as well as the use of simplified method according to [2], are on the side of safety. Ratios between damage accumulation indexes corresponding to two ways of considering railway service load mentioned above and the damage accumulation index corresponding to actual traffic load are presented in Table 1.

The results of the fatigue assessment show very small damage accumulation indexes of the observed bridge members for all presented approaches. It means that service trains determined for fatigue assessment in the standard [1] do not cause significant fatigue damage of the observed bridge members due to small stress ranges and also due to investigated detail not very prone to fatigue

damage. Ratios of damage accumulation indexes emphasise very small stress ranges caused by actual traffic load effects for all the observed bridge members excluding diagonal D5, where the stress ranges due to actual traffic load effects are very close to stress ranges caused by heavy traffic according to standard [1]. The big ratio differences of upper chord H5 and bottom chord S5 result from the smaller stress ranges of these bridge members and lower frequency of the biggest stress ranges compared to bridge members H4 and S4.

At the present time, our research activity is focused on the investigation of the actual railway traffic load effects of the members of the bridge deck. Since the previous experiment was focused only on the main girders, another experimental measurement was necessary. Consequently, the more detailed numerical model was processed using the program IDA NEXIS. At the time, numerical simulations of the actual trains on the observed railway bridge are being realised. These effects will by again confronted with the effects of service load defined in EN 1991-2 [1].

Comparison of the fatigue assessment results   Table 1

	$\dfrac{D_{\text{traffic load by EC1}}}{D_{\text{actual traffic load}}}$	$\dfrac{D_{\text{simplified method by EC3}}}{D_{\text{actual traffic load}}}$
H4	3.41	4.38
H5	5.50	9.67
S4	8.14	9.48
S5	33.21	73.21
D5	1.12	1.39
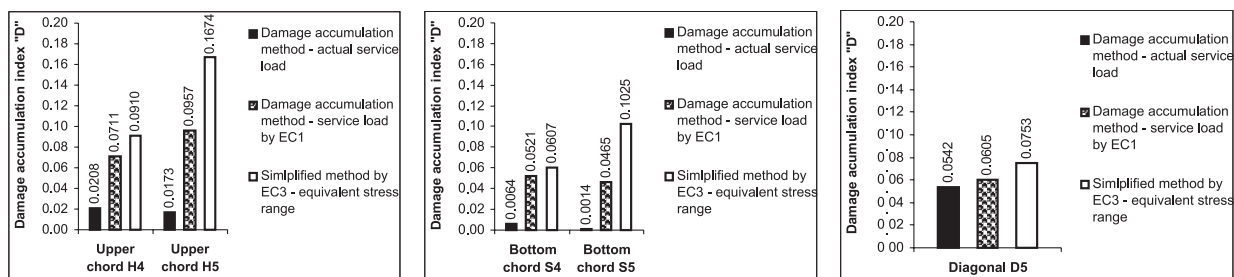
Fig. 6 Comparison of the fatigue assessment results

References

[1] EN 1991-2 *Actions on structures – Part 2: Traffic loads on bridges*, Brussels 2003.
[2] EN 1993-2 *Design of steel structures – Part 2: Steel bridges*, Brussels 2003.
[3] EN 1993-1-9 *Design of steel structures – Part 1.9: Fatigue*, Brussels 2003.
[4] MINER, M. A.: *Cumulative damage in fatigue*, Journal of Applied mechanics, 12, 1945, No. 3, p.p. 159–164

Milan Moravčík *

DYNAMIC PROPERTIES OF THE RAILWAY TRACK

The paper is focused on different aspects of track dynamics and train-track interaction. The dynamic modeling of railway track response and of the interaction of vehicle and track at low and mid frequencies, that are significant for the track deterioration, is presented. Dynamic properties of the track structure as a whole is described and evaluated including the dynamics of compound train-track system. The dynamic amplification resulting from the simulated passage of the locomotive of the type E 499.0 (85t) is presented.

1. Introduction

The use of a railway track structure by vehicles initiates dynamic loading, which gives vibrations of the interacting systems of the train and the track. The vibration behaviour of the railway track structure includes the wide frequency range, from the low frequencies (1–100 Hz) that corresponds the low-frequency vibration of track, through the mid frequencies (100–1500 Hz), and high frequencies (1500–5000 Hz) that corresponds transfer of the wheel-rail interaction forces and the sound radiation. These aspects deserve the attention and can be exploited as a performance indicator of the track structure status and a guiding instrument in track maintenance. One of the research goals at the Department of Structural Mechanics in the Track Mechanics field is to develop suitable methods for the evaluation of dynamic properties and the dynamic behaviour of a track structure that are focused on a conventional ballast track. With this purpose the program of theoretical and experimental works studying the interaction dynamic problems of a vehicle/track mechanical system focused on the track structure and the its dynamic behaviour has been undertaken and it comprises:

- Development of theoretical methods and mathematical models for solving interaction dynamic problems of the vehicle/track.
- Computer simulations and calculation to predict the dynamic response parameters of track – deformations, the strain and stress in the superstructure and in the substructure.
- In situ measurements of the response parameters of track structure.
- Static and dynamic laboratory tests of the track structure components – sleepers, fostering systems, resilient pads, the sleeper/ballast interaction, etc.

This paper is devoted to mathematical models and computer simulations of the dynamic behaviour of the track. Results of theoretical dynamic analyses are compared with the experimental results.

2. Dynamic characteristics of the track structure

One way to investigate the dynamic properties of a railway track is to load the track with a sinusoidal force. At frequencies up to approximately 100 Hz this can be carried out by using a mechanical or hydraulic exciter. If one wants to investigate the track response at higher frequencies, the track may be excited by an impact load. The most employed excitation models for determination the track dynamic characteristic are shown in Fig. 1. The response of the track can be found in either the time or the frequency domain. The response of the track usually is searched as a displacement or acceleration at the point of excitation, the direct rail receptance, interaction forces, etc. The excitation models in Figs. 1 are appropriate for comparing the calculated and measured testing of the track – passages of characteristic vehicles, a vibrator or impulse hammer dynamic tests.
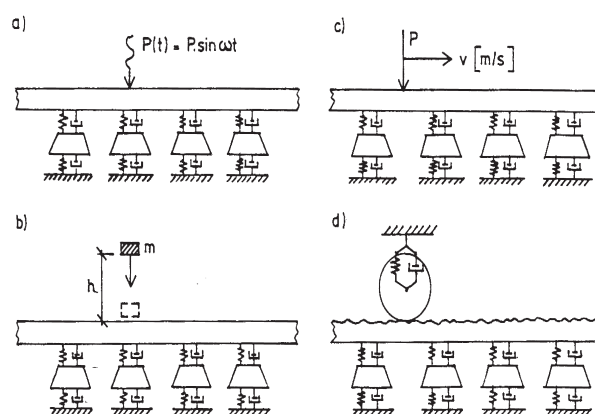

Fig. 1 Excitation models for the track structure

* Milan Moravčík
Department of Structural Mechanics, Faculty of Civil Engineering, University of Žilina, Slovakia, E-mail: Milan.Moravcik@fstav.uniza.sk

In order to examine the effect of variable track stiffness conditions, the five characteristic vertical ballast track stiffness $^{(i)}k_b$, $i = 1 \div 5$ were considered to model low, medium, and high track stiffness conditions. The mean values of the vertical ballast stiffness $\overline{k_b}$ and the vertical pad stiffness $\overline{k_f}$ are shown in Tab. 1.

Mean values of the modelled vertical stiffness of track   Table 1

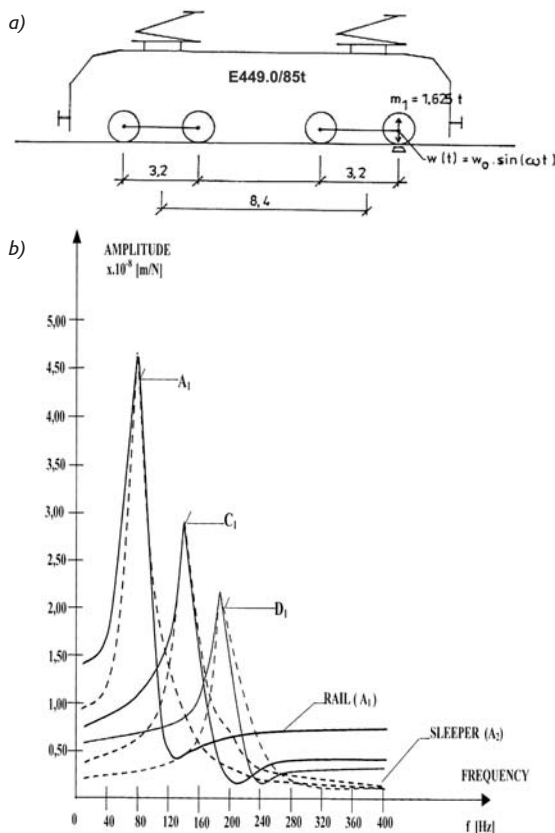| Track type (i)	Level of Support Stiffness	Vertical Ballast Stiffness $^{(i)}\overline{k_b}$ [N/m]	Vertical Pad Stiffness $\overline{k_f}$ [N/m]		Damping coefficient $\overline{C_f}$ [Ns/m]
A	low	40.106	1	150.10⁶	
			2	60.10⁶	
B	Medium (1)	80.106	1	150.10⁶	
			2	60.10⁶	
C	Medium (2)	120.106	1	150.10⁶	50.103
			2	60.10⁶	
D	high	220.106	1	150.10⁶	
			2	60.10⁶	
E	very high	480.106	1	150.10⁶	
			2	60.10⁶	

Fig. 2 The track response in the frequency range corresponding to the kinematics excitation - the vertical rail displacement amplitude $w_R(f)/P$ for the kinematics excitation by the first locomotive wheelset, for the track stiffness A_1, C_1 and D_1

Some results for the stationary point kinematics track excitation by the locomotive wheelset (Fig. 2a) for the driving frequency $f\langle 0-400 \text{ Hz}\rangle$, applied on the first wheelset, and the track response-vertical rail displacement in the frequency range $w_R(f)$, are presented in Fig. 2b.

3. Modeling and simulation of the dynamic track in the time domain

The track behaviour under a moving vehicle is usually reproduced by an interactive dynamic model with three model components: the dynamic model of vehicle, the linear track model, and the stiffness of discrete rail supports.

- *The conventional dynamic models* represent a railway track as an Timoshenko beam, or if we neglected both the effect of shear and the effect of rotatory inertia we obtain the classical Bernoulli – Euler beam model rested on the Winkler linear elastic foundation governed by equation

$$EI \frac{\partial^4 w(x, t)}{\partial x^4} + \mu \frac{\partial^2 w(x, t)}{\partial t^2} + 2\mu\omega_b \frac{\partial w(x, t)}{\partial t} +$$
$$+ \kappa\, w(x, t) = p(x, t) \tag{1}$$

where: $w(x, t)$ is the vertical displacement of the rail, EI is the bending stiffness of the rail, μ is the constant mass per unit length of the rail, ω_b is the circular frequency of damping of the rail, κ is the coefficient of Winkler foundation, and $p(x, t)$ is a external track load.

The force track loading is modeled as a vertical wheel force P_k, see Fig. 3. This model is deficient in several respects, in particular it neglects:
- The discrete nature of the support provided by the sleepers
- Elasticity of the railpad between rail and sleeper
- The ballast mass on the dynamic response
- The effect of variable track stiffness conditions.

This standard 1D Winkler beam on the elastic foundation modeling the track structure is schematic presented in Fig. 3.

- *In the finite elements approach (FEA)* the rail is modelled as an elastic beam on discrete supports. The 2D plain interaction model created in the Department of Structural Mechanics [6] is schematically shown in Fig. 5. This model is concerned with the study of low and mid frequencies $f = 0 - 300$ Hz. In this model the four beam elements belong to one sleeper bay. The track model which has been used (see Fig. 5) consists of the 36 sleepers, which are modeled as rigid bodies. The fastenings (pads) are modeled as a viscoelastic foundation with a linear (bilinear) stiffness k_f and viscous damping C_f. The ballast is also modeled as linear (bilinear) springs k_b and viscous dampers C_b in parallel. Resilient couples connecting the track components – the rail, sleepers, and the ballast are shown in Fig. 4.
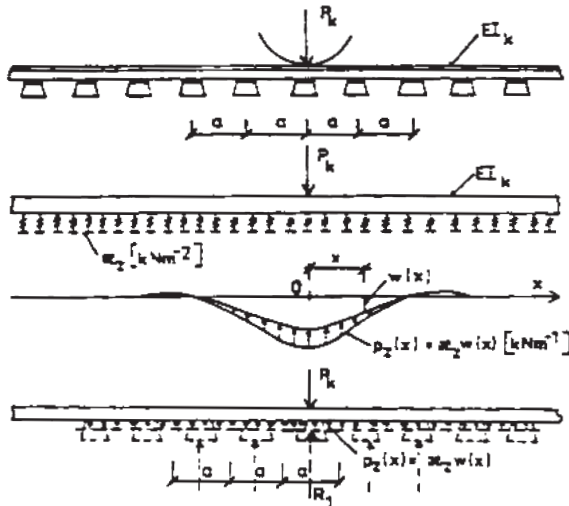
Fig. 3 Standard Winkler beam on the linear elastic foundation modelling the track structure
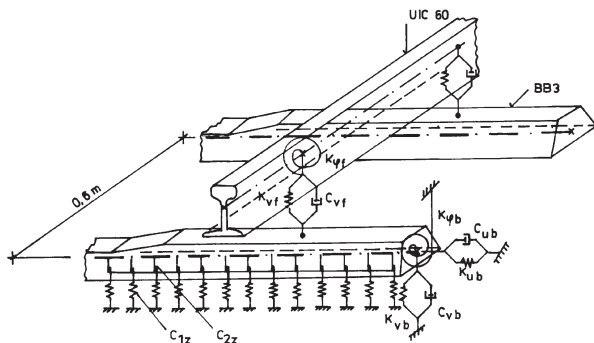

Fig. 4 The resilient couples connecting track components in the railway grid.
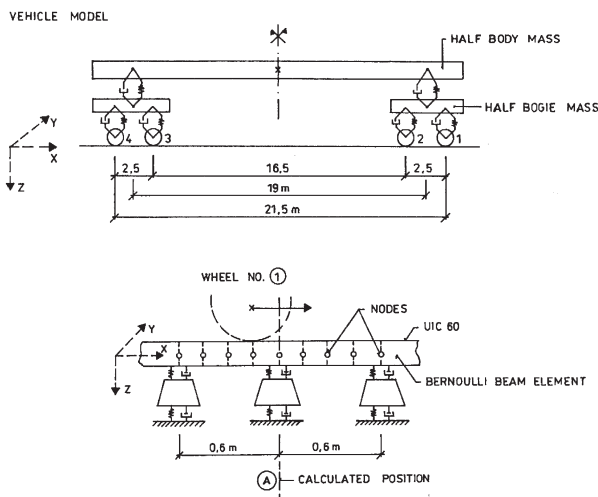

Fig. 5 The scheme of vehicle – track interaction model for FEA

The mechanical properties of the track components are modeled by a set of springs and dampers in one or two layers. The characteristics of springs and dampers can be determined by the laboratory load tests of these components or the field measurements in the typical track conditions.

The track behaviour under the dynamic loading conditions is reproduced by an interactive dynamic model with three model components:
– the dynamic model of vehicle,
– the linear track model,
– the stiffness of discrete rail supports.

The Finite Element Method is used for modeling of the track and the Composite Element Method is used for the modeling of vehicle. The resulting FEM motion equations of the track structure are:

$$[M][\ddot{U}] + [C][\dot{U}] + [K][U] = [P] \tag{2}$$

where $[M]$, $[C]$ and $[K]$ are the mass, damping and stiffness matrices of the track structure respectively, and $\{P\}$ is the nodal load vector. $\{U\}$ is the nodal vertical displacement vector.

The vehicle is modelled by the Composite Element Method as a system described by three quantities: its mass $[m]$ or inherent properties, its internal force elements (springs and dampers $[c]$, $[k]$) and the generalised coordinates $[u]$. The equation of the vehicle mass parts then describes analogous process as in Eq.2:

$$[m][\ddot{u}] + [c][\dot{u}] + [k][u] = [F] \tag{3}$$

where: $[m]$, $[c]$ and $[k]$ are the mass, damping and stiffness matrices of the vehicle system respectively, and $\{F\}$ is the nodal load vector. $\{u\}$ is the nodal vertical displacement vector.

Applying the above-mentioned equations of the finite element method and time-step integration, one can obtain simulation results including chosen amplitudes $Y(t)$ of the dynamic track response:

$$Y(t) = (w_R(t), w_S(t), R_{S-b}(t), M_R(t), ...) \tag{4}$$

where: $w_R(t)$, $w_S(t)$ are the rail and sleeper deflections in the position above sleeper "A", see Fig. 5, $R_{S-b}(t)$ is the sleeper-ballast vertical interaction force under sleeper "A", and $M_R(t)$ is the rail bending moment, etc.

The approach can be helpful in clarifying the influence of vehicle speed, stiffness of subgrade, stiffness and damping of fastenings on the dynamic response of the track. The example of simulation output in the time domain applied for the locomotive Skoda E 499.0 (85t) operating by speeds of 20 m/s are presented in Fig. 6.

• *In applying the commercial FEA programs* the track system can be suitable modeled as a plain grid with resilient couplings between the rail, sleepers, and the subgrade. The five elastic constant $[k]$
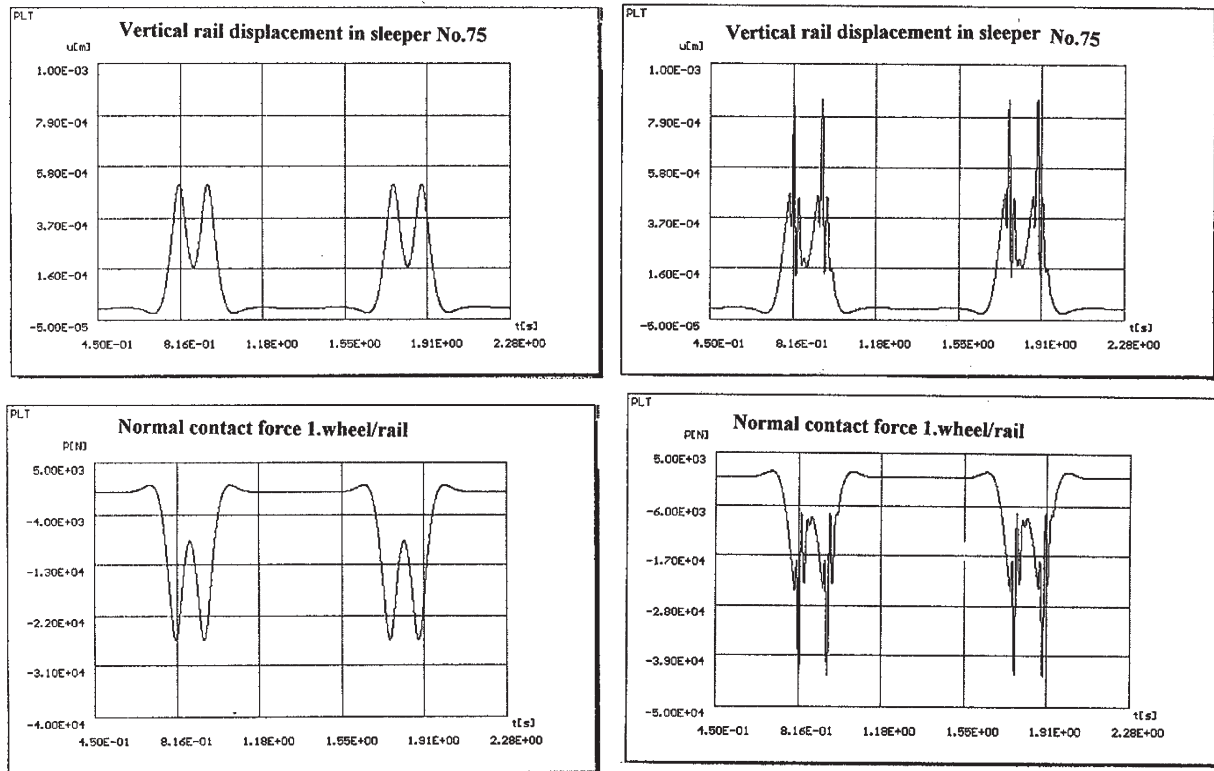
Fig. 6 Vertical dynamic sleeper displacements and the normal contact force for the stationary point force excitation by the locomotive wheelset: a) the locomotive smooth passage, v = 20 m/h, b) The locomotive passage across the single cos. shape irregulation, v = 20 m/h

characterising the resilient properties of subgrade entering as an input data in the computer system FEAT 2000, [7] – three constants k_{1x}, k_{2x}, k_{3x} described the vertical stiffness of subgrade and two constants k_{1y}, k_{2y} described the shear stiffness of subgrade. In regard to the variability of vertical stiffness of the subgrade during the track exploiting, the regular estimation of these constant has the fundamental significance for the respectable results. The model of the railway grid with the resilient couplings modeled in the computer system FEAT 2000 is shown in Fig. 7.

3.1 Dynamic coefficient

A moving vehicle on a track with a stochastic rigidity of the substructure in the vertical direction $\{^{(i)}k_j\}$ generates deflections and stresses in the track structure that are generally greater than those caused by the same vehicle load applied statically or moving on the track with the constant rigidity of the substructure. This actual dynamic wheel loads are approximately represented by equivalent quasi-static load. The simple approach for determining the wheel load $P_{w,dyn}$ uses empirical equations containing an impact factor δ_{dyn} and a wheel load $P_{w,st}$ can be expressed in the form
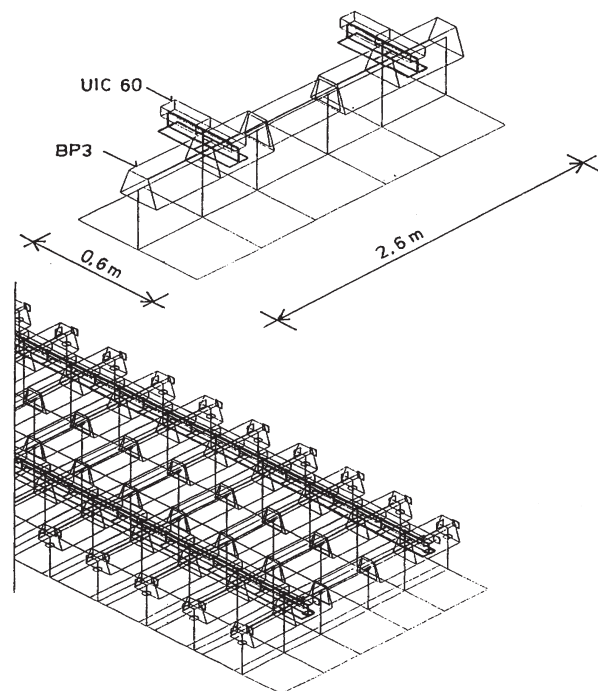
$$P_{w,dyn} = \delta_{dyn} \cdot P_{w,st} \qquad (5)$$

Fig. 7 The railway grid model including resilient component couplings, modeled in the computer program FEAT 2000

The dynamic amplification δ_{dyn} generally has a stochastic character and can be defined as a ratio of the maximum dynamic response of a quantity Y_{dyn}, for example $Y_{dyn} = w_{w,dyn}$ – the rail dynamic deflection, $w_{w,dyn}$, etc. to the static deflection of a quantity Y_{st}.

3.2 Results of numerical simulation

The passage of each vehicle wheelset induces amplitudes of the observed quantity $^{(i)}Y_{dyn(road)}$ and these results may be treated statistically. Thus, the histograms of these amplitudes may be exploited for the statistic expected values of the dynamic coefficient δ_{dyn} for the rail deflection, bending moments, etc.

$$\delta_{dyn} = \frac{^{(i)}Y_{dyn(road)}}{Y_{st}} \qquad (6)$$

The example evaluating of the dynamic coefficients δ_{dyn} from chosen quantities w_{dyn} and P_{S-b} (for the track B1 considering the constant stiffness of supports) are presented in Tab. 2.

Dynamic coefficient δ for the constant stiffness of support, $k_{b,j} = const$.   Table 2

Track type	Amplitude response			Dynamic coefficient	
B1	Y_{st}	Y_{dyn}		$\delta_{dyn} = \dfrac{Y_{dyn}}{Y_{st}}$	
		20 m/s	50 m/s	20 m/s	50 m/s
Rail deflection w_{dyn} [mm]	0.796	0.821	0.908	1.03	1.14
Sleeper-ballast force P_{S-b} [kN]	41.5	42.9	47.7	1.03	1.15

Using the mean values $\mu_{[Y]} = \overline{Y}$ of the response quantities $\overline{Y}$ and the standard deviation $\sigma_{[Y]}$, the dynamic coefficient δ_{dyn} may be evaluated. The dynamic coefficient δ_{dyn} for the constant stiffness of supports, see Tab. 2, is small for the low vehicle speed and it increases with vehicle speed.

The effect of a stochastic rail support stiffness can not be ignored, particularly for the higher vehicle speed, see [4, 5] and some results are in Tab. 3. The results obtained confirm that the higher values standard deviations of the support stiffness can be one of the important factors causing an intensive dynamic response of track components.

4. Conclusion

The purpose of simulating the dynamic track behaviour was to assess the dynamic behaviour of rail $w_R(t)$, sleepers $w_S(t)$ and the interaction force the rail – the sleeper $R_{S-b}(t)$ under the train passages, especially the locomotive passage of the type E 499/85 t in operational conditions. In this paper are presented the simulation approaches for the typical locomotive passage only.

The response of a railway track that includes the uncertainties in the vertical track supports stiffness subjected to moving railway vehicle is solved by the finite element method and time-step integration. Monte Carlo simulation was applied for these cases to estimate the dynamic track response to variations of the subgrade stiffness that was simulated as a stationary randomly distributed ballast stiffness with a standard uniform distribution and a normal distribution. The herein presented simulation results of the dynamic interaction are concerned in the low and mid frequencies, say 0 – 300 Hz, and they are applied to the track with different vertical stiffness. The dynamic amplification resulting from the simulated passage of a vehicle over the simulated track section can be calculated as the ratio of the maximum dynamic response Y_{dyn} (deflection w, bending moment M, etc.) to the static response Y_{st} on given track stiffness level. Some obtained results can be summarised as follows:

- The dynamic response results due to the tracks with the constant stiffness of supports (deterministic cases) show a low dynamic amplification $\delta = 1.05 – 1.2$, for the track response quantities $Y = (w, P, M,$ etc.$)$ in relation to the vehicle speed c.
- The dynamic response due to the stationary randomly distributed stiffness of supports $k_{b,j}$, with the standard uniform and normal distribution, follows the results of the static analysis and they show how the vehicle speed influences the track response.

Dynamic coefficient δ for the Uniform distribution of support stiffness $k_{b,j}$,   Table 3

Track type	Support stiffness $k_{b,j} \in \langle 60.10^6 - 100.10^6 \text{ N/m}\rangle$					
B1	$\delta_{dyn} = \dfrac{Y_{dyn}}{Y_{st}}$		$\delta_{dyn} = \dfrac{(\overline{Y}_{dyn} + \sigma_\gamma)}{Y_{st}}$		$\delta_{dyn} = \dfrac{(\overline{Y}_{dyn} + 2\sigma_\gamma)}{Y_{st}}$	
	20 m/s	50 m/s	20 m/s	50 m/s	20 m/s	50 m/s
Rail Deflection w_{dyn} [mm]	1.03	1.15	1.18	1.33	1.33	1.51
Sleeper-ballast Force P_{S-b} [kN]	1.01	1.14	1.17	1.5	1.32	1.50

In these cases the effect of the stochastic rail support stiffness can not be ignored, in particular for the higher vehicle speeds.

– While the mean value of the response amplitudes $\bar{Y}$ and the corresponding dynamic coefficients δ_{dyn} attain no high values for these cases, the individual response amplitudes $\{Y\}$ can attain values that can not be ignored. The standard deviations of support stiffness σ_γ is an important factor affecting the dynamic response on a given level of support stiffness.

References

[1] KNOTHE, K., GRASSIE, S. L.: *Modelling of Railway Track and Vehicle/Track Interaction at High Frequencies*, Vehicle System Dynamic 22, 1993

[2] MORAVČÍK, M.: *Experience in Railway Track Testing for Validation of Theoretical Dynamic Analysis,* Communications – Scientific Letters of the University of Zilina 1/99, Žilina

[3] MORAVČÍK, M.: *Vertical Track Stiffness in Service Conditions (in Slovak),* Technical report for the Slovak Railways, University of Žilina, 1996, p. 148

[4] MORAVČÍK, M., MORAVČÍK, M.: *Mechanics of the Railway Tracks I, II – Theoretical Analysis and Simulation of Problems in the Railway Tracks Mechanics (in Slovak)*, EDIS, Žilina, 2002

[5] MORAVČÍK, M., MORAVČÍK, M.: *Mechanics of the Railway Tracks III – Experimental Analysis for Straining and Distortions of the Railway Track Components (in Slovak)*, EDIS, Žilina, 2002

[6] SIČÁR, M.: *Vehicle-Track Interaction Concentrated to the Track Response (in Slovak)*, PhD Thesis, University of Žilina, 1996, p. 180

[7] Manual FEAT 2000, Praha, 2000.

Libor Ižvolt – Ján Kardoš – Martin Mečár *

REINFORCED SUBBASES AND APPLICATION OF OTHER CHOSEN PARAMETERS IN SLEEPER SUBGRADE DIMENSIONING

The paper focuses on reinforced subbases which are frequently applied to modernised railway tracks of Slovak Railways (ŽSR) despite certain theoretical and normative deficiencies. Based on the evaluation of laboratory measurements other parameters which are to be taken into consideration when dimensioning a sleeper subgrade construction are specified.

1. Introduction

Integration of the Slovak Republic into the EU makes new, higher demands on the railway transport and it is inevitable to accept them. Besides this, when modernising the railway infrastructure of Slovak Railways (ŽSR), it is necessary to respect required parameters based on European Agreement on Main International Railway Lines (AGC) and European Agreement on Important International Combined Transport Lines and Related Installations (AGTC). Implementation of these agreements is obligatory on 916 km (4 corridor localities) out of 3662 km of the Slovak railway tracks. Modernisation of the railway tracks improves their technical parameters, namely the adaptation of directional conditions to 160 km.h^{-1} and the adaptation of the railway substructure to the axle force of 225 kN. At the same time new modern materials, components and technologies are applied, which is represented mainly by the use of geosynthetics in the railway substructure construction. Its application depends on its function in the sleeper subgrade (isolating, filter, reinforcing, draining, protective or tightening).

Geosynthetics has been applied into a large number of modernised railway corridor localities and approximately 80 km of the modernized railway tracks have been put into operation. Regarding the qualities which geosynthetics offers in the railway substructure, mainly the geosynthetics with the reinforcing function suffers from the insufficient normative basis for dimensioning of reinforced construction layers (with respect to its characteristics and characteristics of its geological surroundings).

2. Design of reinforced subbases in railway substructure – current state

The required deformation resistance of the sleeper subgrade construction (detected by a static plate loading test – SPLT) and protection of the subgrade surface against the influence of frost are two main indicators which determine the required subbase thickness on the subgrade consisting of fine-grained soil (Fig. 1). The assumed value of the static deformation module of the subgrade surface E_0 and the required value of the static deformation module on the level of the railway substructure E_{ekv} are in accordance with the methodology given in [1] the required input parameters for the subbase design (i.e. design of construction structure, type of applied material and its dimensions). These values are determined in a relevant railway technical standard depending on a speed zone (1–5). In the case that the assumed value of the static deformation module of the subgrade surface reaches lower values than required, it is possible to use several solutions how not only to increase the deformation resistance, but reach the required value E_{ekv} on the level of the railway substructure, as well. One of possibilities is to design a sleeper subgrade construction No. 3 – s*leeper subgrade with subbase reinforced by geosynthetics*. When applying this solution, a choice of suitable reinforcing geosynthetics and suitable material (aggregate) of the subbase would follow. At present, in accordance with the requirements given by Slovak Railways Authorities, it is possible to use only such geosynthetics which is authorized by Slovak Railways on the basis of accredited tests realized in testing laboratories, in situ or, if it was authorized according to the Regulation No. 61/1999. However, the certificate issued by Slovak Railways does not declare the reinforcing effect of geosynthetics for example by *TBR* parameter (*Traffic Benefit Ratio*) or *BCR* parameter (*Base Course Reduction Ratio*); it is based only on the reached value of the static deformation modules from SPLT, although (as it will be proved hereinafter) SPLT cannot sufficiently evaluate the efficiency of reinforcing geosynthetics [2], [3]. After the selection of proper reinforcing geosynthetics it is possible to proceed in dimensioning of the reinforced subbases as follows:

- respecting the results of particular geosynthetics given by a producer (distributor), or based on the certificate issued by Slovak Railways the required thickness of the reinforced subbase is determined for particular conditions of the subgrade surface deformation resistance;

* Libor Ižvolt, Ján Kardoš, Martin Mečár
  Department of Railway Engineering and Track Management, Faculty of Civil Engineering, University of Žilina, Slovakia,
  E-mail: libori@fstav.uniza.sk, jan_kardos@vahostav-sk.sk, mecar@fstav.uniza.sk
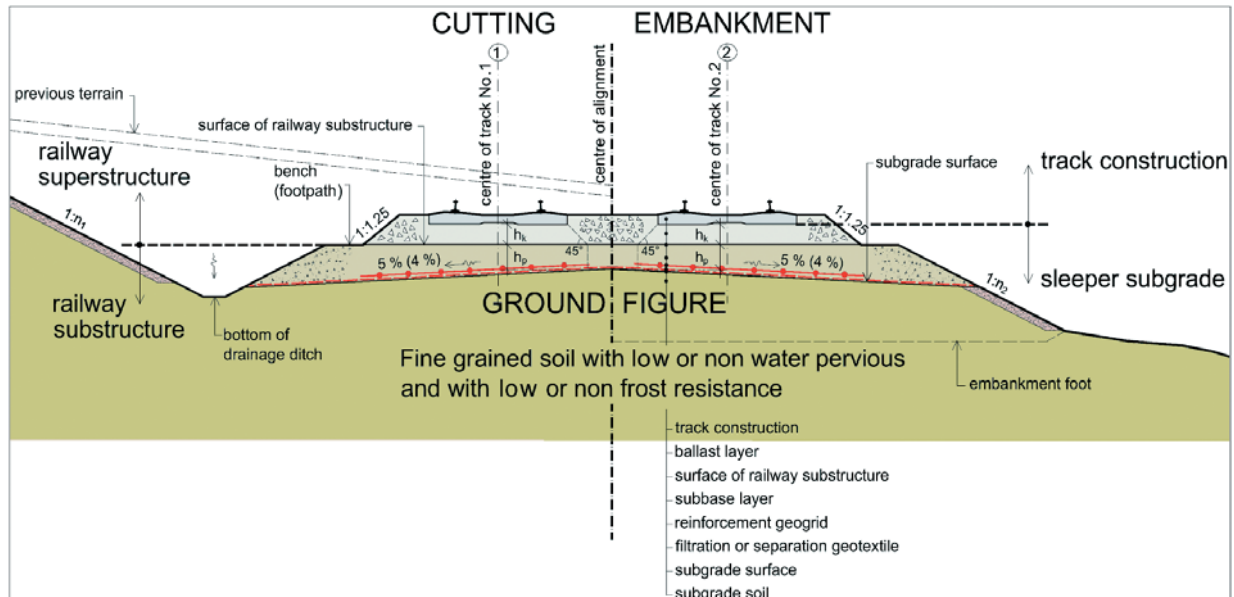
Fig. 1 Front view of double track – sleeper subgrade type No. 3

- according to the regulation [1] DORNII method may be used, and in the case that the subbase reinforced by stiff biaxial geogrids is designed, it is possible to use the deformation module value of the reinforced subbase $E_i = 80 - 140$ MPa,
- again, according to the regulation [1] DORNII method may be used, when the unreinforced subbase is designed at first, and it is subsequently reduced with *Deutsche Bahn AG* or *Czech Railways (ČD)* dimensioning method in the following way:
  - DB AG – if the subbase thickness is more than 0.50 m and at the same time, if the deformation module of the subgrade surface E_0 is 10 – 30 MPa (from SPLT according to DB), the subbase thickness may be reduced in 0.10 m ($BCR \leq 20$ %) [4],
  - ČD – if reinforcing geosynthetics in the gravel subbase is used, the subbase thickness may be reduced in 25 % ($BCR \leq 25$ %) and in the case of the crushed rock subbase in 30 % ($BCR \leq 30$ %) [5].

When dimensioning the reinforced subbase according to all the above mentioned methods, the result is a construction with an unknown value of *TBR* and consequently with an unknown durability or economic return. This situation is caused by inadequately specified conditions for issuing the certificates which further follow from the insufficient normative basis for the reinforced subbase diagnostics. Research on the reinforced subbases that has been already done shows the necessity of using a diagnostic device with cyclic loading (stationary, non-stationary) for diagnostics of these constructions. The reason is that it simulates transport loading more reliably because the reinforcing effect of any geosynthetics is connected with an accumulation of permanent deformations emerging from the compaction of the subbase material (this applies mainly to geogrids).

Despite the above mentioned arguments the certificates have continuously been accepted due to the insufficient normative basis at Slovak Railways. These certificates are based only on the results obtained by SPLT and their evaluation for each particular use of the aggregate and quality of its compaction. The results of many measurements on the railway substructure models and in situ measurements realized by the Accredited laboratory of the Department of Railway Engineering and Track Management (AL DRETM) served as a basis for the certificates issued to distributors and producers of reinforcing geosynthetics. Since 1998 ca *267* constructions have been diagnosed in situ and *217* in the laboratory which represents ca *484* realized and evaluated static plate loading tests.

3. Analysis of experimental research results on reinforced subbases

Description of the subgrade surface model and methods of laboratory measurements are given in [6]. This paper presents the analysis and evaluation of the measurements with the focus on the methodology of the reinforced subbase dimensioning and the importance of the compaction degree on the overall deformation resistance of the sleeper subgrade construction.

In 2006 several measurements of the biaxial stiff welded geogrid efficiency were realized in the Accredited laboratory of DRETM (with various deformation resistance of the subgrade surface – ca 5, 10, 15, 20 and 25 MPa) which finally served as a basis for issuing the certificate for the tested type of geogrid and designed structure and dimensions of the reinforced construction layers in the railway substructure. The comparative measurements on constructions without the applied geogrid were carried out in order to prove the efficiency of the applied tested geogrid. The results of

the measurements realized on the reinforced and unreinforced construction with the equivalent deformation module of the subgrade surface E_0 = ca 5.0 MPa (where the maximum reinforcing efficiency of the applied geogrid was assumed) will be analyzed and evaluated in the following text. The structure of the compared sleeper subgrade constructions is shown in Tab. 1.

The static plate loading tests were successively realized on particular subbase construction thicknesses of 0.30 m, 0.50 m a 0.70 m. The compared construction was identical regarding material and geometry, only the reinforcing geogrid was not applied in it. The material of the subgrade surface was classified as *sandy clay* and the equivalent deformation module of the subgrade surface E_0 = ca 5.0 MPa was obtained when water content w reached ca 23.5 %. Crushed rock with the fraction of 0/63 mm was applied into the subbase (its technical parameters are shown in Tab. 2. Technical parameters of the built-in reinforcing geogrid are shown in Tab. 3. The ratio between efficient fraction calibre of d_{50} and the size of the geogrid aperture is 3.12 or 3.20, which presupposes an efficient concurrence between the aggregate and geogrid. The disadvantage of the applied geogrids is the height of the tensile element which reaches the values of 0.80, or 0.95 mm depending on the applied geogrid. Based on a known theoretical assumption, this fact may cause a small crushing resistance (during interlocking of aggregate particles and geogrid) and thus reduce compactness between the geogrid and aggregate. Another disadvantage of the components applied in the tested construction is a small ratio value between the surface area of the geogrid and the surface area of the geogrid apertures (75.7 – 77.4 %), which is caused by wide tensile elements of the geogrid (6 – 8 mm). This fact may cause the insufficient penetration of the aggregate into the geogrid apertures and may result in forming of a slip surface on the geogrid level.

There were 72 SPLTs realized in 2 cycles of measurement in order to evaluate the effect of the geogrid built in the construction layers of the railway substructure (so called reinforced subbase of the sleeper subgrade). There were 6 SPLTs realized on each partial layer of the subbase and after the realization of SPLTs and the compaction of crushed rock on the last two construction layers, another 3 SPLTs were realized. The influence of the compaction degree on the deformation resistance of the reinforced/unreinforced construction was tested in this way. The summary of the results

Structure of the compared constructions   Table 1

Construction I - reinforced	Construction II - unreinforced
– subgrade surface with the equivalent deformation module E_0 = ca 5.0 MPa	– subgrade surface with the equivalent deformation module E_0 = ca 5.0 MPa
– filtration geotextile	– filtration geotextile
– geogrid GG – A	– ——————
– crushed rock with the fraction 0/63 mm and thickness 0.30 m	– crushed rock with the fraction 0/63 mm and thickness 0.30 m
– geogrid GG – B	– ——————
– crushed rock with the fraction 0/63 mm and thickness 0.40 m	– crushed rock with the fraction 0/63 mm and thickness 0.40 m

Technical parameters of the applied geogrids   Table 3

Type of geogrid / Characteristics	GG – A	GG – B
Tensile strength (kN.m^{-1})	34	25
Strength during 2% elongation (kN.m^{-1})	11	8
Strength during 5% elongation (kN.m^{-1})	23	17
Strain at maximum load (%)	10	10
Type of polymer	polypropylene	
Type of geogrid	stiff biaxial geogrid of the extruded straps connected by laser welding	
Mesh size A x B (mm)	44 x 43	44 x 44
Height and width of the rib (mm)	0.95 x 7.0	0.80 x 6.0
Open area to overall area (%)	75.7 %	77.4 %

obtained by testing the reinforced and unreinforced construction (average values of deformation resistance and compaction degree) is shown in Tab. 4 and its graphic representation in Fig. 2.

Table 4. and the diagram of the deformation module of the reinforced and unreinforced construction show that small differences between the compared constructions occurred in real thickness, the acquired compaction degree of the subbase, and modelling of the deformation resistance of the subgrade surface. Despite the

Technical parameters of the compared constructions   Table 2

Effective grain size dx (mm)		Fraction ratio (%)		Further characteristics	
d_{10}	0.445	f	4.919	Number of uneven granularity C_U	42.182
d_{30}	5.062	s	14.134	Number of curvature C_C	3.074
d_{50}	13.779	g	78.508	Water content w (%)	3.560
d_{60}	18.751	cb	2.439	Wash-off particles b (%)	4.489
d_{100}	64.281	b	0.000	Filtration coefficient k_f (m.s^{-1})	0.01742
Classification of subbase material according to USCS:				Maximum density ρ_{max} (kg.m^{-3})	2130
				Minimum density ρ_{min} (kg.m^{-3})	1440
$G2 = GP - Cb$ – gravel with poor granularity with admixture of stones					

Resulting average values of the tested parameters on the reinforced and unreinforced construction   Table 4

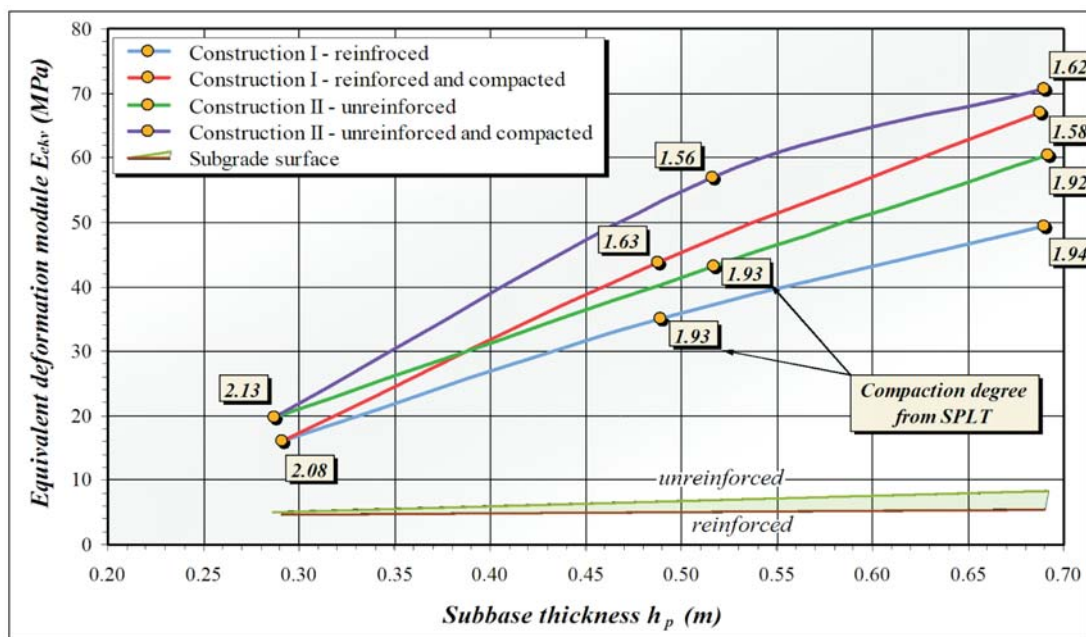| Testing construction		Construction I - reinforced				Construction II - unreinforced			
		E_{ekv} (MPa)	M_z	Real thic-kness of subbase (m)	Day of measuring	E_{ekv} (MPa)	M_z	Real thic-kness of subbase (m)	Day of measuring
Measurement level	Subgrade surface before testing cycle	4.64	2.24	–	0	4.99	3.06	–	0
	Subbase thickness 0.30 m	16.04	2.08	0.291	6	19.72	2.13	0.287	14
	Subbase thickness 0.50 m	35.04	1.93	0.489	8	43.28	1.93	0.517	22
	compacted	43.83	1.63	0.488	9	56.97	1.56	0.516	26
	Subbase thickness 0.70 m	49.30	1.63	0.690	9	60.38	1.92	0.692	31
	compacted	67.06	1.58	0.688	10	70.74	1.62	0.690	33
	Subgrade surface after testing cycle	5.52	2.70	–	15	8.27	2.11	–	36

Fig. 2 The equivalent deformation module of the reinforced and unreinforced construction depending on the subbase thickness and compaction degree

effort put into the construction of two identical models, they were not completely identical. Duration of the experimental measurements presents a considerable problem when making a comparison, because it causes the increase of the deformation resistance of the subgrade surface on individual subbase layers during the measurement. The increase of the deformation resistance of the subgrade surface after the subbase removal is in the unreinforced construction 3.7 times higher than in the reinforced construction. This fact is caused by a longer period of the measurements on the construction in 21 days. Based on the above mentioned reasons, the results had to be further analysed in order to exclude these small differences and find a functional dependence between the following variables:

- the equivalent deformation module of the subgrade surface E_0 (MPa) in the specific time of measurement of the equivalent deformation module on a particular construction layer E_{ekv} (MPa),
- the equivalent deformation module on a particular construction layer E_{ekv} (MPa),
- thickness of the subbase (reinforced/unreinforced) h_p (m),
- the acquired compaction degree M_z.

It was inevitable to reduce the number of four variables into two variables in order to obtain the required functional relation. The equivalent deformation module on a construction layer E_{ekv} and the equivalent deformation module of the subgrade surface E_0 were replaced with a parameter of the equivalent deformation module increase ΔE_{ekv} which was determined from the equation:

$$\Delta E_{ekv} = E_{ekv} - E_0 \quad \text{(MPa)} \tag{1}$$

The equivalent deformation module of the subgrade surface E_0 was determined with a linear interpolation from the deformation module values of the subgrade surface according to the time and location of the measurement on a particular construction layer and thus the deformation resistance increase of the subgrade surface during the measurement on a particular construction was taken into consideration, as well. The deformation module increase made it possible to remove a small difference between the deformation resistance of the subgrade surface on the reinforced and unreinforced construction, as well. Another assumption which had to be taken into consideration was connected with a linear relation between the equivalent deformation module increase ΔE_{ekv} and thickness of the subbase h_p. A parameter which describes the given assumption is labelled as k and is calculated according to the equation:

$$k = \frac{\Delta E_{ekv}}{h_p} \qquad (\text{MN.m}^{-1}) \qquad (2)$$

There were two variables obtained through these procedures: the compaction degree M_z and the parameter k. These variables may be easily analysed and it is possible to determine their functional relation from measured values with the method of regression and correlation analysis. There were 4 out of 24 pairs of the measured values excluded (the level of importance 0.95) on both the reinforced and unreinforced constructions. The graphic representation of regression and correlation analysis is shown in Fig. 3. Having used a simple regression function of an exponential form, the correlation coefficient reached the value $R = 0.869$ for the reinforced and $R = 0.889$ for the non-reinforced construction.

Having completed the obtained regression functions with the equations (1) and (2) the equations for the calculation of the equivalent deformation module E_{ekv} or the required thickness of the subbase h_p depending on the type of construction (reinforced/ unreinforced) and on the acquired compaction degree M_z were derived. Equations applying to the reinforced construction are as follows:

$$h_p = \frac{(E_{ekv} - E_0) \cdot M_z^{2.67}}{313} \quad (\text{m}); \text{ or}$$

$$E_{ekv} = \frac{313 \cdot h_p}{M_z^{2.67}} + E_0 \quad (\text{MPa}) \qquad (3)$$

Equations applying to the unreinforced construction are as follows:

$$h_p = \frac{(E_{ekv} - E_0) \cdot M_z^{2.28}}{276} \quad (\text{m}); \text{ or}$$

$$E_{ekv} = \frac{276 \cdot h_p}{M_z^{2.28}} + E_0 \quad (\text{MPa}) \qquad (4)$$

When analysing the equations (3) and (4) it is obvious that the equivalent deformation module E_{ekv} of the reinforced construction layer is always lower than that of the unreinforced construction. This phenomenon is probably caused by the insufficient interlocking of the aggregate into the geogrid apertures because the small height of the tensile elements (ribs) of the geogrid

cannot activate the sufficient crushing resistance. At the same time the flat ribs probably cause that the aggregate particles lie on them and this does not prevent their movement; on the contrary, the flat ribs support the formation of a slip surface by lowering the friction between the geogrid and aggregate. [8]. The geogrid with flat tensile ribs may thus serve only as a membrane. Another fact that might impede the detection of reinforcing effect of the geogrid is the process of SPLT itself because it simulates the real loading only marginally. Since the current directives are based on the expected acquired equivalent deformation module from SPLT, it is neither appropriate nor possible to start with the reduction of the subbase thickness in this case (with the application of *BCR*) as it is mentioned in *Chap. 2.* When applying diagnostic devices with a more reliable simulation of the real operational loading (multiple cyclic loading) in the detection of the geosynthetics reinforcing effect, it will be possible to obtain parameters *TBR* depending on the type of the applied geosynthetics. At the same time it will be possible to specify the influence of various physical characteristics of geosynthetics and aggregate on their reinforcing effect in the subbase and thus, together with economic indicators, to design an optimum construction as for price and quality. Till then it is possible to reinforce the subbases only with the assumption of the coefficient *TBR* increase, whose exact indicators are not known at present. It follows that the economic indicators of a particular geosynthetics application are unknown, as well.

The analysis of the equations (3) and (4) shows that the acquired compaction degree is a parameter which remarkably influences the final equivalent deformation module based on SPLT. The current dimensioning methodology [1] does not take into consideration the compaction degree but it uses another variable in calculation, namely a material deformation module of the construction layer E_i. Under certain circumstances the material deformation module of the construction layer E_i may represent the material compactness because in the case of reaching a low deformation module, the material has the insufficient compaction (which means that it has a high compaction degree from SPLT). However, it is very difficult to measure the material deformation module and therefore its values are only estimated at certain intervals according to Tab. 5.9. given in [1]. On the contrary, the compaction degree based on SPLT characterizes properly the material conditions and the assumption of its future behaviour because the material compacted to a low compaction degree resists further loading with a lower deformation (decrease). One of the advantages of this method is a possibility of using measurement technique installed in the compaction machinery (vibratory rollers). They are able to monitor the decrease during compaction, evaluate the acquired compaction degree and thus determine the assumed deformation module on the construction layer indirectly. It is possible to use a dynamic plate loading test with a relative sensor of deflection for the evaluation of the compaction degree, as well. Its realization is easy and does not require much time [5]. Inclusion of the compaction degree into the dimensioning method would make it possible to design the construction thickness with regard to the compaction technology and to simplify diagnostics of a given construction, as well.
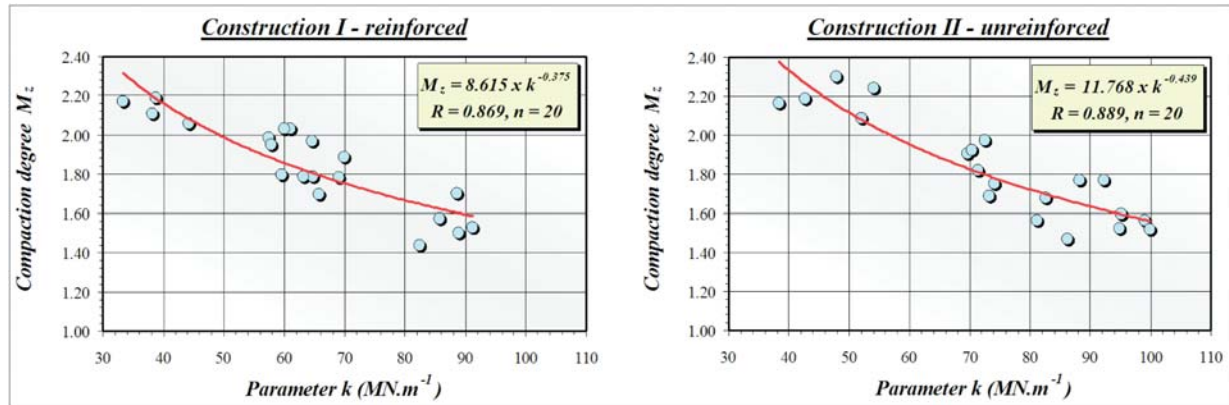
Fig. 3 Regression and correlation analysis of dependence between the compaction degree M_z and the parameter k

Having transformed the equation (4) for the unreinforced construction into the graphic representation (Fig. 4) a dimensioning nomogram has been created. This nomogram may serve (when taking into consideration the required deformation module increase ΔE_{ekv} and the assumed compaction degree M_z) as a basis for determination of the required subbase thickness h_p, or on the contrary, for determination of the required compaction degree M_z in a particular designed subbase thickness h_p. Validity of this dimensioning nomogram is for the subgrade surface with the equivalent deformation module E_0 = ca 5.0 MPa (possibly for the range of 2.50 MPa

– 7.50 MPa). The graph (Fig. 4) shows an isoline determined by DORNII method according to [1] which presupposed the application of aggregate and the deformation module E_i = 80 MPa. It is possible to determine from the graph that the results of the calculation method are approximately identical with the experimental values for the acquired compaction degree M_z = ca 1.95. If the required deformation module increase ΔE_{ekv} = 40 MPa and the assumed compaction degree M_z = 1.70, it is possible to reduce the subbase thickness hp in 0.15 m = ca in 40 % (as the result of a higher compaction), as opposed to the calculation dimensioning
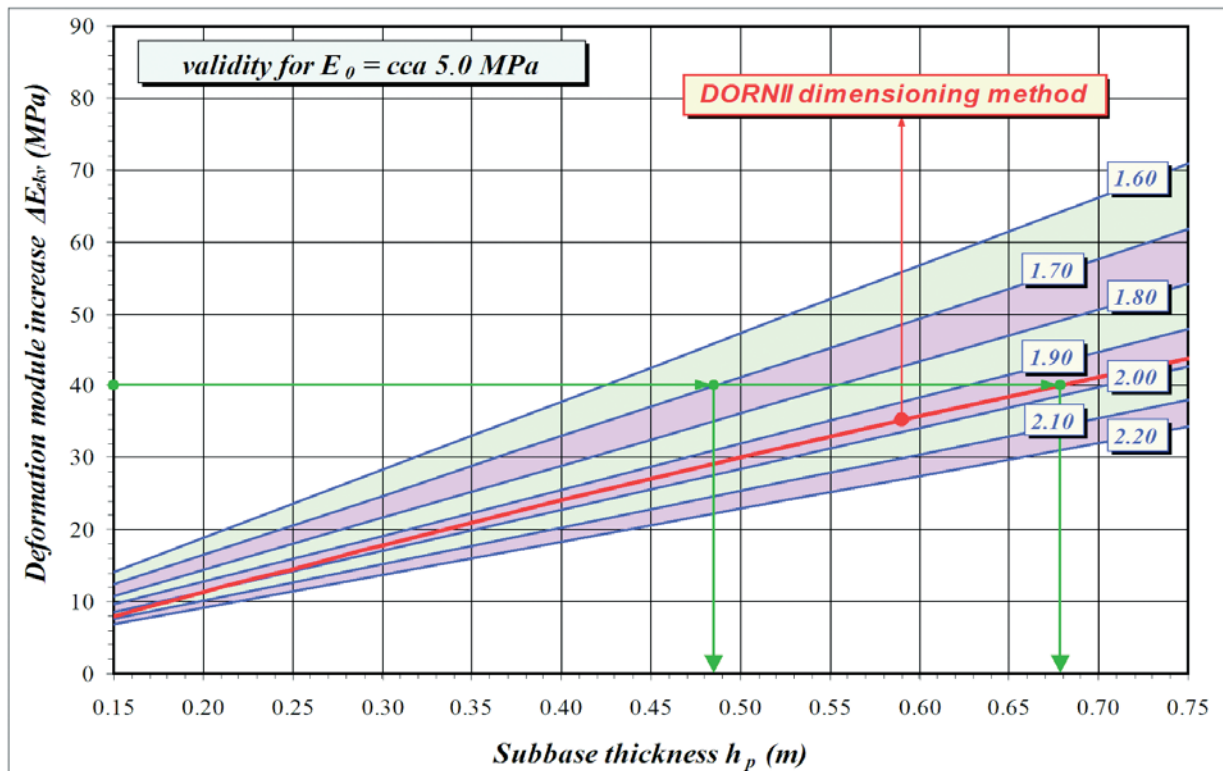

Fig. 4 Dimensioning nomogram for determination of the subbase thickness taking into consideration the compaction degree of the subbase material

method. Evaluation of the experimental measurements in other values E_0 = 10, 15, 20 a 25 MPa assumes that the above mentioned tendencies will be proved and it will be possible to develop a new dimensioning method which will be able to evaluate the influence of the compaction degree precisely. Based on the application of the specific aggregate (Tab. 1) it will be inevitable to verify the aggregate with a different fraction and granularity curve and to monitor its effect on the relation between the subbase thickness hp and the deformation module increase ΔE_{ekv}, or to determine a possible degree of the effective compaction. It may be assumed that differences in granularity will not have a substantial influence on the equivalent module of deformation in a given compaction degree. However, according to the existing experience, granularity will be a significant factor for compactibility with regard to energy demands for the acquirement of the same compaction degree (density).

3. Conclusion

The process of design of the reinforced and unreinforced subbases at Slovak railways has suffered many deficiencies. Reinforcement of subbases is based only on the unconfirmed assumption of the construction durability increase without its detailed quantification. After the evaluation of laboratory measurements it is obvious that the application of *BCR* coefficients or determination of *TBR* will be possible only after their determination on a given construction via cyclic loading tests. This is one of the reasons why the laboratory of DRETM plans to utilise an electro-hydraulic pulsator which is able to generate loading with variable frequency, variable deflection and thrust. Another step will be based on the necessity to establish a normative basis and conditions for issuing

the certificates, which will apply these new possibilities of diagnostics in practice. It will be essential to monitor and determine the factors of the reinforcing geosynthetics and aggregate which influence their mutual efficiency in the subbase. Consequently, based on these factors a system for the evaluation of geosynthetics applicability will be developed with respect to particular conditions (deformation module of the subgrade surface, speed zone, type of aggregate, etc.).

The deformation resistance of the subbase is influenced mainly by the compaction degree which is very difficult to evaluate precisely by the current dimensioning methodology [1]. Based on the already obtained results and on the evaluation of further measurements realized at DRETM a new empirical dimensioning method covering further relevant factors is to be developed. Fig. 4 shows that current criteria for the maximum values of the acquired compaction degree from SPLT (for minimum compaction) are to be revised. It would put the current limit value of 2.20 closer to the value corresponding to DORNII method, i.e. 2.00 which would guarantee the fulfilment of the acquired deformation resistance in dimensioning calculation. At the same time it is important to realise that the influence of the acquired compaction degree on the acquired deformation resistance is increased together with the construction thickness. It follows that it is inevitable to determine not only general criteria for the compaction degree, but the criteria depending on the construction thickness, as well (bigger construction thickness = stricter criteria for compaction degree).

References:

[1] *Railway technical standard 73 6312 – Subbase construction layers designing,* GR ŽSR, August 2005.
[2] IŽVOLT, L., KARDOŠ, J.: *Reinforcing of sleeper subgrade construction layers,* Expert opinion for PRODEX(r) spol. s r.o., Žilina, July 2006.
[3] GÖBEL, C., LIEBERENZ, K.: *Handbuch Erdbauwerke,* Der Bahnen, Eurailpress Tetzlaff-Hestra Gmbh&Co.KG, 2004, ISBN 3-7771-0317-9.
[4] Instruction S4 of Czech Railways *"Railway substructure".*
[5] IŽVOLT, L., KARDOŠ, J., LEĽAK, J., MEČÁR, M.: *Diagnostics of the track substructure model and its practical use,* Communications – Scientific letters of the University of Zilina, Žilina, April 2005, ISSN 1335-4205.
[6] IŽVOLT, L., LEĽAK, J., KARDOŠ, J.: T*he results of the reinforced subbase layers laboratory tests,* Theoretical Foundation of Civil Engineering, XV Russian-Slovak-Polish Seminar, Moscow-Rostov, September 2006, ISBN 83-908083-7-4.
[7] Instruction S4 of Slovak Railways "*Railway substructure*", NADAS, January 1988.
[8] IŽVOLT, L., KARDOŠ, J., LEĽAK, J.: *Factors influencing efficiency of biaxial geogrid in subbase*, Proc. IV International Conference GEOSYNTHETICS in Civil Engineering, Žilina, February 2007, ISBN 978-80-8070-646-3.

Ján Čelko – Marek Drličiak – Andrea Gavulová *

TRANSPORTATION PLANNING MODEL

The traffic congestion represents a very important problem of the cities at present. The results are a frustration of motorists; longer travel times; an increase of accidents and fuel consumption and negative effect to the environment. The transport relations modeling by exact analysis of the real traffic state is a complex solution. This solution enables a determination of the future demands depending on traffic forecast. The article presents the main process of transport modeling based on four-step solution. This process is completed by its practical using in the town of Žilina. The transport relation analyses, the modal split and traffic distribution are described. The focus of the article is approaching the transport-modeling dilemma.

1. Introduction

The traffic requirements are increasingly more extensive and demands for the road network expand. The exact traffic forecast is one of basic assumptions of sustainable transport. It allows to determinate the future transportation relations and a network loading. The requirements to the new infrastructure elements would be defined.

The transportation model became one of the basic tools of transportation engineers. The model is wide-spectrum and it would be oriented to the wide area but also to the individual intersection. However, the real state of traffic is an imperative assumption of the model. So the quality of the model is directly depending on input parameters.

The phase in a four steps model became the wide-spread. The process of determination of the future traffic demands includes, first, a trip generation, second, a trip distribution, third, a modal split and fourth, a traffic assignment. The result of the four step analysis is forecast of the infrastructure and intersections loading and specification of the demands for future network developing.

Two types of models are generally used. The disaggregate model is used above all at present. Contrary to the aggregate model, the disaggregate model evaluates the habitants from the point of view of effect to the transport behaviour in dependence on a trip purpose.

The North Region of Slovakia and Žilina especially is a rapidly developing area. The new investments launched, above all, the development of car industry. The industry expansion brought new problems in infrastructure loading, especially in the road infrastructure. Creation of an exact transport model has a markedly accruing account. The Department of Highway Engineering of Civil Engineering Faculty collects the essential data for the model creation in frame of its research activities. The PTV VISION software is used as a modelling tool.

2. Trip generation

Trip generation deals with productions and attractions of the parts of the region. The solved region is divided to zones depending on selected parameters which are defined by a detailed analysis of urban, transport, economic, and sociological conditions. The basic parameter needed for traffic forecast is the generation of the trips by origin zones. Žilina was divided into 36 zones to analyse the internal transport; and new six fictive zones were created to define the origin, destination and transit transport. The fictive zones are located on the town periphery.

The number of trips depends on a zone character, above all. The greatest source of the trips is a living zone. The majority of the trips are connected with a household. The home based trips mean that one end of the trip is at home (home – work, sport – home, etc). On the other hand the industry zones are the most attractive for trips inducing by destination zone.

The most important parameters of the trip generation are regional economics, regional demographics, and population of the zone and distribution of the subzonal traffic relation. The described parameters markedly affect the car ownership. Philosophy of the zone creation is a very important factor.

2.1 The zone creation

The exact definition of the zone functionality is inevitable. The function determines the type of transport, the trip's purpose and attractiveness. The zone functionality represents the land uses of the area, the population, employment, retail space etc.

The models included a big territory define from 5 to 8 types of the zone. The minimal 4 types of zone are necessary for forecast of the traffic demands:
– habitable,
– industry,

* **Ján Čelko, Marek Drličiak, Andrea Gavulová**
  Department of Highway Engineering, Civil Engineering Faculty, University of Žilina, Slovakia, E-mail.: jan.celko@fstav.uniza.sk,

– service,
– recreation.

Each zone is characterized by a number of inhabitants, employment offer, school capacity, commercial service and recreation abilities. The division of Žilina to the zones is shown in Fig. 1. The 7 external zones for transit transport were created besides 42 internal zones.
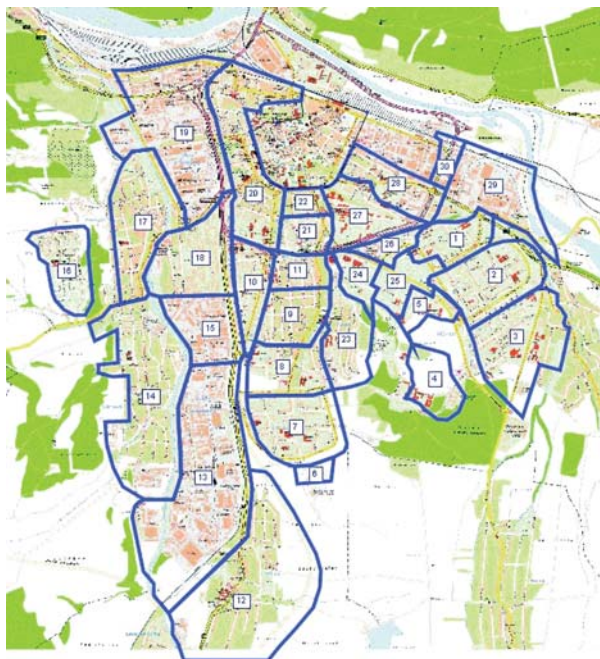

Fig. 1 Zones in Žilina

2.2 Transport potential

The transport potential of the zone is the transport production depending on possibility of a trip generation. The potential depends on more factors; the car ownership is very important. The average number of vehicles per household is used for calculation the most frequently. The car ownership defines the basic group for calculation of traffic generation by individual car transport. The economically active people without car are the basic group for generation of the traffic by public transport. These two groups of habitants are the source of essential traffic. The generated traffic potential of the zone D_i involves also next groups of habitants – students, unemployed, children etc.

The employment offer and service providing are a secondary source of the potential and they are used as a source of attractiveness above all.

The solution of Zilina region issues from transport-sociological analysis. The present specimen is more than 3000 inhabitants, which is about 4%. The process of data collection continues. The specimen 6% of inhabitants is an aim of research team. The homoge-

nous groups characterised by uniform transport behaviour were crested by division of the inhabitants to the specific groups.

The next groups were created:
- $E+c$ Employed persons. car available
- $E-c$ Employed. no car available
- $NE+c$ Not Employed persons. car available
- $NE-c$ Not Employed. no car available
- Child Children
- Stud Students
- Pens Pensioners

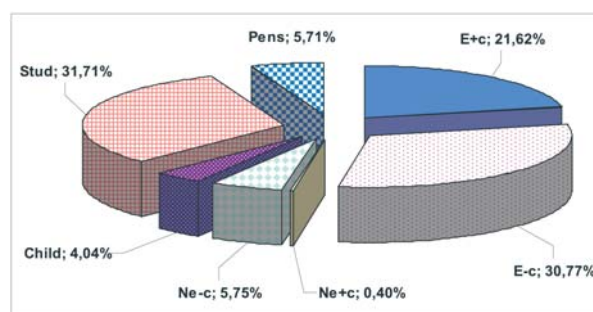The division of inhabitants to the groups is shown in Fig. 2.

Fig. 2 Inhabitants' groups

The mobility of the groups of inhabitants was the source of a trip number generation for each zone. The average mobility in Žilina is 2.26 trips per day. The mobility is shown in Fig. 3.
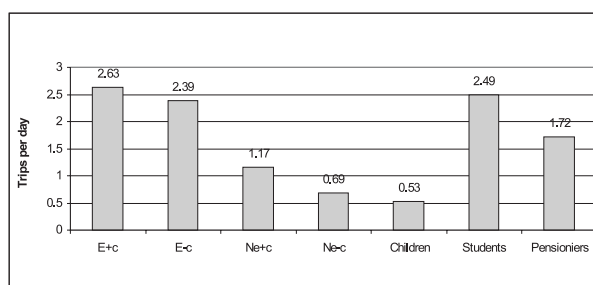

Fig. 3 Mobility of groups

3. Trip distribution

When speaking of a trip generation, a 'trip' is defined as travel between two places of activity. The analysis deals separately with *trip productions*, which are trips generated by residential zones to serve a need, and *trip attractions*, which are trips generated by activities such as employment, retail services etc. and are related to satisfaction of a need. The traffic volumes induced by potential of the zone must be predicted to the interzonal travel volumes $D_{i,j}$ as a function of the attractiveness of the destination zone and expe-

dience of the offers of next zones. The traffic volumes are defined by the following parameters:
- transported subject D
- origin of transport (zone i)
- destination of transport (zone j)
- travel time t
- transport mode m
- transport purpose p
- transport route r.

The chains of activities of inhabitants were created by results of the analysis. The chain represented a structure of movements during day and forms a traffic relation between zones. So, the volume of origin transport is described by formula (1)

$$Do_{ip} = a_{ip} \times t_p \times X_{ip} . \tag{1}$$

Volume of destination transport is described by formula (2)

$$Dd_{jp} = a_{jp} \times t_p \times X_{jp} \tag{2}$$

Where Do_{ip} (Dd_{jp}) is the volume of origin (destination) transport of zone i (j) by purpose p, a_{ip} (a_{jp}) is specific moving of an structural element X_{ip} (X_{jp}); X_{ip} (X_{jp}) is a structural element of beginning or ending activity; t_p is proportion of the trips during observed period for purpose p.

The volume of transport is divided between the solved zones in the next step and O-D Matrix is created by a trip distribution.

3.1 Methodology of the trip distribution

The simpliest method for calculation of the trip distribution is a method of growth factor. The predicted trips are depended on observed trips at present and some growth factor, outgoing from the zone development forecast. The more effective and the most common method is the gravity model derived from Newton's Gravitation Law. The basic structure of the model is as follows:

$$D_{i,j} = \frac{D_i \times D_j \times k_i \times k_j}{w_{ij}} . \tag{3}$$

Where $D_{i,j}$ is the number of trips between zone i and j, D_i is the total trips produced in zone i, D_j is the total trips attracted to zone j, k_i, k_j are constants derived so the model could satisfy the production and attraction constraints, w_{ij} is a deterrence function that describes a disutility of travel.

A very simple gravity model substitutes the total trip produced in zone i and attracted to zone j by number of inhabitants and deterrence function that is described only by a distance between the zones (4).

$$D_{ij} = \frac{\alpha \times O_i \times O_j}{d_{ij}^2} \tag{4}$$

Where α is factor of region, O number of inhabitants, d distance between zones i-j.

The gravity model arises on the dependence of direction of transport flows by determination of the probability P_w of the transport relation between zones i-j. The function is named deterrence function $F(w_{ij})$. The classical deterrence function has the shape:

$$F(W_{ij}) = \frac{1}{f(W_{ij})} = \frac{1}{W_{ij}^\alpha} . \tag{5}$$

This type of deterrence function suits the overvaluation of traffic flows in specific conditions. The different shapes of the function are presented in Fig. 4 [2].
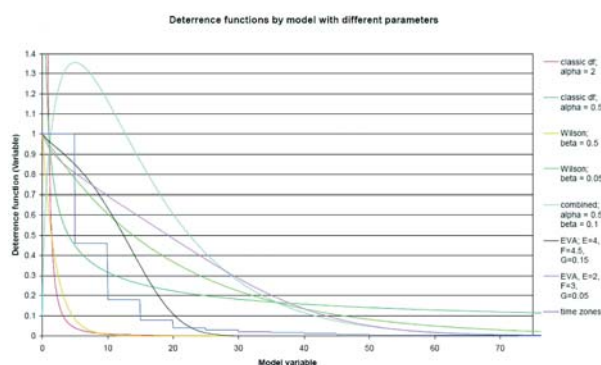

Fig. 4 Deterrence functions

The most frequently used formulae for the function description are:

- Wilson model:

$$f_{ij} = W_{ij}^{-\alpha} \exp(-\beta W_{ij}) \tag{6}$$

- EVA formula (Bayesian formula by Lohse and Lätzsch 1997):

$$f_{ij} = \frac{1}{(1 + W_{ij})^{\varphi(W_{ij})}}; \quad \varphi(W_{ij}) = \frac{E}{1 + \exp(F - G \times W_{ij})} \tag{7}$$

Where E, F, G are parameters of travel mode, W_{ij} is resistance of the route, $\varphi(W_{ij})$ is deterrence function.

- Another author's models.

The next methods used for the trip distribution are Fratar's method, Detroid's method, method of entropy. Fratar's and Detroid's method established the local growth factor for definition of the region development. The entropy method is defined as a rate of uncertainty in a process of trip direction distribution

3.2 O-D Matrix

The result of the trip distribution is O-D Matrix (origin - destination). The origin (rows of matrix) represents the zone responsible for producing a trip; destination (columns of matrix) represents the zone responsible for attracting the trip. So in the same cell appear both the home to work and work to home trips; the sum of

row values represents origin trips from the zone and the sum of column represents destination trips to the zone.

It is very important than the trip generation describes origin traffic volumes and the trip distribution describes interzonal relation. *O–D* matrix includes all the trips between the zones independent on type and transport mode. The *O–D* matrix can be seen in Fig. 5.

from i / to j	1 ...	j	...	n	Σ	
1	D_{11}				O_1	
.	.				.	
.		.			.	
i		D_{ij}			O_i	$(=\sum_j D_{ij})$
.			.		.	
.				.	.	
m				D_{nm}	O_m	
Σ	D_1 ...	$D_j(=\sum_i D_{ij})$	...	D_n	D	$(=\sum_i O_i = \sum_j D_j)$

Fig. 5 O-D matrix

4. Modal split

The third step of the transportation modelling is modal split among the available modes of travel. The travel mode must be allotted to each trip. The travel modes are defined like a one-person mode (cycle, car driver) and group's mode (walk, public transport, car passenger). PTV software uses a multimodal model with 5 modes. These models consider the time, costs and other characteristics of each mode. The characteristics determine a proportion of travellers which will choose each mode.

In the process of modal split the probability of particular mode choice is found. The logit model is the most frequently used for this activity. The logit model predicts the probability that an individual will choose a particular alternative (mode m) as follows:

$$P_{gij}(m) = \frac{e^{U_{gij}(m)}}{\sum_{k=1}^{M} e^{U_{gij}(k)}} \qquad (8)$$

Where *i, j* are indices of the zones, *g* is the group of inhabitants, *m* is index of travel mode, $U_{gij}(m)$ is a group-specific utility if transport mode *m* is chosen to get from *i* to *j*. The quality of model is dependent above all on utility that accents a resistance of the travel mode to the route. PTV Vision defines this function by formula

$$U_{gij}(m) = -p_{1gm} * T_{ij}(m) - p_{2gm} * Z_{ij}(m) +$$

$$+ p_{3gm} * \log(D_{ij}/p_{4gm}) - p_{5gm} \times C_{ij}(m) + p_{6gm} \qquad (9)$$

Where $T_{ij}(m)$ is travel time from *i* to *j* by transport mode *m*, $Z_{ij}(m)$ is a sum of access time *i* and egress time *j* for transport mode *m*, $C_{ij}(m)$ is a travel cost from *i* to *j* by transport mode *m*, $D_{ij}(m)$ is a distance from *i* to *j*, $A_{ij}(m)$ is an additional supply attribute, p_{igm} is parameter of utility.

The described coefficients are determined for each travel mode separately. The KONTIV 89 coefficients (PTV VISION) are nonfactual for Slovak conditions, so new ones are solved at present. Besides the logit model the *binary model* is used for two modes. The more complicated models are used in case of more travel modes (by example *NESTED model*).

The solved modal split in Žilina is presented in Fig. 6 for all the observed groups.
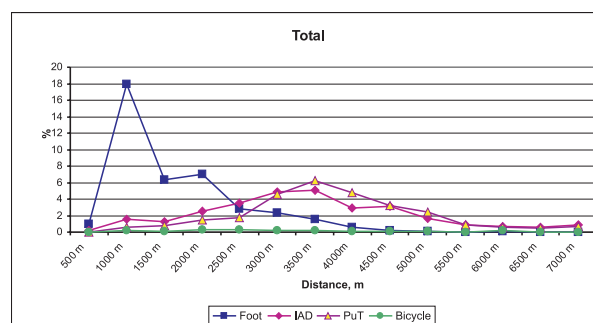

Fig. 6 Modal split according to distance

5. Traffic assignment

The final step of modelling is traffic assigning to the transport network using traffic assignment models. These essentially represent travellers' route choice decisions and would indicate the number of elements travelling between zones *i* and *j*.

The traffic assignment process requires traffic volumes between zones described by vehicle flows depending on car and public transport occupancy, and parameters of network, the capacity determination, of course. The parameters of network parts determine the travel time of the link. The more different methods are used for traffic assignment – equilibrium, self-teaching. The method of limited capacity is mostly used. First, the shortest path (in terms of travel time) between each origin and each destination is found. The assignment is realised by calculation of the capacity sufficiency and next routes are found in the next steps.

5.1. The model calibration

The model would be the working tool only in case of its comparability with the real conditions. O-D Matrix created from the realised analyses defines real matrix of interzonal transport relations. In addition the traffic censuses were realised within the of Žilina to compare real and calculated traffic loading of the road network. The complement of the model by further sociological and transport censuses will be the source of its next precision. The first results from the traffic analyses of Žilina can be seen in Fig. 6.

Fig. 7 Traffic loading of Žilina road network

6. Conclusions

Transport development is a very important part of the town's policy. Sustainable development of the regions needs the necessary increase of public transport depending on increasing demands of individual transport including traffic loading, parking problems etc. The complex traffic model is one of the best ways of exact and immediate solution of current problems.

References

[1] ROSE, G.: *An introduction to four step transportation planning models,* Monash University, 2002.
[2] KÖLBL, R., J.: *A bio-physical model of trip generation/trip distribution,* A thesis submitted for the degree of Doctor of Philosophy, Department of Civil and Environmental Engineering, University of Southampton, United Kingdom, December 2000.
[3] ČELKO, J., GAVULOVÁ, A., DRLIČIAK, M.: *The influence of regional development intention on transport in the town of Žilina,* International Conference Regional Development and Transport Logistics, Proc. ISBN 80-8070-621-2, Žilina, December 2006, pp. 151 – 157.
[4] ČELKO, J. et al: *General City Plan of Žilina,* Additional censuses and analyses - transport and transportation facilities, Žilina, July 2006.
[5] PTV_VISION User Manual, Karlsruhe, 2002.

Jozef Komačka – Martin Korenko – Jaroslav Piala *

RELATION OF TEMPERATURE CHANGES IN ASPHALT PAVEMENTS TO PAVEMENT BEARING CAPACITY EVALUATION

Temperature changes in asphalt pavements have to be taken into account at the diagnostic and evaluation process of pavements bearing capacity. Theoretical calculations resulting from general theory are not suitable for the practical use. Therefore the experimental test section with flexible and semi-rigid pavement was built and the temperatures were measured at different depths. The examples of typical temperature gradients for the hot summer and cold spring day are presented and their similarities are stated. The development of the simple method for the determination of mean temperature of pavement asphalt layers is described and the correction values relative to the temperature of pavement surface are shown for the time interval from 20^{00} to 8^{00} and the asphalt layers thickness of 210 mm.

1. Introduction

Highways and roads as the important part of the traffic infrastructure must have sufficient structural performance to satisfy traffic requirements. Diagnostic and evaluation of bearing capacity of road pavements is one of the most important activities in evaluation procedures of road structural performance. In Slovakia the top layers of road pavements consist of asphalt. As stiffness of asphalt and consequently pavement response (measured deflections) changes according to temperature this parameter must be taken into account during the process of pavement bearing capacity evaluation. According to Slovak provisions [1] and [2] measured deflections or backcalculated moduli of asphalt layers have been "recalculated" to the "equivalent" temperature of 20 °C. Although different equations have been used the temperature of asphalts at the depth of 40 mm below the pavement surface is generally an input to the recalculation (it is assumed the temperature at this depth is mean temperature of asphalt layers). But in practice the temperature at the depth of 40 mm is usually measured only at the first testing point and it is considered as the representative mean temperature of asphalt layers for whole test section. As the pavement temperature changes along the test sections the differences in temperatures could be a cause of mistakes when the measured deflections are recalculated to the equivalent temperature. From this point of view the measurement of air and pavement surface temperature at each testing point seems as inevitable for the determination of right mean temperature of pavement asphalt layers.

2. Theoretical background

Different methods could be used for the pavement temperature calculation. Generally all methods are related to solar radiation, heat transfer and energy balance on the pavement surface. As stated

at [3] the net rate of heat flow to and from a body q_{net} can be calculated from the equation

$$q_{net} = q_s + q_a + q_t \pm q_c \pm q_k - q_r \tag{1}$$

where: q_s – energy absorbed from direct solar radiation

q_a – energy absorbed from diffuse radiation (scattered from the atmosphere)

q_t – energy absorbed from terrestrial radiation (for the pavement can be considered to be 0)

q_c – energy transferred to or from the body as a result of convection

q_k – energy transferred to or from the body as a result of conduction

q_r – energy emitted from the body through outgoing radiation

Then, by writing each of the above flow rates in terms of temperatures the following equation for the calculation of the pavement surface temperature can be obtained

$$422\alpha\tau_\alpha^{1/\cos z} \cdot \cos z + \epsilon_a \sigma T_a^4 - h_c(T_s - T_a) -$$
$$- \frac{k}{d}(T_s - T_d) - \epsilon\sigma T_s^4 = 0 \tag{2}$$

where: α – surface absorptivity to the solar radiation

τ_a – transmission coefficient for unit air mass

z – angle between the zenith and direction of the sun's rays

ϵ_a – $0.49 \cdot (10^{-0.074 \cdot \rho})$

ρ – vapour pressure varying between 1 and 10 mm of mercury

σ – Stefan-Boltzman constant = $5.68 \cdot 10^{-8}$ [W.m^{-2}. K^{-4}]

T_a – air temperature [K]

* Jozef Komačka, Martin Korenko, Jaroslav Piala
Department of Highway Engineering, Faculty of Civil Engineering, University of Žilina, Slovakia
E-mail: komacka@fstav.uniza.sk

T_s – surface temperature [K]
h_c – average convective heat transfer coefficient of surface [$W.m^{-2}.C^{-1}$]
k – thermal conductivity [$W.m^{-1}.C^{-1}$]
d – depth below the surface [m]
T_d – temperature at depth d [K]
ϵ – emissivity

Thermal diffusion theory can be used for the calculation of temperature changes in the pavement structure. According to Fourier law the thermal diffusion and the changes of heat flow can be described by equations published in [4]

$$q(x,t) = -\lambda \cdot \frac{\partial T(x,t)}{\partial x} \qquad (3)$$

$$\frac{\partial q(x,t)}{\partial x} = -\rho \cdot c \frac{\partial T(x,t)}{\partial t} \qquad (4)$$

The final equation resulting from the formulas (3) and (4) is then

$$\frac{\partial T(x,t)}{\partial t} = \frac{\lambda}{\rho \cdot c} \cdot \frac{\partial^2 T(x,t)}{\partial x^2} \qquad (5)$$

where: $q(x,t)$ – density of heat flow at the point x and time t [$W.m^{-2}$]
λ – thermal conductivity coefficient [$W.m^{-1}.K^{-1}$]
$T(x,t)$ – temperature at the point x and time t [K]
ρ – bulk density of the material [$kg.m^{-3}$]
c – thermal capacity of the material [$J.kg^{-1}.K^{-1}$]

Various computing method can be used to solve equation (5) but they are complicated in general and not very suitable for the practical applications. Therefore different empirical methods are used too and they differ according to their purpose. When pavement bearing capacity is tested, diagnostic equipment has usually the possibility to measure the air and pavement surface temperature at each testing point. The empirical method for the determination of mean temperature of pavement asphalt layers using these two temperatures has been developed at the Highway Engineering Department of the Civil Engineering Faculty.

3. Experimental measurements

The test section consists of flexible and semi-rigid pavement was built in Žilina (about 330 m above see level) to measure the temperature in pavement layers. The type and thicknesses of asphalt layers is given in table 1. The temperature sensors were installed at different depths below the pavement surface (table 2) to measure

Asphalt layers of pavements   Table 1

Semi-rigid pavement	Flexible pavement
AC 11 mm 40 mm	AC 11 mm 40 mm
AC 16 mm 90 mm	AC 16 mm 80 mm
AC 22 mm 80 mm	AC 22 mm 100 mm

continually the temperature distribution in the pavement. Moreover the air temperature at 2 m above earth surface has been recorded automatically.

Positions of thermometers   Table 2

Semi-rigid pavement		Flexible pavement	
Thermometer number	Depth below the pavement surface	Thermometer number	Depth below the pavement surface
I/13	5 mm	II/13	5 mm
I/12	40 mm	II/12	40 mm
I/11	130 mm	II/11	80 mm
I/10	180 mm	II/10	120 mm
I/9	210 mm	II/9	170 mm
		II/8	220 mm

Results of measurements confirm the theoretical assumptions from equation (2). The temperature of pavement surface is related to the air temperature but do not depend only on this temperature (Fig. 1).
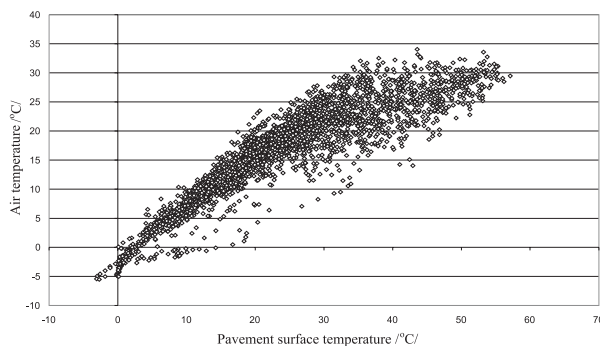

Fig. 1 Relationship between the temperature of air and pavement surface

Other outputs concern the temperature distribution in the pavement structure. It is evident the temperature at the different depths of pavement changes not only during long time period (month, year) but the changes occur within an individual day too and they are significant during hot summer days (Fig. 2). That means the temperature gradients at pavement layers change too and the mean temperature of asphalt layers varies at different hours of a day.

The temperature gradients at the different hours of cold spring and hot summer day are presented in Fig. 3. The similarities of gradients can be stated as:
- relatively small temperature change on the bottom of the lowest asphalt layer in comparison with the temperature changes on the pavement surface;
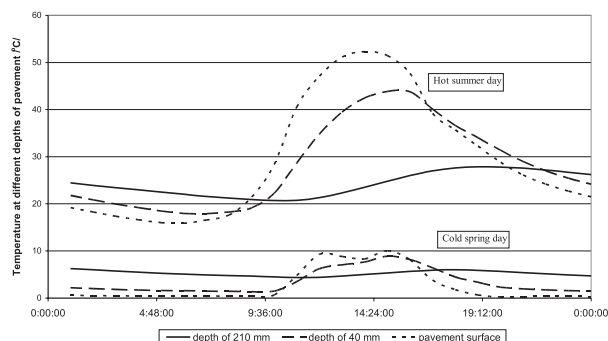
*Fig. 2 Example of the temperature changes
in the asphalt pavement layers*

• steady temperature distribution in the asphalt layers and the approximately equal temperature gradient between the temperature at the top of pavement and at the bottom of the lowest asphalt layer; for the hot summer day it is from 23^{00} to 6^{00} and for the cold spring day from 20^{00} to 9^{00}.

4. Development of the empirical method

For a consideration the experimental measurements the development of the empirical method for the determination of mean temperature of pavement asphalt layers using the air and pavement surface temperature was divided to two main stages regarding the time interval during a day. The first time interval is from 20^{00} to 8^{00} and the second from 8^{00} to 20^{00}. The former is less compli-

cated with the highest temperature at the bottom of the lowest asphalt layer and the lowest temperature at the top of pavement. The similar shape of the temperature gradients aside from the pavement and air temperature is other important fact.
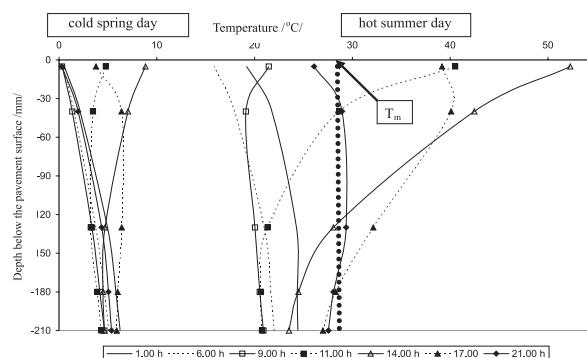

Fig. 3 Example of the temperature gradients in the asphalt layer

The mean temperature of asphalt layers (T_m) was determined for each hour within the time interval from 20^{00} to 8^{00}. As the mean temperature were considered the temperature where the areas between the temperature gradient line and the chosen vertical line (the area on right and left side from the chosen vertical line) were approximately equal (see Fig. 3, thick dotted line, hot summer day, 21.00 h). Then the difference between the pavement surface temperature and the mean asphalt layers temperature were determined. This procedure was carried out for the asphalt layers thickness of 130 mm and of 210 mm (to cover the most frequent

The correction values for the asphalt layers thickness of 210 mm   Table 3

Time interval	The range of pavement surface temperature					
	0 – 5 °C	5 – 10 °C	10 – 15 °C	15 – 20 °C	20 – 25 °C	25 – 30 °C
20:00 – 21:00	Tp + 1 °C		Tp + 2 °C			
21:00 – 22:00						
22:00 – 23:00			Tp + 3 °C			
23:00 – 0:00	Tp + 2 °C					
0:00 – 1:00						
1:00 – 2:00						
2:00 – 3:00						No data available
3:00 – 4:00		Tp + 3 °C		Tp + 4 °C		
4:00 – 5:00						
5:00 – 6:00						
6:00 – 7:00						
7:00 – 8:00					Tp + 2 °C	
Tp - the temperature measured at the top of pavement						

thickness of asphalt layers in pavements). All differences were processed according to the air temperature and the correction values were determined for the both asphalt layers thickness above (table 3). It is evident the pavement surface temperature is lower than the mean asphalt layer temperature and the difference varies according the time interval and the pavement surface temperature. At present the same procedure has been applied for the time interval from 8^{00} to 20^{00}.

5. Conclusions

The temperature of asphalt layers influences their stiffness and response to loading. It is very important to take into account the temperature distribution in the asphalt pavement when pavement bearing capacity is evaluated and to determine the mean temperature of asphalt layers at the moment of diagnostics. The mean asphalt layers temperature depends on the pavement surface temperature, time interval within a day when measurement is carried out, asphalt layers thickness and weather tendency (heating, cooling and settled). The temperature gradients in the asphalt pavements are less complicated during the time interval from 20^{00} to 8^{00} with the highest temperature at the bottom of the lowest asphalt layer the lowest temperature at the top of pavement and the similar shape of the temperature gradients aside from the pavement and air temperature.

The analysis of experimental measurements showed that it is possible to determine the mean temperature of pavement asphalt layers during the time interval from 20^{00} to 8^{00}. The simple method was developed for this purpose using the temperature of pavement surface measured at the moment of pavement bearing capacity diagnostics.

References

[1] TP 01/2004 *Repairs and reconstructions of pavement, Strengthening of asphalt pavements,* Technical provisions, Ministry of Transport, Posts and Telecommunications SR, 2004

[2] TP 02/2006 *Measurement and evaluation of asphalt pavements bearing capacity using FWD,* Technical provisions, Ministry of Transport, Posts and Telecommunications SR, 2006

[3] SOLAIMANIAN, M., KENNEDY, T., W.: *Predicting maximum pavement surface temperature using maximum air temperature and hourly solar radiation,* Transportation Research Record 1417, pp. 1-11, TRB, National Research Council, Washington D.C., 1993

[4] ČOREJ, J., ČELKO, J., TROJANOVÁ, M.: *Water and thermal regime of pavements and rail subgrade (in Slovak),* Chap. 3.2.1, p. 43, VŠDS Žilina, 1994.

Emília Juhásová *

EFFECTS OF STRUCTURAL INTEGRITY ON IMPROVING THE RESISTANCE TO DYNAMIC LOADS

The paper deals with the approaches to the dynamic response analysis when non-linear response of the structure including its partial damage is expected. This concerns the building and other structures executed near transport lines and possibly subjected to seismic effects from transport or earthquakes. Seismic response is here analysed under the action of near field earthquake that was considered and applied as 6DOF seismic input and 2DOF seismic input. A typical reinforced concrete frame with masonry infills was chosen as the prototype for the experimental tests and next analysis. Two storey one bay 1:1 model was tested on a large shaking table with sequentially increasing intensity of seismic input. The specimen was designed according to the rules of Eurocode 8 and the masonry infill was strengthened with horizontal polymer grids placed in prescribed bed joints. The non-linear behaviour is analysed in view of pushover analysis approach and limits of interstorey drift. General behaviour of the analysed frame showed reasonable seismic resistance that was supported by sufficient integrity and limited cracks appearance.

Keywords: space seismic input, near field earthquake, polymer grids, interstorey drift, R/C frame, masonry infills, seismic resistance capacity

1. Introduction

The response spectra approach became a popular tool for the structural seismic response analysis and design. Both advantages and disadvantages of response spectra characteristics are well known, the simplicity of calculations is pushing designers and researchers to utilise the extended related application tools as pushover analysis, non-linear seismic response analysis in time domain, combined with the verification of deformations and stresses. If the deformation and stress states do not conform the safety requirements, the key action is the application of the appropriately chosen additional materials and measures that support the enhanced dynamic resistance of the structure against transport, accidental and/or seismic effects, see e.g. [Anicic et al., 1990], [Colombo and Negro, 2000], [Paulay and Priestley, 1992].

Structures in seismic regions shall be designed and constructed in such a way that two basic requirements are met, each with an adequate degree of reliability. This concerns the no-collapse requirement and damage limitation requirement (EN 1998-1: 2004).

To meet the *no-collapse requirement*, the structure shall be designed and constructed to withstand the design seismic action without local or global collapse, thus retaining its structural integrity and a residual load bearing capacity after a seismic event. The design seismic action is expressed in terms of the reference seismic action associated with a reference probability of exceedance P_{NCR}, in 50 years (usually 10%) or a reference return period T_{NCR} (usually 475 years) and completed with importance factor of an analysed structure.

To meet the *damage limitation* requirement the structure shall be designed and constructed to withstand a seismic action having a larger probability of occurrence than the design seismic action, without the occurrence of damage and the associated limitations of use, the costs of which would be disproportionately high in comparison with the costs of the structure itself. The seismic action to be taken into account has a probability of exceedance P_{DLR} in 10 years (usually 10%) and a return period T_{DLR} (usually 95 years).

Since the seismic performance of a structure is largely dependent on the behaviour of its critical regions or elements, the detailing of the structure in general and of these regions or elements in particular, shall be such as to maintain the capacity to transmit the necessary forces and to dissipate energy under cyclic conditions. The resistance and energy-dissipation capacity to be assigned to the structure are related to the extent to which its non-linear response is to be exploited [Juhásová, 1991], [Hájek, 1994].

The tested and analysed R/C frame model was subjected to the sequence of seismic inputs with increasing intensity of acting seismic motion. The near field earthquake record was used as a base for shaking table tests.

2. Properties of applied near field earthquake motion

The near field earthquakes are characterised by short duration, large initial amplitude of acceleration and higher vertical component that is equal or higher than horizontal ones. The applied

---

* Emília Juhásová
Institute of Construction and Architecture Slovak Academy of Sciences, Dúbravská cesta 9, 845 03 Bratislava, Slovakia, E-mail:usarjuha@savba.sk

seismic input used time history of near field earthquake recorded at Nocera during the Central Italy 1997 Umbria earthquake. This record contains high amplitudes of accelerations (nearly 0.5 g in each direction). It was recorded at a distance about 11 km from the epicentre. The magnitude $Mw = 6.0$. The general features of this record show that the large amount of energy comes during the first 5–6 sec. The original record lasted 45 sec, but for tests and analysis purposes it was sufficient to consider the length of 25 sec. The applied time histories of input accelerations and displacements include also calculated rotations roll, pitch, yaw, see Figs. 1 and 2 [Juhásová et al., 2000, 2004]. The response spectra for damping 2% and 5% are in Figs. 3 and 4.

In general, an actual seismic ground motion is interconnected with wave fields that consist of components of different frequencies and waves lengths. Some structures might be sensitive to spatial varying vertical excitation; a vertical ground motion propagating in any horizontal direction is expected to promote a rocking of the structure, concurrent with the rocking provided by the horizontal excitation along that direction. The contribution of horizontal ground motions to torsion seismic input either increases the torsion response of asymm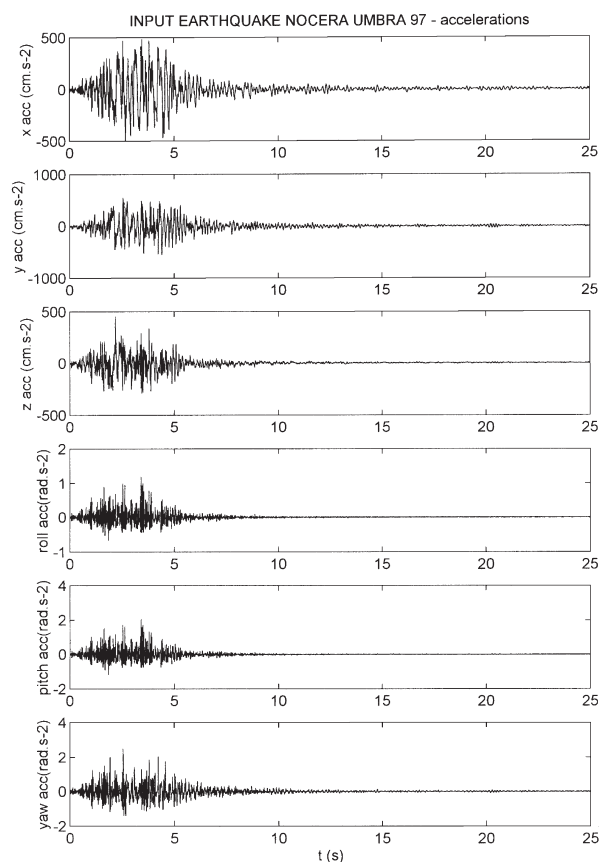etrical structures or creates torsion response in case of symmetrical structures. The rotation input acting at the ground level arrives with a phase shift in relation to respective translate input. Both time histories and response spectra are influenced by this phase shift and the frequency value. The calculated rotation input time histories could be used in those cases when no direct information about rotation seismic motion of the ground exists. However, lately new sensors and instruments of different type were developed for direct measurement of rotation motions. This represents the promise for the future in the form of actual rotation seismic motions recorded during a seismic event [Juhásová, 1999, 2004].
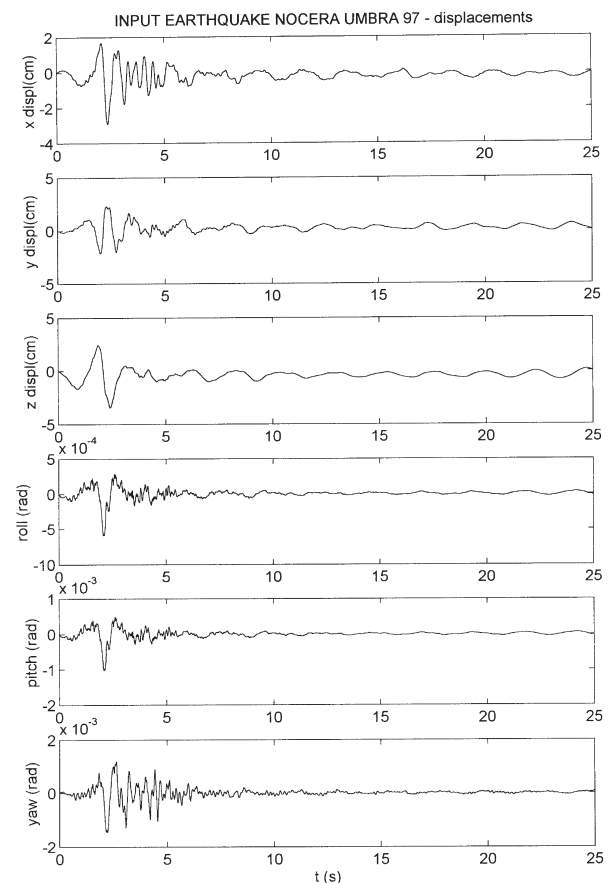

Fig. 2 Displacement and rotation time histories related to Umbria, Italy 1997 earthquake, Nocera record, dt = 0.005 s; used as the seismic input for shaking table tests

3. Full scale reinforced concrete frame specimen tested on the shaking table

More realistic data on the behaviour of R/C frame structures can be obtained on actual structures or on large scale models. A large 1:1 R/C one bay two storey frame model with solid brick masonry infills was tested on the shaking table. The seismic loading was introduced in the sequence of increasing intensity modelled through the input specified in Figs. 1 to 4. The frame system was
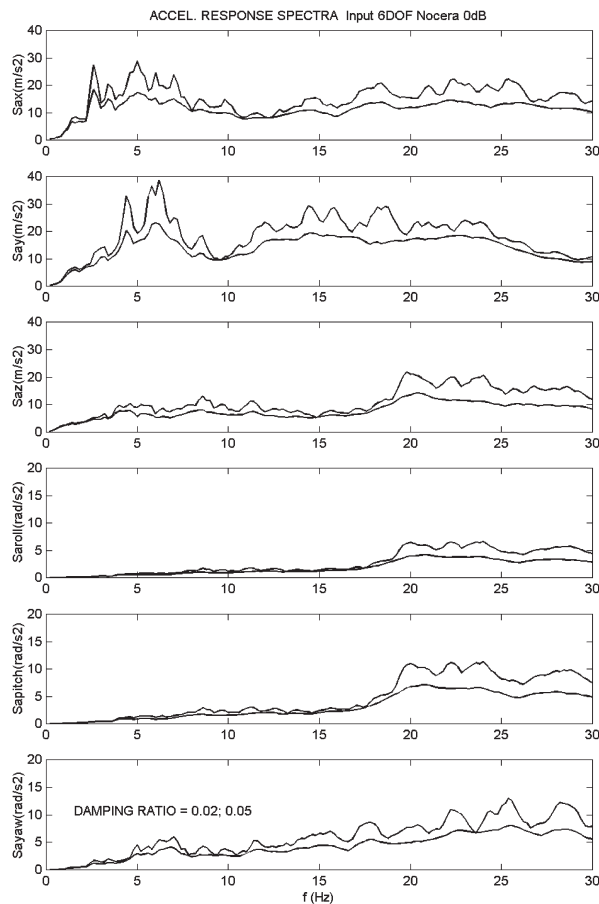

Fig. 1 Translate and rotation acceleration time histories related to Umbria, Italy 1997 earthquake, Nocera record, dt = 0.005 s; used as the seismic input for shaking table tests

Fig. 3 Acceleration response spectra of Nocera 1997 seismic input
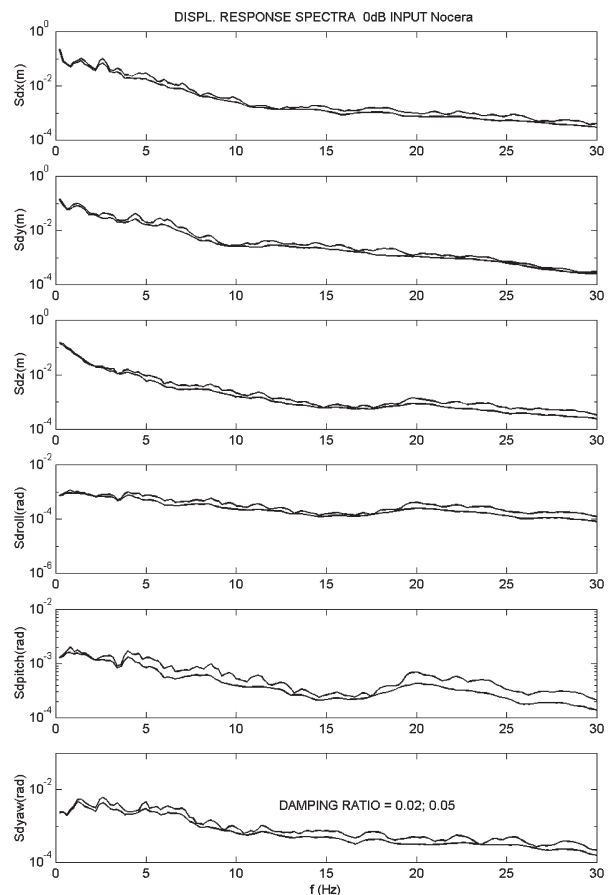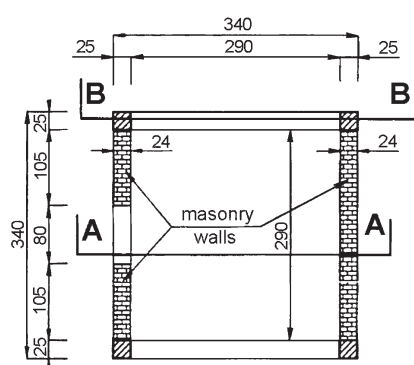

Fig. 4 Displacement response spectra of Nocera 1997 seismic input
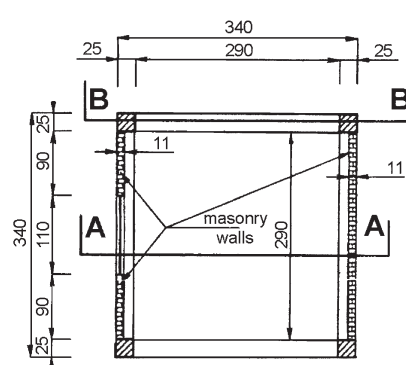
SECTION FIRST FLOOR

SECTION SECOND FLOOR

Fig. 5 R/C frame model with masonry infills – horizontal sections

designed according to the rules of Eurocode 8 with doubled stirrups. The dimensions of the model and its reinforcement are given in Figs. 5 to 7.

The model was constructed as symmetrical in *y* direction and asymmetrical in *x* direction. Its dimensions in plan were 3.5 ×

× 3.5 m, height was 5.9 m. R/C columns were of square cross section 0.25 × 0.25 m, girders 0.25 × 0.30 m, floor slabs were 10 cm thick. Two opposite masonry walls were constructed from solid bricks of thickness 24 cm in the first storey and 11 cm in the second storey. The front wall had a door in the first storey and a window in a second storey, the back wall was full. Lime-cement
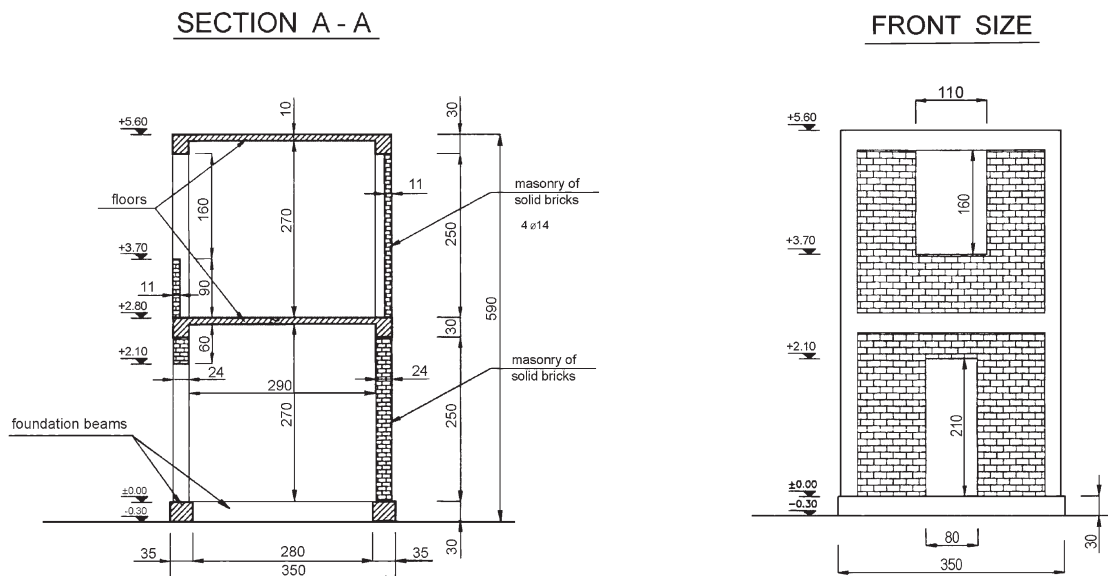
SECTION A - A

FRONT SIZE

Fig. 6 R/C frame model with masonry infills – vertical section and front elevation

SECTION B - B

SECTION C-C
C1, 2, 3, 4

8 ⌀14
Stirrups ⌀ 6/10 (15) L = 98
Stirrups ⌀ 6/10 (15) L = 74
hcr (0.60 cm) Stirrups ⌀ 6/10
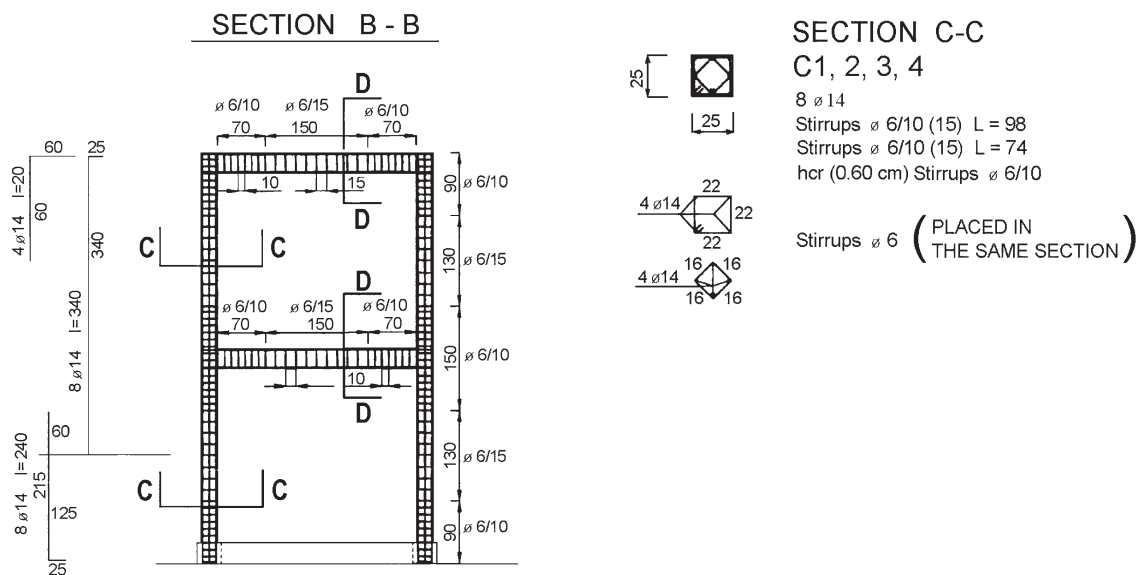
Stirrups ⌀ 6 (PLACED IN THE SAME SECTION)

Fig. 7 R/C frame model with masonry infills – steel reinforcement

mortar was used in masonry together with polymer grid Tensar SS20 reinforcement in horizontal bed joints, applied in each fifth row. The polymer grids, with slender ribs and solid integrated joints, inserted in the bed layers are uniformly distributing the tensile stresses and by the sandwich effect any stress concentration is prevented. The polymer grids are effective prevailingly in tension and to some degree in shear [Sofronie et al., 2003], [Bairrao et al., 2006]. 64 channel data acquisition system was used to follow accelerations, strains and displacements in appropriately chosen points. The registration of data ran continuously in time with sampling frequency 200 Hz. The view of model with position of sensors is in Fig. 8.

4. Procedure of test and main test results

The tests comprised impact tests, sweep sine tests and earthquake like x, y, z, θx, θy and θz common excitation with increasing intensity of seismic input [Juhásová, 1999, 2004]. However, the short duration of strong earthquake phase did not allow to develop low cycle fatigue like behaviour with development of hysteresis loops in critical sections of a system. The strength in critical points was decisive and redistribution of stresses during the response was affected both by input and natural modes of vibration. Table 1 gives the schedule of applied test steps.
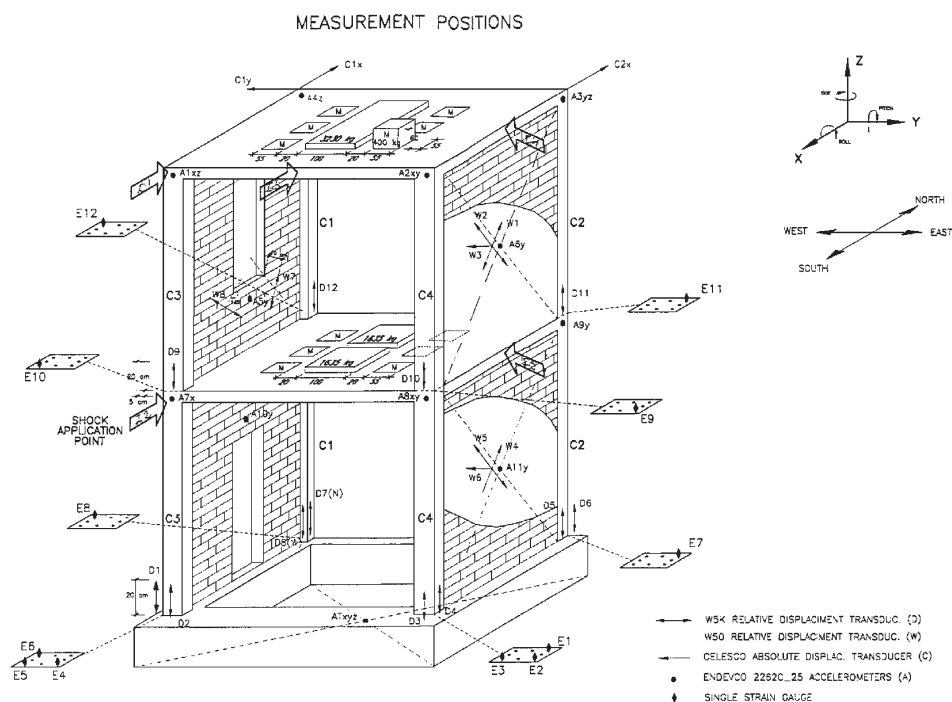
MEASUREMENT POSITIONS

Fig. 8 Position of sensors on tested R/C frame with masonry infills

Review of applied test steps – R/C frame with masonry infills   Table 1

Test No.	Loading	max aTx (g)	max aTy (g)	max aTz (g)	Test No.	Loading	max aTx (g)	max aTy (g)	max aTz (g)
T1	Impact I1, table down	–	–	–	T18	seis. -6dB 6DOF	–	–	–
T2	Impact I2, table down	–	–	–	T19	seis. -3dB 6DOF	0.567	0.585	0.407
T3	Impact I3, table down	–	–	–	T20	seis. 0dB 6DOF	0.867	0.797	0.706
T4	Impact I4, table down	–	–	–	T21	seis. 2dB(e) 6DOF	0.087	0.103	0.095
T5	Impact I5, table down	–	–	–	T22	seis. 2dB r 6DOF	0.945	0.986	1.156
T6	sweep sine x	–	–	–	T23	seis. 3dB 6DOF	1.124	1.063	0.932
T7	sweep sine x	0.0114	0.0084	0.0051	T24	seis. 3dB r 6DOF	0.990	1.142	0.518
T8	sweep sine y	0.0039	0.0112	0.0018	T25	seis. 4dB 6DOF	1.132	1.270	0.600
T9	Impact I3 table up	–	–	–	T26	seis. 0dB 2DOF	0.693	0.068	0.356
T10	Impact I3 table up	–	–	–	T27	seis. 5dB 2DOF	–	–	–
T11	Impact I3 table down	–	–	–	T28	seis. 6dB 2DOF	1.0732	0.132	0.845
T12	sweep sine z	0.0086	0.0154	0.0118	T29	seis. 7dB 2DOF	–	–	–
T13	seis. -18dB 6DOF	–	–	–	T30	seis. 8dB 2DOF	2.412	0.144	1.147
T14	seis. -15dB 6DOF	–	–	–	T31	sweep sine x	0.0118	0.0014	0.0014
T15	seis. -18dB 6DOF	–	–	–	T32	sweep sine y	0.0018	0.0112	0.0020
T16	seis. -12dB 6DOF	–	–	–	T33	sweep sine z	0.0059	0.0098	0.0122
T17	seis. -9dB 6DOF	–	–	–					

The impact loading was applied in appropriately chosen points denoted in Fig. 8 by I1, I2, I3, I4 and I5. 6DOF seismic input was introduced during the tests T19 to T25. Next tests T26 to T30 introduced only 2DOF seismic input (x + pitch), thus securing the higher excitation in the direction of infill walls. Representative data from tests are in Tables 2 to 4.

Measured and recalculated natural frequencies
of tested R/C frame with masonry infills
Table 2

Natural frequencies (Hz)	$(x-\theta)_1$	$(x-\theta)_2$	$(\theta-x)_1$	$(\theta-x)_2$	y_1	y_2
Impact(1) table down	8.3	27	13.1	37	3.5	10.3
Impact(2) table up	12.0	27.5				
Sweep sine x	11.4	24.4	12.8	37?	2.9	9
Sweep sine y					2.75	9
Seismic Test 19	4.78		6.24	9.76	2.70	7.18
FEMA 273 Test 19 ini	4.41				2.35	
FEMA 273 Test 25 aft.	3.92				1.80	
Sweep sine x after Test 30	2.46	7.44	5.39	8.24		
Sweep sine y after Test 30					1.62	5.68
Total mass = 31.46 tons						

On the basis of the obtained experimental results it is worth to pick up following observations:

a) The experimental dynamic identification of the model was successfully completed. The impact and sweep sine tests served directly for dynamic identification purposes. The seismic tests enable to recognize the response and damage development. With increasing intensity of test the R/C frame and masonry stiffness were decreasing. Sweep sine test in z-direction gave the floor slabs natural frequencies of values 17 Hz for second storey and 19 Hz for the first storey.

b) The structural system is symmetrical in y-direction, where both natural frequencies were clearly identified. In x direction the asymmetry of infills exists and coupled vibration $x-\theta$ was identified as expected. Next contribution came from boundary conditions. There exists evident difference between the impact tests in the case of shaking table down – in parking position and in operating – up position of the shaking table. With increasing seismic input the natural frequencies were decreasing. At a low level of excitation the damping was very low. Especially in y-direction the damping ratio reached during sweep sine test only 1.5 – 2.0 %. However, it was increasing at a higher seismic input and due to the effect of partial damage.

c) The asymmetrical structure with a symmetrical reinforced concrete frame showed a considerable contribution of reinforced infill masonry to the total stiffness and strength. Having general earthquake like 6DOF seismic input, the yielding appeared firstly in the steel reinforcement of columns and it was followed by separation in the upper horizontal and vertical connections between the frame and infill masonry. The result of this process aimed at separate cantilever like vibration of left masonry panel in the second storey of the model. It should be expected that during the longer stage of extreme seismic input the out of plane failure of masonry would appear as the first one. The view of cracks in and near R/C frame joints can be seen in Figs. 9 to 11. Fig. 12 presents the cracks in masonry walls at the end of the tests (after T30). Actually, the introduced seismic excitation is considerably above the levels of seismic inputs usually expected during the seismic events.

The obtained results suggest that the applied technique provided the system with higher seismic resistance with uniformly distributed seismic capacity through the structure since the beginning of the model failure.

The interstorey drift is another characteristic that should be treated in relation to the non-collapse and damage limitation requirements (see e.g. EN 1998-1: 2004). The values of this characteristic are in Table 4, as they were recalculated from the experimental data. For reference points position 1, 2, 3, 7, 8, 9, see Fig. 8.

For the non-collapse requirement the second-order effects ($P-\Delta$ effects) need not be taken into account if the following condition is fulfilled in all the storeys:

$$\delta = \frac{P_{tot}\, d_r}{V_{tot}\, h} \le 0.10 \qquad (1)$$

where
δ is the interstorey drift sensitivity coefficient;
P_{tot} is the total gravity load at and above the storey considered in the seismic design situation;
d_r is the design interstorey drift, evaluated as the difference of the average lateral displacements ds at the top and bottom of the storey;
V_{tot} is the total seismic storey shear; and
h is the interstorey height.

Chosen measured extremes in seismic response of the tested specimen
Table 3

Test N.	Input (dB)	Input (DOF)	Milistrains (steel)	Relative deflections (concrete) (mm) reference length = 200mm
19	−3 dB	6DOF	$E1 = 1.37$;	D1 = 0.26 mm; D4 = 0.27 mm
20	0 dB	6DOF	$E1 > 2$; $E1res = 1.48$;	D1 = 0.59 mm; D4 = 0.33 mm
21	2 dB	6DOF	$E1 > 4 - broken$; $E7 > 5$; $E7res = 3.9$;	D4 = 2.13 mm;
22	2 dB rep.	6DOF	$E7 = 11.9$; $E7res = 7.6$; $E2 = 4$; $E2res = 0.8$;	D4 = 2.2 mm;
25	4 dB	6DOF	$E6 = 6.3$; $E6res = 1.9$;	D5 = 2.1 mm; D8 = 2 mm;
30	8 dB	2DOF	–	D11 = 1.6 mm;

Reached interstorey drifts during chosen shaking table tests   Table 4

Test 19, max aTx = 0.57 g, 6DOF; h_s = 2.8 m				Test 19, max aTy = 0.58g, 6DOF; h_s = 2.8 m			
$\Delta 1-7x$	$\Delta 2-8x$	$\Delta 7-Tx$	$\Delta 8-Tx$	$\Delta 2-8y$	$\Delta 3-9y$	$\Delta 8-Ty$	$\Delta 9-Ty$
9.32 mm	7.41 mm	9.89 mm	5.38 mm	13.85 mm	13.74 mm	14.65 mm	19.77 mm
0.33 %	0.26 %	0.35 %	0.19 %	0.49 %	0.49 %	0.52 %	0.71 %
Test 25, max aTx = 1.13 g, 6DOF; h_s = 2.8 m				Test 25, max aTy = 1.27 g, 6DOF; h_s = 2.8 m			
$\Delta 1-7x$	$\Delta 2-8x$	$\Delta 7-Tx$	$\Delta 8-Tx$	$\Delta 2-8y$	$\Delta 3-9y$	$\Delta 8-Ty$	$\Delta 9-Ty$
20.89 mm	23.65 mm	17.25 mm	15.40 mm	51.03 mm	43.42 mm	53.47 mm	45.39 mm
0.75 %	0.84 %	0.62 %	0.55 %	1.82 %	1.55 %	1.91 %	1.62 %
Test 30, max aTx = 2.41 g, 2DOF; h_s = 2.8 m				Test 30, max aTy = 0.14 g, 2DOF; h_s = 2.8 m			
$\Delta 1-7x$	$\Delta 2-8x$	$\Delta 7-Tx$	$\Delta 8-Tx$	$\Delta 2-8y$	$\Delta 3-9y$	$\Delta 8-Ty$	$\Delta 9-Ty$
51.05 mm	38.61 mm	32.88 mm	31.65 mm	11.79 mm	8.02 mm	9.48 mm	7.70 mm
1.82 %	1.38 %	1.17 %	1.13 %	0.42 %	0.29 %	0.34 %	0.27 %

The values of δ determined from the experiment maximum drifts in the first storey are:

for y-direction: $\delta = 31.46 \times 9.81 \times 0.05347/(180 \times 2.8) = 0.0327$;
for x-direction: $\delta = 31.46 \times 9.81 \times 0.05105/(340 \times 2.8) = 0.0165$,
which are lower than the limit in Eq. (1).

Thus, the values from Table 4 and Fig. 16 suggest that for similar low R/C frame structures (as represented by the tested specimen) the second order effects need not be taken into account.

The damage limitation requirement prescribes the limits of interstorey drift as follows:
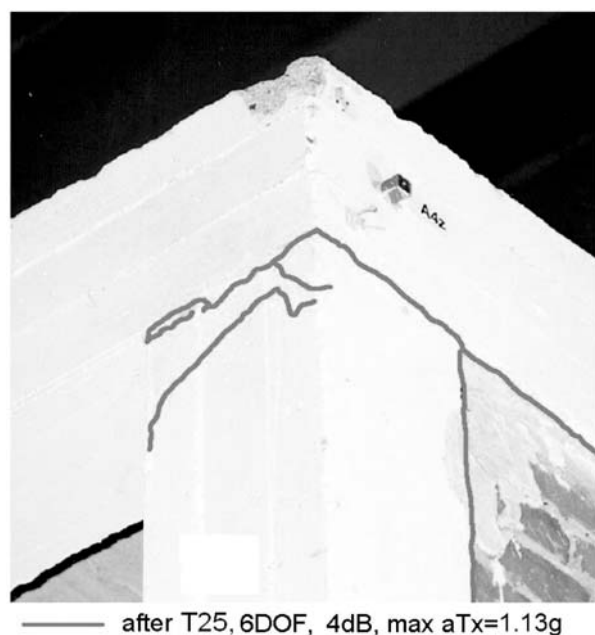
$$d_r v \le 0.010h \qquad (2)$$

provided that the non-structural elements are fixed in a way so as not to interfere with structural deformations, or there are no non-structural elements.

Taking the value $v = 0.5$ and the largest reached value of d_r, there is for y-direction:

$$0.05347 \times 0.5/2.8 = 0.0095 < 0.01$$

which suggests that the first storey drifts remained just below the limit value.

after T25, 6DOF, 4dB, max aTx=1.13g

*Fig. 9 Cracks in critical sections of R/C frame at the end of test
– top of the frame*

– – – – after T19, 6DOF, -3dB, max aTx=0.57g
───── after T25, 6DOF, 4dB, max aTx=1.13g
─ · ─ · after T30, 2DOF (x + pitch), 8dB, max aTx=2.41g

*Fig. 10 Cracks in critical sections of R/C frame at the end of test
– frame joint at the first floor*

--- --- after T19, 6DOF, -3dB, max aTx=0.57g
——— after T25, 6DOF, 4dB, max aTx=1.13g

Fig. 11 Cracks in critical sections of R/C frame at the end of test – frame joint at the base
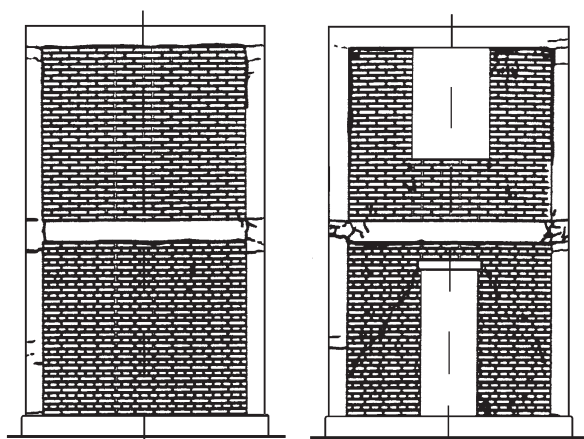

Fig. 12 Cracks in masonry at the end of test: left – solid wall; right – wall with openings

5. Using of pushover approach in the test data analysis

The pushover analysis applies the static non-linear analysis for determining the dependence between the base shear force and control displacement of a structure. The control displacement may be taken at the centre of mass of the roof of the building (see EN 1998-1: 2004 or FEMA 273: 1997). The lateral load is considered like distributed in the first modal shape. A similar approach can be applied in the test data analysis. Having in mind the inertial forces acting during the seismic response, distribution of masses and data about response acceleration and displacement, experimental control parameters could be determined for different states of the speci-

men during execution of seismic tests. Tests T19, T25 and T30 were the subject of such analysis.

Accelerations were measured in points as shown in Figure 8. The allocation of concentrated masses to sensor points at the floor levels and respective horizontal direction follows the known rule used for calculation of concentrated masses for multi mass dynamic models. The relations between seismic input and maximum absolute acceleration in *x* and *y* directions indicate the non-linear response effects (Figure 13). Similar charts for relations between seismic input and maximum relative displacement are in Figure 14.

The relation between the control displacement (roof horizontal displacement) and the base shear can be calculated on the basis of a built analytical model, using changes in non-linear stiffness, e.g. according to FEMA 273 or EN 1998-1, see Fig. 15.

Actual relation between the mean top relative displacement of the tested specimen and the base shear force is given in Figure 16. Such development of the base shear is interconnected with the reached maximum strains in critical sections and reached inter-storey drifts, see Tables 3 and 4. Fig. 16 illustrates the clear distinction between the base shear force capacity in *y*-direction (the resistance is mobilised only by R/C frame) and in *x*-direction (the resistance is mobilised both by R/C frame and masonry infills supported by horizontal polymer grids).

The test T25 significantly participated in the softening of a system, the crack widths, strains, the increasing and deterioration of the frame and masonry. However, polymer grids in bed joints supported the integrity of a system and prevented it from a significant damage. Even if these grids are locally fixed to the R/C frame, the system exhibits reasonable behaviour under higher near field seismic inputs. Reference changes of natural frequencies with the use of Figs. 15 and 16 and rules of FEMA 273 are in Table 1, giving a reasonable agreement with the measured values.
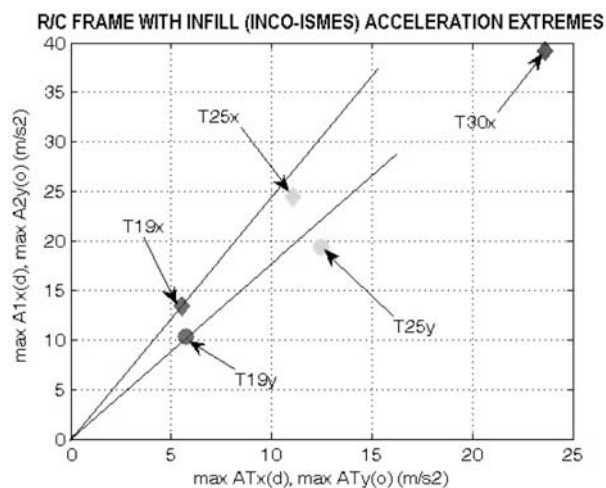

Fig. 13 Absolute accelerations at the top of frame versus seismic input (Tests 19, 25, 30)

It should be mentioned that the lower bound of yield stress of used steel rebars was 490 MPa, the yield strain was above 50 milistrain and strength was 590 MPa with ductility of 150 milistrain. The compression strength of concrete was 30 MPa. Considering these data and strain in tension rebars of value 10 milistrain, the theory for concrete column resistance gives the calculated value of base shear 186 kN for *y*-direction and test T25. The agreement with Fig. 16 and inertial forces is evident.
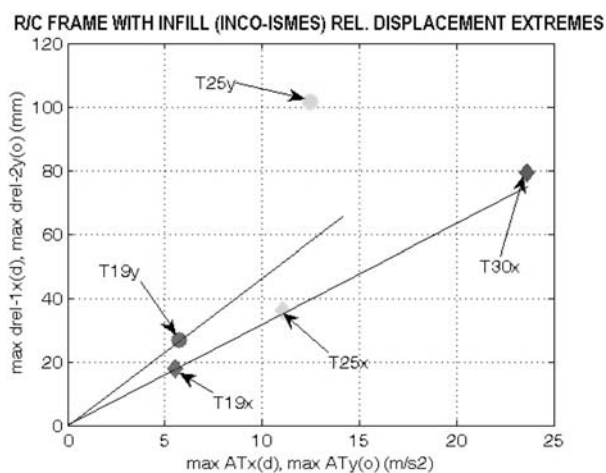

Fig. 14 Relative displacements at the top of frame versus seismic input
(Tests 19, 25, 30)
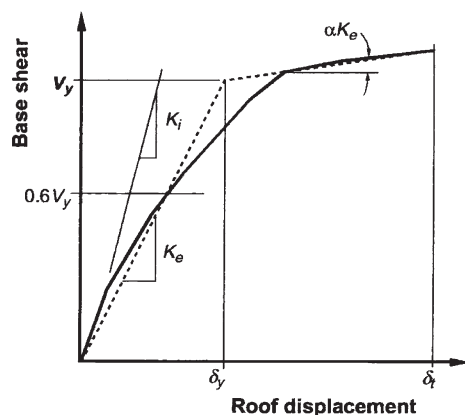
Fig. 15 FEMA 273 dependences between top displacement and base shear for pushover analysis

6. Conclusions

The tests of a full scale model on a large shaking table were realised using the original, appropriately modeled 6DOF seismic input based on actual strong earthquake. The numerous obtained data describe redistribution of seismic resistance between R/C frame, masonry infills, boundary joints and the polymer grid reinforcement in the masonry infills.
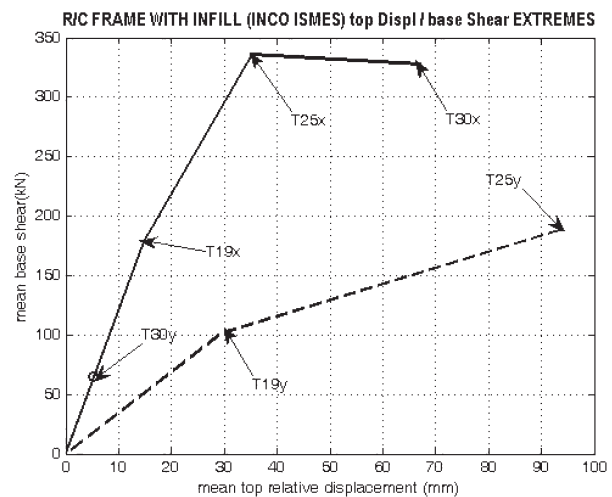
Fig. 16 Relations between the top relative displacements and base shear of tested frame (Tests 19, 25, 30)

The space seismic response differs from the plane one. Therefore, both the structural model and inputs should be built in a space mode. Such an approach implies changes in natural frequencies and modes of vibration. Different positions of initiative failure regions should be expected in relation to the used structural model and inputs.

The necessity of the continuous control of seismic resistance capacity in critical parts of the structure should be emphasised. Simultaneously, the appropriate changes should be introduced into the structural model depending on the degree of its non-linear behaviour. The verifications of stresses in critical parts give the answer whether the design is sufficient or should be modified. The described case study proved that it is possible to reach such a combination of the reinforced frame with infill masonry walls which gives nearly uniform seismic resistance capacity and remarkable contribution of infills to total seismic resistance of structure.

The tools which are used in response analysis and the knowledge from experimental research should be reasonably applied to improve the structure resistance capabilities. If ductility is supposed to be beneficial, the cracks can be accepted provided that neither loss of structure integrity nor instability can appear. The proper detailing and the appropriate measures for increasing the total resistance capacity are the key design and execution activities in construction industry. The described technology underlines an integrity role in the increase and securing dynamic resistance capacity. To this end, not only safety aspects in case of natural or terrorist hazards, but also protection against undesirable transport effects and settlements can be reasonably and conveniently solved.

References

[1] ANIČIĆ, D., FAJFAR, P., PETROVIĆ, B., SZAVITS-NOSSAN, A. and TOMAŽEVIĆ, M. (1990), *Earthquake Engineering*, Gradevinska knjiga, Beograd.

[2] BAIRRAO, R., FALCAO SILVA, MJ., JUHÁSOVÁ, E., CAMPOS COSTA, A., COELHO, E. (2006), Shaking table tests of an asymmetrical limestone building. *Proceedings of the 1st European Conference on Earthquake Engineering and Seismology,* Geneva, Switzerland, Sept. 3–8, 2006; p. 636/1–10.

[3] COLOMBO A., NEGRO P. (2000), Advanced materials for strengthening, rehabilitation and repair of structures. Experimental activities at ELSA, In: *Mitigation of Seismic Risk Support to Recently Affected European Countries,* Proc. of Workshop held in Belgirate, Italy in 27–28 Nov. 2000, JRC EC Ispra, 2000; p. 5/1–7.

[4] Eurocode 8, EN 1998-1: 2004, *Design of Structures for Earthquake Resistance.* Part 1. General Rules, Seismic Actions and Rules for Buildings, CEN, Brussels.

[5] FEMA 273: 1997, NEHRP *Guidelines for the Seismic Rehabilitation of Buildings.* BSSC, Washington, October 1997.

[6] HÁJEK, J. (1994), *Deformations of Concrete Structures.* VEDA, Bratislava.

[7] JUHÁSOVÁ, E. (1991), *Seismic Effects on Structures.* Elsevier, Amsterdam.

[8] JUHÁSOVÁ, E. (1999), Seismic effects on R.C. frames with infills including torsion input, *Structural Dynamics, Eurodyn '99*, 1999, Praha, Balkema, Rotterdam, p. 1147–1152.

[9] JUHÁSOVÁ, E. (2004), Effect of structural integrity in improving the resistance to dynamic loads – some studies. *Journal of Struct. Engng.*, India, Vol. 31, No. 1, p. 65–72.

[10] JUHÁSOVÁ, E., SOFRONIE, R, CONTRI, P. (2000), Real time testing of reinforced infills. In: *Proceedings of 12WCEE Auckland* 27, Jan. – 3, Feb. 2000, p. 921/1–8.

[11] JUHÁSOVÁ, E., SOFRONIE, R., JUHÁS, M. (2004), The key role of structure integrity and new materials. *Proceedings of the Conference Building for European Future,* Maastricht, October 14–15, 2004, ECCREDI, Brussels, Vol. 1, p. 527–544.

[12] PAULAY, T., PRIESTLEY, M.J.N. (1992), *Seismic Design of Reinforced Concrete and Masonry Buildings.* John Wiley & Sons, New York.

[13] SOFRONIE R., JUHÁSOVÁ E. , GREENING P. (2003), Seismic strengthening of masonry, *SECED Newsletter,* Vol. 16, No. 4, May 2003, p. 6–7.

Ján Bujňák – Kazimierz Furtak *

RESEARCH ON SHEAR CONNECTION DESIGN IN COMPOSITE BEAMS

The paper deals with a way of determining concrete pressure strength when calculating load carrying capacity of steel perfobond strip connectors. This type of strip connectors has been used in composite bridges only recently and no precise methods of calculating them have been worked out so far. The effect of axial forces on bearing capacity of classical stud shear connectors is also given in the paper as a result of research.

1. Introduction

There is no explicit definition of concrete pressure strength because there are no standard principles of defining this strength. This is why it may be difficult to adopt design values for particular classes of concrete in actual engineering practice. Moreover, the experimental investigations in this field are done on different samples for different areas of pressure. Hence, significant discrepancies exist in the propositions by various authors, and even norm values.

The stud connector's behaviour depends not only on their bearing and shear resistance. The axial forces may modify importantly the ultimate load bearing capacity. The effect of this action is also given in the paper as a result of research.

2. Test elements and research methodology

In case of perfobond strip connectors, there are special conditions of concrete pressure. It is a pressure of two cylindrical surfaces of small dimensions. The strips thickness range can be from $t = 12$ mm to 20 mm, and the diameter of holes is from $\Phi = 30$ mm to 40 mm.

Moreover, the distribution of pressure stress on the concrete-strip contact area differs in comparison to classical cases. It can be assumed to be close to the one adopted by Hertz's formulae. However, these formulae cannot be adopted for calculating $\bar{f}_{end}$ because of significant non-homogeneity of concrete and big differences between mechanical characteristics of aggregate and cement set. Moreover, the relatively thin steel strip acts on concrete like a wedge.

Due to the specific character of problems of concrete pressure in perforated strips, the only solution seems to be experimental investigations. They are recommendable also because of the limited range of values of the essential parameters, i.e. strip thickness, hole diameters and concrete class.

The sizes of the elements used in tests are shown in Fig. 1. The elements were cubes of a side $a = 150$ mm, with an additional bulge in the shape of a half-round of diameter matching the diameter of the holes in the perforated strips used in steel-concrete composite structures. The pressure force has been transferred by a steel element with a half-round of the same diameter as the bulge on the concrete cube and the thickness corresponding to the thickness of the strip.
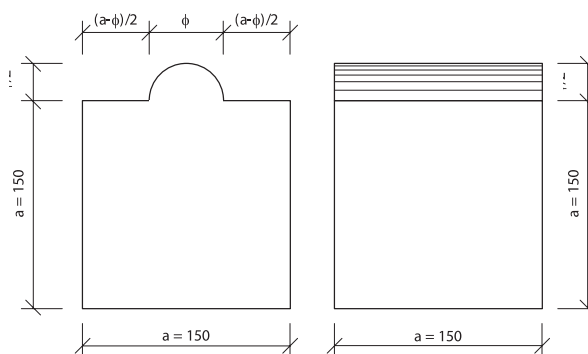

Fig. 1 Shape and dimensions of test samples

For the adopted shape of the test elements, concrete ultimate pressure strength was obtained, which can be used directly in calculating perfobonds load carrying capacity. To this aim, the following test parameters were adopted: thickness of perfobonds, diameters of holes and concrete class.

Three classes of concrete were used: C30/37, C40/50 and C50/80 with three diameters of holes: $\Phi = 20$, 30 and 40 mm and

* **Ján Bujňák[1], Kazimierz Furtak[2]**
[1]Faculty of Civil Engineering, University of Žilina. Komenského 52, 010 26 Žilina, Slovakia. E-mail: bujnak@fstav.uniza.sk
[2]Department of Bridges and Tunnels Building, Faculty of Civil Engineering, Cracow University of Technology. Warszawska 24, 31155 Cracow, Poland

three thickness of the strips: t = 12, 16 and 20 mm. The basic parameters used were: the concrete class C40/50, the diameter of a hole Φ = 30 mm and the strip thickness t = 16 mm. As a total, the 114 elements have been examined.

The tests were run on a standard testing machine. The rate of loading was 0.4 MPa.s^{-1}, the given stress was calculated by dividing the pressure force by the product of strip thickness and hole diameter. The tests elements were stored in normal laboratory conditions.

3. Test results and their analysis

The tests of strength characteristics of the concrete from which the test elements were made had provided the following values of concrete mean compressive strength $\bar{f}_c$ and tensile strength $\bar{f}_t$:

- Concrete class C30/37: $\bar{f}_c$ = 34.80 MPa $\bar{f}_t$ = 2.36 MPa,
- Concrete class C40/50: $\bar{f}_c$ = 45.96 MPa $\bar{f}_t$ = 3.08 MPa,
- Concrete class C50/80: $\bar{f}_c$ = 61,10 MPa $\bar{f}_t$ = 4.10 MPa.

The concrete compressive and tensile strength for splitting were determined on cubes of sides of 150 mm. For strength characteristics tests ($\bar{f}_c$, $\bar{f}_t$), each series have contained six elements. The tests were done in a standard way. The cubes for $\bar{f}_c$ and $\bar{f}_t$ were stored in natural conditions, similarly as samples for compressive tests.

The results of the compressive tests are shown in Figs 2 to 5. Fig. 2 illustrates the effect of strip thickness for different concrete classes, while Fig. 3 the effect of diameter of holes. As it can be clearly seen, there is a strong decreasing tendency of compressive strength $\bar{f}_{cud}$ with the increase of strip thickness and hole diameters. The approximately linear change of concrete strength $\bar{f}_{cud}$ dependence on t and Φ is worth to underline.

For design purpose, it is much more useful to have concrete compressive strength $\bar{f}_{cud}$ as a function of the pressure area A_p = $t \cdot \Phi$. This pressure can be defined as a product of the strip thickness t and the diameter of holes Φ. This is a simplification due to adopted assumption of the mean values of stresses. In reality, the distribution of stresses on the pressure semi-perimeter is quite variable, especially in the case of homogeneous materials.

The effect of pressure area A_p on concrete strength $\bar{f}_{cud}$ is illustrated in Fig. 4. The dependence is clearly non-linear and may be well approximated by a logarithmic function. Generally, with the larger pressure area the lower $\bar{f}_{cud}$ strength results. However, it should be noted that the decrease of pressure strength in real practical ranges of pressure area is even doubled.

Fig. 5 shows the dependence of the concrete pressure strength $\bar{f}_{cud}$ on its class (represented by compressive strength $\bar{f}_c$) and pressure area A_p.

The results of experimental investigations illustrated in Figures 2 to 5 are an arithmetic mean obtained from the whole series of 3

$$\bar{f}_{cud} = -26.4737 \cdot t + 781.5$$
$$\bar{f}_{cud} = -12.7838 \cdot t + 475.043$$
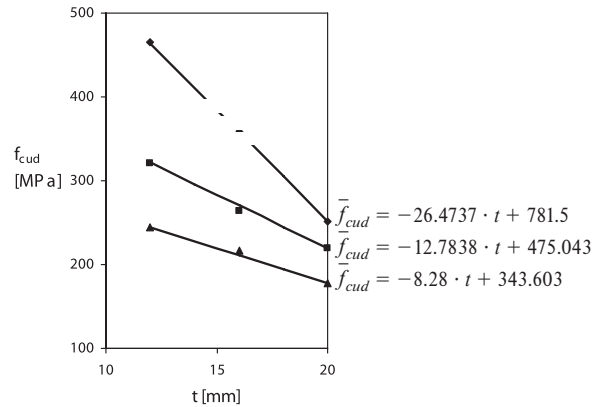$$\bar{f}_{cud} = -8.28 \cdot t + 343.603$$

Fig. 2 Effect of strip thickness on pressure strength of concrete class C40/50

to 6 elements. The figures show approximation curves, which can be used for determining concrete pressure strength when designing perforated strips in composite structures.
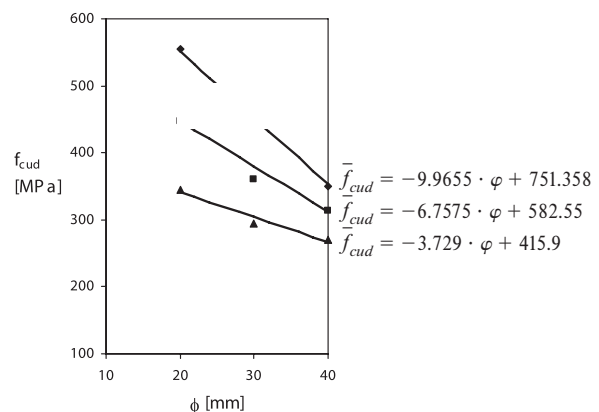

$$\bar{f}_{cud} = -9.9655 \cdot \varphi + 751.358$$
$$\bar{f}_{cud} = -6.7575 \cdot \varphi + 582.55$$
$$\bar{f}_{cud} = -3.729 \cdot \varphi + 415.9$$

Fig. 3 Effect of hole diameter on pressure strength of concrete class B40

$$\bar{f}_{cud} = -228.655 \cdot \ln(A_p) + 1776.52$$
$$\bar{f}_{cud} = -224.41 \cdot \ln(A_p) + 1651.7$$
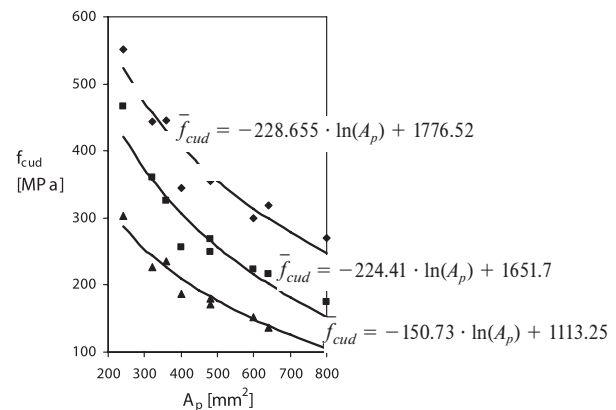$$\bar{f}_{cud} = -150.73 \cdot \ln(A_p) + 1113.25$$

Fig. 4 Effect of pressure area on pressure strength of concrete

For design purposes, it can be preferable to have a simultaneous dependence of concrete pressure strength $\bar{f}_{cud}$ on compressive

strength $\bar{f}_c$ and pressure area A_p. Dependence $\bar{f}_{cud} = \bar{f}_{cud}(\bar{f}_c, A_p)$ can be written as:

$$\bar{f}_{cud} = (8.30 \cdot \bar{f}_c - 56.70) \cdot \kappa \tag{1}$$

$$\kappa = 1.46 \cdot \lambda^{0.4} + 2.46 \tag{2}$$
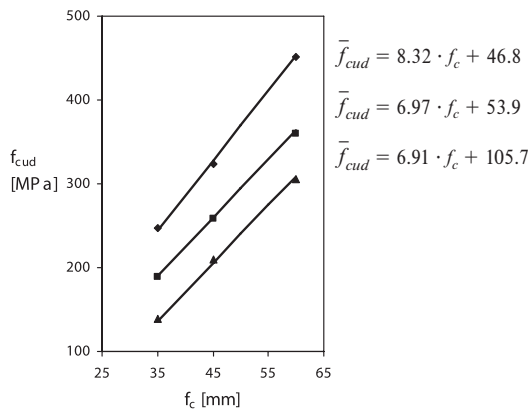
$$\lambda = \frac{A_p}{360} \tag{3}$$

$$\bar{f}_{cud} = 8.32 \cdot f_c + 46.8$$
$$\bar{f}_{cud} = 6.97 \cdot f_c + 53.9$$
$$\bar{f}_{cud} = 6.91 \cdot f_c + 105.7$$

Fig. 5 Dependence of pressure strength on concrete class and pressure area

In the formulae above $\bar{f}_c$ and $\bar{f}_{cud}$ are expressed in [MPa] and the pressure area $A_p = t.\Phi$ in [mm^2]. Formula (1) is valid for 360 mm$^2 \leq A_p \leq 600$ mm^2. It gives the mean strength. The characteristic strength $\bar{f}_{cudk}$ and design one $\bar{f}_{cud}$ can be determined using the same calculations as for concrete compressive strength.

4. Influence of axial forces on shear strength

The normal forces across the concrete and steel interface in the direction of the axis of the stud connector shank apply concentrated local loads. Bearing of the slab onto the steel beam flange resists the axial compressive forces and they rarely pose a problem. In contrast, the axial tensile actions can cause a separation between the composite elements or more often embedment concrete slab cracking. The shear strength of stud connectors is strongly influenced by the axial force across the steel and concrete interface. This resulting strength of push-test in which the base is free to slide [4] is substantially less than in the case of the fixed base [6]. This reduction in shear strength is due to the change of the resultant axial force at the interface from compression when the base is fixed to tension for the studs in the case of sliding base. The shear strength of headed studs can be degraded up to a third when the base is free to slide. The value of embedment forces in composite beams is generally considerably less than in the push-tests because of the difference between the boundary restraint conditions in the two systems.

The axial load can cause failure of the stud shank at the axial tensile strength
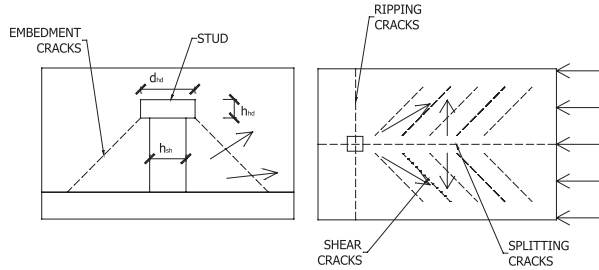

Fig. 6 Conical failure plane, dimensions of the stud connector

$$N_d = A_{sh} \cdot f_u, \tag{4}$$

where A_{sh} is the cross-sectional area of the stud shank and fu its design tensile strength.

Alternatively, the connector can be pulled out of the slab forming a concrete cone around it (Fig. 6). The surface area of this conical failure plane is used for deriving the following axial embedment strength

$$N_d = 1.5 \cdot \sqrt{f_{ck}} \cdot h_{sh}(h_{sh} + d_{hd}), \tag{5}$$

in which f_{ck} is the compressive cylinder strength of the concrete and the remaining dimensions are defined in Fig. 6.

The shear dowel strength of stud connectors is given by a standard equation

$$P_d = 0.8 \cdot f_u \cdot \frac{\pi \cdot dsh^2}{4}, \tag{6}$$

the other equation should control shear connector steel shank strength

$$P_d = 0.29 \cdot \alpha \cdot d_{sh}^2 \cdot \sqrt{f_{ck} \cdot E_{cm}}. \tag{7}$$

5. Interaction between shear and axial forces

The axial forces on the shear connection can produce the elements separation. As a result, the tensile force at the stud head increases and the probability of embedment failure becomes greater. The critical tensile failure in the weld collar zone is in the same time more likely to fail when the axial tensile forces are applied. It is therefore necessary to determine the interaction between shear and axial effect.

The elliptical interaction curve proposed in [5] is

$$\left(\frac{P_{Sd}}{P_d}\right)^{\frac{3}{2}} + \left(\frac{N_{Sd}}{N_d}\right)^{\frac{3}{2}} = 1.0 . \tag{8}$$

This failure envelope is represented in Fig. 7.

The alternative method of considering effect of axial forces on the shear strength of connectors is based on changing the tensile strength of the connector [6]. If the axial tensile stress $\sigma_{Sd} = N_{Sd}/A_{sh}$
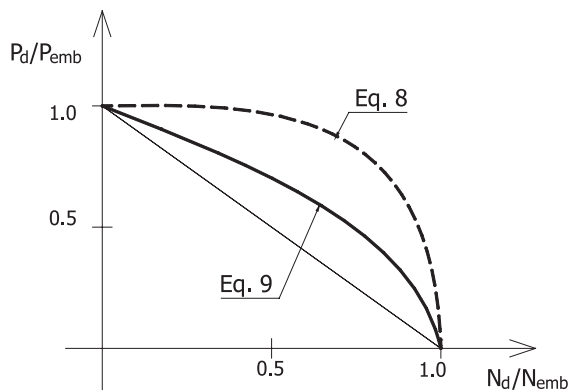
Fig. 7 Shear-axial failure envelope

mining $\bar{f}_{cud}$ have been based on the results of the experimental investigations, which were done within the framework of the grant of the Committee for Scientific Research.

The formulae quoted are valid for the parameters of strip thickness, hole diameters and concrete class adopted in the research. They cannot be extrapolated beyond the extreme values of Φ (20 $\div$ 40 mm), t (12 $\div$ 20 mm) and A_p (360 $\div$ 600 mm^2). Interpolation is possible in the range of the given maximum values.

In design of a composite concrete slab with a steel girder using perforated strips, it can be considered as minimum value of pressure strength $f_{cp} = \omega \cdot f_c = 4 \cdot f_c$ with pressure area not larger than 600 mm^2 and concrete class at least B30. With pressure area not exceeding 360 mm^2 and concrete class at least B30 even $\omega = 5$ can be adopted.

Mechanical connectors impose very high concentrated load onto the concrete element. The load is transferred from the steel beam to the concrete through the dowel action of the connectors. The tensile cracks caused by shear and splitting actions can be avoided by design procedures in [7]. The embedment cracks caused by tension, resisting separation at the steel and concrete interface of composite beam can be assessed according to the described procedure.

is applied, the equivalent design tensile strength of a connector is reduced by relationship

$$R_{d,ekv} = \left(1 - \frac{\sigma_{Sd}}{f_u} \right) \cdot R_d \,. \tag{9}$$

It can be seen in Fig. 7 that the expression for quantifying the effects of axial forces on the shear strength of stud connector is a lower bound to the previous failure envelope.

6. Conclusions

The paper deals with concrete pressure strength $\bar{f}_{cud}$ in strip connectors of composite structures. The propositions of deter-

References

[1] PN-B-03264: 1999: *Concrete, Composite Steel and Concrete Structures (in Poland)*, Obliczenia statycznei projektowanie.
[2] PN-84/B-03264: *Concrete, Composite Steel and Concrete Structures (in Poland)*, Obliczenia statyczne i projektowanie.
[3] PN-91/S-10042: *Bridge Objects – Concrete, Composite Steel and Concrete Structures (in Poland)*, Projektowanie
[4] OLLGAARD, J. O., SLUTTER, R. G., FISHER, J. W.: *Shear Strength of Stud Connectors on Light Weight and Normal Weight Concrete,* Engineering Journal AISC, April 1971
[5] BUJŇÁK, J.: *Designing of Composite Steel and Concrete Beams (in Slovak),* Vydavateľstvo ŽU v Žiline, 1997
[6] BUJŇÁK, J., FURTAK, K.: *Structural Elements from Steel and Concrete (in Slovak),* Vydavateľstvo ŽU v Žiline, 1999
[7] BUJŇÁK, J., FURTAK, K., VIČAN, J.: *Structure Designing by Eurocods (in Slovak)*, EDIS, Žilinska univerzita, Zilina, 2003.

Ruzica R. Nikolic – Jelena M. Veljkovic – Jozef Vican *

DESIGN OF COLUMNS CENTRICALLY LOADED IN COMPRESSION

Design of centrically loaded columns by the axial compressive load is considered in this work. The three methods results are compared: theoretical ω-procedure and calculations according to standards JUS U.E7.081 and Eurocode 3. The analysis is illustrated on an example of a column with a complex cross-section. By comparison between the calculated normal stresses and should be allowable stresses for all the three procedures, one can see that the stresses calculated using both standard procedures are significantly smaller than stresses calculated using the theoretical procedure. This shows that the standard procedures of calculations and design are much more on the safety side, especially in the case of Eurocode 3.

1. Introduction

The columns loaded in compression must be checked for stability, i.e., against the possibility of buckling. There exist numerous methods for these calculations; from the classical Eulerian procedure, through Engesser – Karman corrections, to the application of generally adopted international standards. The intention here is to compare the three design (calculations) procedures, one theoretical, the so-called ω-procedure, and the two standards' prescribed procedures, by the JUS and Eurocode 3. It will be shown which procedure gives the best estimate of the load carrying capacity of the compressed column and which procedure(s) are on the safety side and for how much.

2. The design of columns centrically loaded by compressive load

Load-carrying capacity of axially loaded columns, by using the *ω-procedure*, is written as, [1–3]:

$$\sigma_\omega = \frac{N}{A}\,\omega \le \sigma_{dop}\,, \tag{1}$$

where coefficient ω depends on effective slenderness ratio, λ.

Load-carrying capacity of axially loaded columns, with a single-part cross-section, by using *the standard procedure JUS U. E7. 081/198* [4], is written as:

$$\sigma_N = \frac{N}{A} \le \sigma_{i,dop} = \chi\sigma_{dop}\,, \tag{2}$$

where: N is the calculated normal force for appropriate case of loading, A is the cross-sectional area, σ_N is the calculated normal stress, $\sigma_{i,dop}$ is the allowable buckling stress, σ_{dop} is the allowable normal stress, χ is the buckling reduction factor, which depends on relative slenderness $\overline{\lambda}$, shape of cross-section and degree of equivalent geometric imperfections.

Dependence of the column's cross section and degree of equivalent geometric imperfections are expressed by column belonging to one of the buckling curves, A_0, A, B, C or D, Figure 1, [4].

Relative slenderness ratio $\overline{\lambda}$ is the relation between the effective slenderness ratio λ and slenderness ratio at yield strength, λ_v:

$$\overline{\lambda} = \lambda/\lambda_v \tag{3}$$

Effective slenderness ratio is a quotient of the effective length of the column, ℓ_{ki} and competent radius of gyration i:

$$\lambda = \ell_{ki}/i\,. \tag{4}$$

Load-carrying capacity of axially loaded columns, with a single-part cross-section, *according to Eurocode 3*, should be verified against buckling as follows, [5]:

$$\frac{N_{Ed}}{N_{b,Rd}} \le 1.0\,, \tag{5}$$

where: N_{Ed} is the design value of the compression force; $N_{b,Rd}$ is the design buckling resistance of the compression member.

For members with non-symmetric Class 4 sections allowance should be made for the additional moment ΔM_{Ed} due to the eccentricity of the centroidal axis of the effective section.

* **Ruzica R. Nikolic[1], Jelena M. Veljkovic[2], Jozef Vican[3]**
  [1]Faculty of Mechanical Engineering, University of Kragujevac, Sestre Janjic 6 34000 Kragujevac, Serbia,
  E-mail: ruzicarnikolic@yahoo.com and inikolic@ptt.yu
  [2]Executive research manager, "RAPP-ZASTAVA" Factory, Trg Topolivca 4, 34000 Kragujevac, Serbia, E-mail: vkatarina@ptt.yu
  [3]Faculty of Civil Engineering, University of Zilina, Komenskeho 52, 01026 Zilina, Slovakia, vican@fstav.uniza.sk
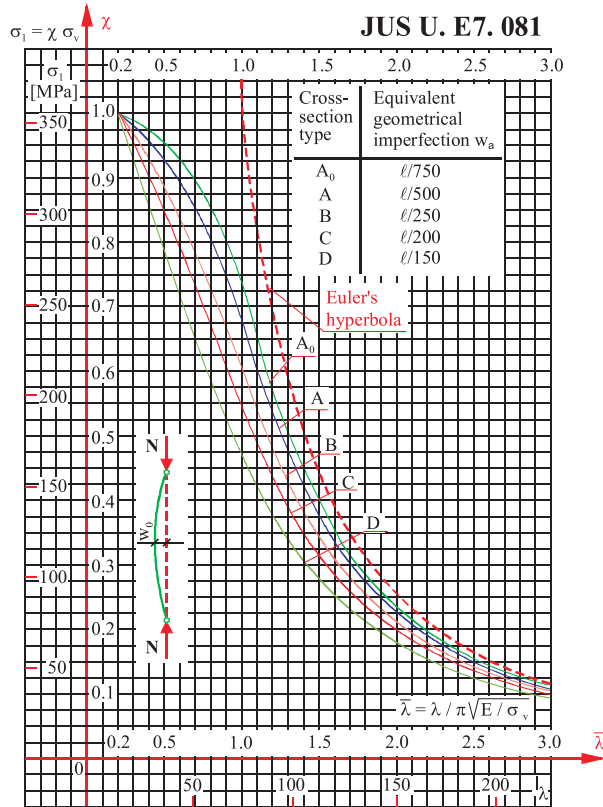
Fig. 1 Buckling curve according to the standard procedure
JUS U. E7. 081/198

The design buckling resistance of a compression member should be taken as for Class 1, 2 and 3 cross-sections

$$N_{b,Rd} = \chi A f_y / \gamma_{M1} \qquad (6)$$

and for Class 4 cross-sections:

$$N_{b,Rd} = \chi A_{eff} f_y / \gamma_{M1}, \qquad (7)$$

where χ is the reduction factor for the relevant buckling mode, f_y is the yield stress and γ_{M1} is partial factor for resistance to instability.

For axial compression in members, the value of χ for the appropriate non-dimensional slenderness $\bar{\lambda}$ should be determined from the relevant buckling curve according to

$$\chi = 1/(\Phi + \sqrt{\Phi^2 - \bar{\lambda}^2}), \qquad (8)$$

but $\chi \le 1.0$, where $\Phi = 0.5[[1 + \alpha(\bar{\lambda} - 0.2) + \bar{\lambda}^2]]$ with:

$$\bar{\lambda} = \sqrt{A f_y / N_{cr}} \text{ and } \bar{\lambda} = \sqrt{A_{eff} f_y / N_{cr}}, \qquad (9)$$

for the Class 1, 2 and 3 and for the Class 4 cross-sections, respectively,

where: α is an imperfection factor. The imperfection factor α corresponding to the appropriate buckling curve should be obtained from Tables 1 and 2.
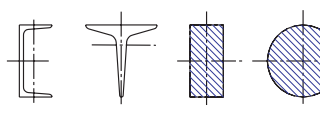
Imperfection factor for different   Table 1.
buckling curves (Table 6.1, [5])

Buckling curve	a_0	a	b	c	d
Imperfection factor α	0.13	0.21	0.34	0.49	0.76

Buckling curves for various   Table 2.
cross-sections (Table 6.2, [5])

	Cross section	Buckling about axis	Buckling curve
	...	...	...
U, T- and solid sections		any	c
	...	...	...

N_{cr} is the elastic critical force for the relevant buckling mode based on the gross cross sectional properties.

Values of the reduction factor χ for the appropriate non-dimensional slenderness $\bar{\lambda}$ may be obtained from Figure 2.
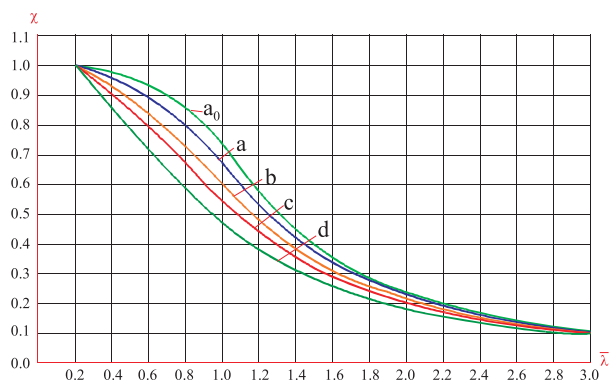

Fig. 2 Buckling curves according to Eurocode 3, [5].

For slenderness $\bar{\lambda} \le 0.2$ or for $N_{Ed}/N_{cr} \le 0.04$ the buckling effects may be ignored and only cross sectional checks apply.

The non-dimensional slenderness $\bar{\lambda}$ is given by:

$$\bar{\lambda} = \sqrt{A f_y / M} = (L_{cr}/i)(1/\lambda_1) \text{ and }$$

$$\overline{\lambda} = \sqrt{A_{eff}f_y/N} = (L_{cr}/i)\left(\sqrt{\frac{A_{eff}}{A}}/\lambda_1\right),\tag{10}$$

for the Class 1, 2 and 3 and for the Class 4 cross-sections, respectively. Here, L_{cr} is the buckling length in the buckling plane considered; i is the radius of gyration about the relevant axis, determined using the properties of the gross cross-section

$$\lambda_1 = \pi\sqrt{E/f_y} = 93.9\epsilon; \quad \epsilon = \sqrt{235/f_y},\tag{11}$$

where f_y is in N/mm^2.

3. The design procedures for compressively centrically loaded columns comparison

The cross section of the multi-part columns is characterized by the material and non-material (free) axes. The former crosses all the individual parts of the cross section, while the latter does not necessarily pass through all the parts of cross section. The lace sheets and truss bars are positioned perpendicular to the free axis.

The individual element axis is the axis that corresponds to the minimum gyration radius. The carrying capacity control of centrically compressed columns, of the constant, multi-part cross-section, enhances the control of buckling resistance both around the material and around non-material axes.

The problem of design centrically loaded column by compressive load will be illustrated on an example of a column with cross-section shown in Figure 3 (battened built-up members). The column height is $h = 7$ m, and axial compressive force is $F = 840$ kN. The material is Č 0361 (corresponding to S 275 in ENV 1993 [5]).
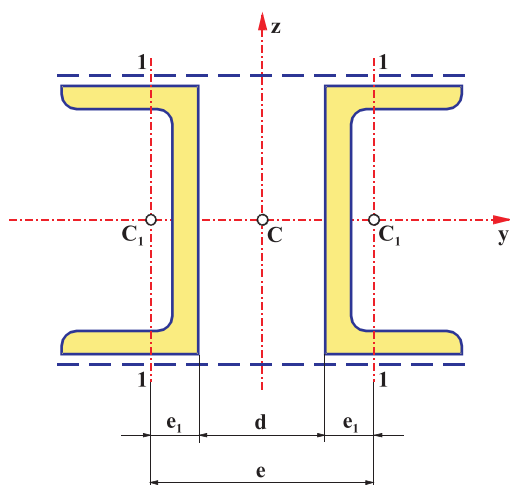

Fig. 3 Cross-section of a column

$\omega_{z_1} = 2 \cdot A_1 \cdot \sigma_{dop}/F = 1.61 \Rightarrow \lambda z_i = 85$, [6], $\lambda_1 = \dfrac{a}{i_1} = \dfrac{100}{2.42} =$

$= 41.32 \approx 41$, ($a = 1000$ mm – distance between the two lacing bars, Figure 4).

In the first place, dimensions necessary to carry actual load, will be determined using the ω - *procedure* [6,7].

Firstly, is selected *U24*, with the following data (Figure 3):

$I_{y_1} = 3600 \cdot 10^4$ mm^4, $I_{z_1} = 248 \cdot 10^4$ mm^4, $A_1 = 4230$ mm^2,

$e_1 = 233$ mm, $i_{z_1} = i_1 = 24.2$ mm, $i_{y_1} = 92.2$ mm

For *2U24* column cross-section is:

$I_y = 2 \cdot I_{y_1} = 7200 \cdot 10^4$ mm^4; $i_y = \sqrt{I_y/A} = \sqrt{2 \cdot I_{y_1}/2 \cdot A_1} =$

$= \sqrt{I_{y_1}/A_1} = i_{y_1} = 92.2$ mm.

$\lambda_y = h/i_y = 75.92 \Rightarrow \lambda_y = 76 \Rightarrow \omega_y = 1.46$, [4].

$\sigma_{\omega_y} = (F/2 \cdot A_1) \cdot \omega_y = 145$ *MPa*;

$\sigma_{\omega_y} = 145$ Mpa $< \sigma_{dop} = 160$ MPa.

The 2U24 cross-section is well selected in view of buckling stability around the y-y axis.

It is necessary to check validity of criterion of stability around the *z-z* axis. Lattice *e*, namely, *d* is unknown, and will be determined under condition that the material is utilized by buckling around that axis up to $\sigma_{dop} = 160$ MPa, [4].

$\sigma_{\omega_z} = (F/A) \cdot \omega_{z_i} = \sigma_{dop} \Rightarrow \omega_{z_i} = 2 \cdot A_1 \cdot \sigma_{dop}/F = 1.61 \Rightarrow$

$\lambda_{z_i} = 85$, [6].

$\lambda_1 = a/i_1 = 41.32 \approx 41$ – (Distance between the two lacing bars is $a = 1000$ mm).

$\lambda_{z_i} = \sqrt{\lambda_z^2 + \lambda_1^2} \Rightarrow \lambda_z = \sqrt{\lambda_{z_i}^2 - \lambda_1^2} = 74.4$; $\lambda_z = \ell_{kz}/i_z =$

$= h/i_z \Rightarrow i_z = h/\lambda_z = 94.1$ *mm*

$I_z = i_z^2 \cdot A = 7490 \cdot 10^4$ mm^4 ;

$I_z = 2 \cdot (I_{z_1} + y_{c_1}^2 \cdot A_1) \Rightarrow e^2 \cdot (A_1/2) = I_z - 2 \cdot I_{z_1} \Rightarrow$

$e = \sqrt{2 \cdot (I_z - 2 \cdot I_{z y_1})/A_1} = 182$ mm.

For $e = 182$ mm $\Rightarrow d = e - 2 \cdot e_1 = 137.4$ mm, thus the value of $d = 160$ mm is adopted.

For d = 160 mm $\Rightarrow d = e + 2 \cdot e_1 = 204.6 \Rightarrow$

$I_z = 2 \cdot (248 \cdot 10^4 + (204.6)^2 \cdot 4230) = 9340 \cdot 10^4$ mm^4.

$i_z = \sqrt{I_z/A} = 105$ mm $\Rightarrow \lambda_z = h/i_z = 67$.

Control of buckling stability around the *z-z* axis:

$$\lambda_{z_i} = \lambda_z^2 + \lambda_1^2 = 79 \Rightarrow \omega_{z_1} = 1.51, \text{ [6]}.$$

$\sigma_{\omega_y} = (F/A) \cdot \omega_{z_1} = 150$ MPa $< \sigma_{dop} = 160$ MPa, *thus the stability checks.*

Control of the distance between the two lacing bars:

$$\lambda_1 = c/i_1 = 41 \leq 50 \cdot (4 - 3 \cdot (\sigma_\omega/\sigma_{dop})) = 59 \Rightarrow$$
$$\Rightarrow \lambda_1 = 41 < 59$$

The cross-section 2U24 is selected with lattice d = 16 cm.

In further analysis is illustrated a design of centrically compressed column according to *the standard procedure JUS U. E7. 081.*

The proof of load-carrying capacity around the material axis *y-y*, is as follows:

$\lambda_{i,y} = \ell_{i,y}/i_y = 75.92; \quad \overline{\lambda}_y = \lambda_{i,y}/\lambda_v = 0.82 \Rightarrow \chi = 0.65$, (Curve "C", Figure 1).

Allowable buckling stress is: $\sigma_{i,dop} = \chi \cdot \sigma_{dop} = 104$ MPa

Calculated normal stress is: $\sigma_N = N/A = 99.3$ MPa, *thus the stability checks.*

The proof of the load-carrying capacity around the nonmaterial axis *z-z*, is as follows:

$$\lambda_z = \ell_{i,z}/i_z = 67 \Rightarrow \lambda_{zi} = \sqrt{\lambda_z^2 + (m/2) \cdot \lambda_1^2} = 78.55 ,$$

with *m* = 2 – number of single elements in a complex cross-section.

$\lambda_1 = c/i_1 = 41.32 \approx 41; \overline{\lambda}_{zi} = \dfrac{\lambda_{zi}}{\lambda_v} = 0.85 \Rightarrow \chi = 0.63$, (Curve "C", Figure 1).

Allowable buckling stress is: $\sigma_{i,dop} = \chi \cdot \sigma_{dop} = 100.8$ MPa, while the calculated normal stress is: $\sigma_N = N/A = 99.3$ MPa, *thus the stability checks.*

Finally, the dimensioning of the compressed columns according to *Eurocode 3*, [5] will be presented.

Checks should be performed for chords using the design chord forces $N_{ch,Ed}$ from compression forces N_{Ed} and moments M_{Ed} at mid span of the built-up member.

For a member with the two identical chords the design force $N_{ch,Ed}$ should be determined from:

$$N_{ch,Ed} = 0.5N_{Ed} + (M_{Ed}h_0 A_{ch}/2I_{eff}),$$

where: $M_{Ed} = (N_{Ed}e_0 + M_{ED}^I)/[1 - (N_{Ed}/N_{cr}) - (N_{Ed}/S_v)]$; $e_0 = L/500$ is the initial bow imperfection; $N_{cr} = \pi^2 EI_{eff}/L^2$ is the effective critical force of the built-up member; N_{Ed} is the design value of the compression force to the built-up member; M_{Ed} is the design value of the maximum moment in the middle of the built-up member considering second order effects; M_{ED}^I is the design value of the maximum moment in the middle of the built-up member without second order effects; h_0 is the distance between the centroids of chords, $h_0 = 204.6$ mm; A_{ch} is the cross-sectional area of one chord; I_{eff} is the effective second moment of area of the built-up member; S_v is the shear stiffness of the lacings or battened panel.

For chords the buckling verification should be performed as follows:

$$(N_{ch,Ed}/N_{b,Rd}) \leq 1.0,$$

where: $N_{ch,Ed}$ is the design compression force in the chord at mid-length of the built-up member and $N_{b,Rd}$ is the design value of the buckling resistance of the chord taking the buckling length L_{ch} from Figure 4.

The shear stiffness S_V should be taken as:

$$S_v = [24EI_{ch}/a^2[1 + 2I_{ch}/nI_b)(h_0/a)]] \leq (2\pi^2 EI_{ch}/a^2) .$$

The effective second moments of area of battened built-up members may be taken as:

$$I_{eff} = 0.5h_0^2 A_{ch} + 2\mu I_{ch} ,$$

where I_{ch} is the in plane second moment of area of one chord, I_b is the in plane second moment of area of one batten, μ is the efficiency factor from Table 3.

Using the previously obtained data from the example, the calculations are as follows:

$$e_0 = L/500 = 14 \text{ mm}; I_{eff} = 0.5h_0^2 A_{ch} + 2\mu I_{ch} =$$

$$= 93496353.4 \text{ mm}^2$$

$$N_{cr} = \pi^2 EI_{eff}/L^2 = 3950728.5 \text{ N}; S_v = 2\pi^2 EI_{ch}/a^2 =$$

$$= 10269759.36 \text{ N}$$

$$N_{b,Rd} = \chi A_{ch}f_y/\gamma_{MI} = 988762.5 \text{ N}; \overline{\lambda} = \sqrt{A_{ch}f_y/N_{cr}} =$$

$$= (L_{ch}/i)(1 + \lambda_1) = 0.54; L_{ch} = a = 1000 \text{ mm};$$

$$\lambda_1 = \pi\sqrt{E/f_y} = 93.9\epsilon = 76.06 \Rightarrow \epsilon = 0.81; \chi = 0.85;$$

$$\gamma_{MI} = 1; M_{Ed} = 31111111.1 \text{ Nmm}; N_{ch,Ed} = 773991.5 \text{ N};$$

$$(N_{ch,Ed}/N_{b,Rd}) = 773991.5/988762.5 = 0.783 \Rightarrow$$

$$(N_{ch,Ed}/N_{b,Rd}) < 1.0$$

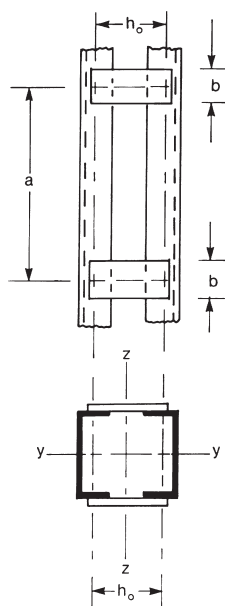*The chosen profile (2U24) satisfies the load-carrying requirements.*

Fig. 4 Battened built up-members, (Figure 6.7, [5]).

Efficiency factor μ, (Table 6.8, [5]). Table 3.

Criterion	Efficiency factor μ
$\lambda \geq 150$	0
$75 < \lambda < 150$	$\mu = 2 - \dfrac{\lambda}{75}$
$\lambda \leq 75$	1.0
where $\lambda = \dfrac{L}{i_0}; i = \sqrt{\dfrac{I_1}{2A_{ch}}}; I_1 = 0.5h_0^2 A_{ch} + 2I_{ch}$	

3. Conclusion

By comparing the calculated normal stress to the allowable stress obtained by the ω – procedure and the standard procedure(s), it can be seen that the stresses obtained by the standard procedures are significantly smaller than stresses obtained by the theoretical procedure. This shows that the standard procedures are much more on the safety side.

The reason for this difference in stresses' values (up to 40 %) is that the calculation by the ω – procedure is done under the assumption that the material is utilized by buckling up to allowable stress, while calculations done by the standard procedures do not consider that assumption. The calculation according to Eurocode 3 is even more on the safety side than that according to standard JUS U. E7. 081. If one compares the buckling curves given by the two standards, it is not difficult to realize that they are identical. The difference in results of calculations stems from the stricter requirements by the Eurocode 3.

References

[1] MILOSAVLJEVIC, M. M., et al.: *Fundamentals of Steel Structures,* The Civil Engineering Book, Belgrade, Serbia, 1986.
[2] OSTRIC, D.: *Metal Structures,* Faculty of Mechanical Engineering, Belgrade, Serbia, 1988.
[3] PETKOVIC Z., OSTRIC, D.: *Metal Constructions in Machine Building - 1,* Institute of Mechanization, Faculty of Mechanical Engineering, Belgrade, Serbia, 1996.
[4] JUS M.B1. GROUP OF STANDARDS: *"JUS standards for construction elements, materials allowable stresses, ..."*, Federal Bureau for Standardization, Belgrade, Serbia.
[5] EUROCODE 3: *"Design of Steel Structures"*: ENV 1993-1-1: Part 1.1: General rules and rules for buildings, CEN, 1992.
[6] NIKOLIC, R., MARJANOVIC, V.: *Metal Structures - Handbook for Calculations,* Faculty of Mechanical Engineering, Kragujevac, Serbia, 1998.
[7] NIKOLIC, R., VELJKOVIC, J.: *"The Analysis of Designing Columns Centrically Loaded by Axial Compressive Load"*, Proc. V Int. Conf. "Heavy Machinery", Kraljevo, Serbia, 28–30 June, 2005, pp. IC29-IC32.

COMMUNICATIONS

Martin Moravcik *

THE LOAD TESTING AND NUMERICAL VERIFYING OF THE PRECAST PRESTRESSED GIRDER

Precasting can solve complicated structural details, ambitious demands to quality of surface arrangements and manage hard terms filling at present. The prestressed precast girders are produced to 30.0 m span and are distributed for the realization of big shopping centers. The design and realization of the prestressed precast tie-beam for a skeleton system is presented in this paper. The experimental and numerical analyses were performed to verify the safety and reliable acting of the girder for the next service.

1. Introduction

The design, realisation and experimental testing of the prestressed precast tie-beam for the skeleton system is presented in this paper. Similar tie-beams are being produced to the span of 30.0 m and applied in the up to date big shopping centres. The experimental testing of the girder was applied on the new technological stressing bed that was constructed in the working plant of Prefa Sucany. The Prefa company started to produce precast rod elements for long span in 2004. Sufficient load carrying capacity for designed and for ultimate load level was approved as the main goal of the experiment. The experimental results were compared with the numerical ones gained from the nonlinear FEM analysis using the ATENA program system.

Precasting is the important component of the building production in civil engineering. Development in precast elements is being done hand in hand with the improvement of material base and structural systems. Complicated structural details, ambitious demands to quality of surface arrangements and a sharp time schedule of work can be satisfied using precasting technology at present. The modern technologies of self compacting concrete (SCC), high performance concrete (HPC) and light weight concrete (LWC) are gradually applied in practice for the precast elements.

The company Prefa Sucany had produced thin slab prestressed elements already in the past. The existing stressing bed with 250 t prestressing capacity was changed to the new one with the length of 84 m and 1000 t prestressing capacity in the year 2004. The company started to produce some rod types of precast prestressed elements for the skeleton and roof systems, mainly for new shopping centres. Rectangular, I, TT, or T shapes are commonly used shapes of girders.

The extension of production of the new types of girders required verification of important physical and mechanical parameters designed and manufactured precast prestressed elements. Experimental testing was carried out in the collaboration with the company Prefa Sucany, Inc., University of Zilina and company Projstar PK, Ltd. The research results are presented in the report [3].

One of such precast tie-beams which were distributed for the shopping centre Kaufland was chosen for experimental and numerical testing.

The original manufactured girder with the length of 24.0 m was reduced in compliance with the purpose of the experiment to the length of 18.0 m. The general aims of the experimental test can be specified as follows:
- to verify the transferring of prestressing force to concrete element and prestressing losses,
- to prove a sufficient load carrying capacity of the girder for the designed load level that was simulated by the real roof coat, see Fig. 1, and Tab. 1,
- to observe the girder behaviour after a crack propagation,
- to achieve the ultimate limit state of the girder.

The proposed skeleton system is manufactured in the 12×18 m module and the 4 roof beam being reacted on the girder in 1/3 of the span. The values of the load according to standard [1] were proposed:
- the permanent load consists of the self-weight of the girder, the weight of concrete roof beams with a trapezium cross-section with the basics of 200 and 300 mm and the depth of 700 mm, the anchored foil, thermal insulation 80 mm + 160 mm fume-insulation and trapezoidal plate (the Ranilla Ran 1 mm).
- a variable load due to electricity distributions, air-condition, etc. The climatic load consists of snow action for the IV snow area, according to [1] and the suck action of the wind.

* Martin Moravcik
Department of Structures and Bridges, University of Zilina, Faculty of Civil Engineering, Komenskeho 52, 010 26 Zilina, Slovakia,
E-mail: Martin.Moravcik@fstav.uniza.sk

Resulted values of the point action F and internal forces are presented in Tab. 1.
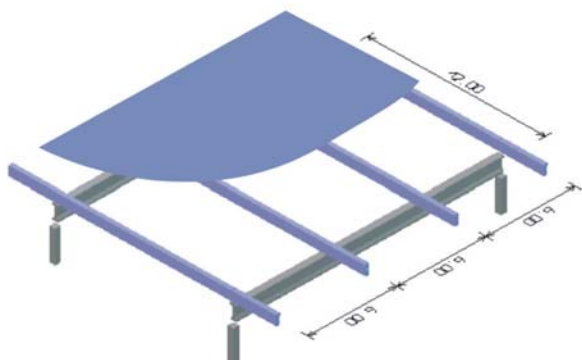

Fig. 1 Scheme of the investigated girder in skeleton system

Designed values of the load and internal forces for the tie-beam — Table 1

	F [kN]	M [kNm]	V [kN]
characteristic value	239.30	1570.48	298.19
design value	307.44	2135.35	372.13

2. Basic parameters of the girder

Considering spatial and manipulation possibility the girder with 18 m span was used for the testing. The girder was designed according to the standard [2]. It has to satisfy the stress conditions and crack width for an element of "second category". That means 0.5 MPa compress stress at least in the permanent tension concrete fibres due to the permanent load action. The computer program "PresBeam" was developed for design of precast prestressed girders.

Depth of the investigated girder is 1050 mm and other geometrical parameters can be seen in Fig. 2. The designed concrete quality is C50/60. Self-weight of the girder is 12.45 t. The real average concrete cube strength was 63.9 MPa. It was 35 days after transferring prestressing to the concrete. The R-type cement was used. Concrete strength had the value of 46.8 MPa in the time of prestressing transfer. Prestresing elements consist of 14 tendons LSA 15.5/1800 MPa. The tendons are arranged to the raster 50×50 mm 4 tendons are included to the bottom 3 rows (tendons A) and the 2 tendons belong to the top row, see Fig. 2. Two other tendons in the bottom row were separated using a greased polyethylene tube of the 2.0 m length (tendons B). The prestressing force was designed 186.8 kN and applied using the PAUL system.

Profiles of φ 10 and 16 mm of the type (R) 10 505 were used for the longitudinal girder reinforcement, and for stirrups the profile of φ 10 mm over 250 mm was used. The distance was

reduced to 100 mm above abutments and manipulate elements for stirrups.

3. Test arrangement

The girder was continually observed from the time of tendons stressing to the load test performing. The following parameters were scanned – the prestressing force (P), the vertical deflections (f), the concrete strain (ϵ), the temperature (t), the crack width (w) and a possible tendon slip (Δ). Possible settlement of abutments was geodetically checked. The prestressing force was recorded using elastomagnetic sensors, Fig. 4b), using Projstar PK system. One sensor was located on top tendon and one was fixed on bottom tendon. Experimentally and theoretically achieved results of the actual prestressing force are presented in Tab. 2 and the registered data from elastomagnetic sensors can be seen in Fig. 3.

Fig. 2 Reinforcement and the cross section of the girder

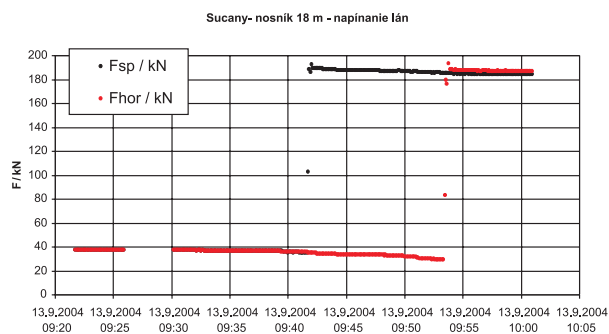*Fig. 3 Stressing force course in the tendons*

Prestressing force measured during prestressing and transferring process   Table 2

Force (kN)	prestressing. theoretic.	prestressing recorded	ratio (–)	transferring theoretic.	transferring recorded.	ratio (–)	immediate losses
bottom tendon	186.8 kN	184.3 kN	0.986	167.5 kN	158.2 kN	.0.944	26.1 kN
top tendon	186.8 kN	186.9 kN	1.001	171.1 kN	161.0 kN	0.941	25.9 kN

The resistance sensors of the type NovoTechnik TR with the range of 50 or 150 mm were used for vertical deflection measuring and for checking the possible tendon slip. Vertical deflection was scanned in 11 points equally distributed along the span, according to Fig. 4a). The concrete strain monitoring was realised using common Hollan mechanical strain gauger and the strain gauges of type HBM 50/120LY41, see Fig. 4b). Five points were defined along the cross section depth, according to Fig. 4a). The crack width was monitored with magnifier with scale and photometric method using digital cameras (3MP and 10x zoom) was also used for crack width calibration.
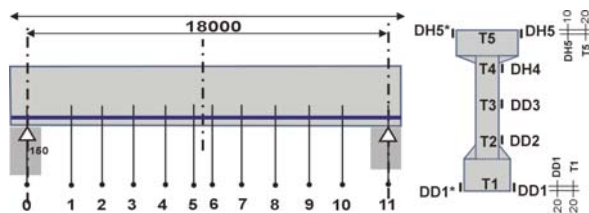
Fig. 4a) Measured points location for the deflection and concrete strains

Fig. 4b) Strain gauges and elastomagnetic sensors

The girder was set on fixed abutments through the elastic bearings. The elastic bearings deformations were recorded too. The concrete panels with dimensions 2.0 × 3.0 × 0.15 m were used as loading elements. Their gravity was exactly determined using the suspension weight equipment. The average one panel gravity oscillated from 2.1 to 2.2 t. Load steps were realised incrementally without unloading steps. One load step includes loading by 4 panels equally assembled to 1 row, see Fig. 5. The 21 rows of panels and 15 load steps were finally performed.
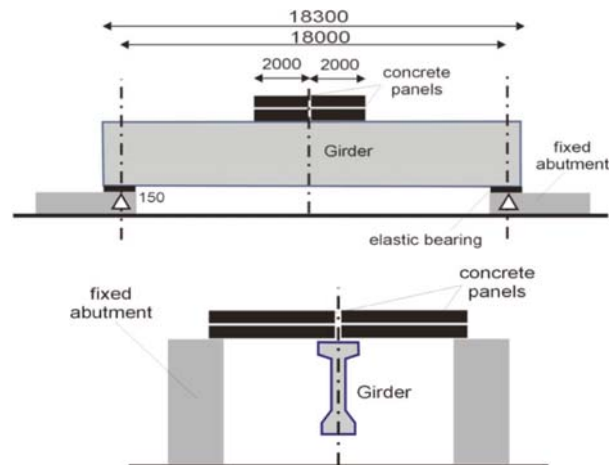

Fig. 5 Loading scheme of the girder

4. Numerical analysis principles

The nonlinear FEM computer program ATENA, [5] was used to analyse this problem to compare theoretical and experimental values of the above mentioned girder mechanical parameters. ATENA system enables to consider material and geometrical non-linearities of concrete structures based on fracture mechanics and nonlinear solution principles.

The constitutive relations are formulated for the plane stress state. A smeared approach is used to model the material properties for cracks and the longitudinal and transversal reinforcement. In that concept the implemented material model SBETA, [5] was used for concrete element, see Fig. 6.

The material model SBETA includes the following effects of concrete behaviour:
- non-linear behaviour in compression including hardening and softening,
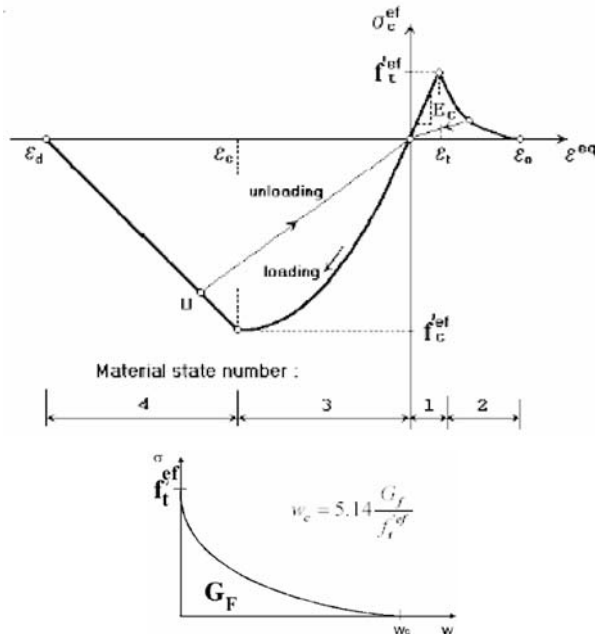- fracture of concrete in tension based on the nonlinear fracture mechanics,

Fig. 6 Uniaxial stress-strain law for concrete - tension and compression.

- biaxial strength failure criterion,
- reduction of compressive strength after cracking,
- tension stiffening effect,
- reduction of the shear stiffness after cracking (the variable shear retention),

The perfect bond between concrete and reinforcement is assumed within the smeared concept. The exponential crack opening law and the fixed crack model was applied as a model of smeared cracks. Tendons are modelled as discrete elements and the bilinear stress-strain relationship for all reinforcement was applied.

5. Results of theoretical and experimental analysis

5.1 Phase of prestressing application

The measurement and numerical analysis of the deflection and the prestressing force transferred to the concrete were realised as first. The short-term losses were about 12 % including the elastic deformation of concrete.
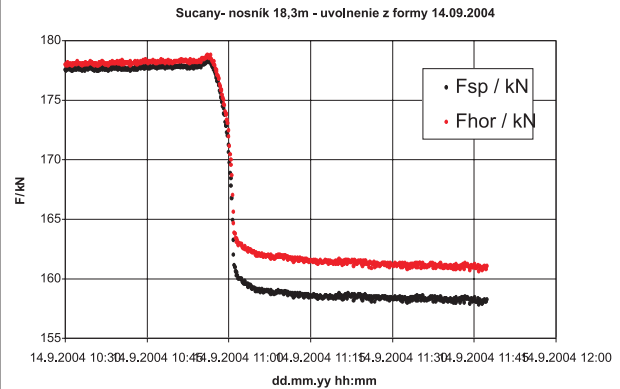

Fig. 7 Transferred prestressing force in bottom flange of the girder.

Real observed values of the camber along the longitudinal axis were gained immediately after the transferring time (around 24 hours) and their value was 44 mm. It was higher value than the designed value of 31 mm, according to the Slovak standard [2], see Fig. 8. Several cracks were detected on the upper flange in the third length on the both side of girder. Their width increased the values up to 0.1 mm. Therefore the numerical nonlinear analysis for the deflection applied on a relatively young concrete deflection was performed including crack propagation effect in the concrete. The value of deflection was 42 mm. Cross section was divided to 3 sections – upper flange, the web and the bottom flange respecting to the concrete modulus of elasticity distribution along cross section, see Tab. 3. Apart from the modulus the compression and tension concrete strength have been changed depending on location in the cross section. The concrete modulus of elasticity was considered as a standard value [2, 4] and values with respect to the actual time (t) adjusted to the concrete temperature (t_T) and the cement type (s), [6]. Two types of the used cement were compared and the time of 1 day was considered in the analysis. The modulus was expressed by the following relationship,

$$E_{ci}(t) = \beta_{cc}(t)^{0.5} \cdot E_{co}[f_{,cm} / f_{,cmo}]^{0,3}, \qquad (1)$$

where $\beta_{cc}(t) = e^{\{s \cdot [1 - (28/(t_T/t1))0.5\}} \qquad (2)$

5.2 The load test phase

Experimental results of the vertical deflection due to the load action increase are presented in Fig. 10. The girder deflection was

Concrete modulus of elasticity depending to the temperature and the cement type
Table 3

Location	Cement RS (52,5)			Cement N, R (32,5 , 42,5)		
	$T(\_t_i)$ [°]	$f_{,cm}(t)$ [MPa]	$E_{ci}(t)$ [GPa]	$T(\_t_i)$ [°]	$f_{,cm}(t)$ [MPa]	$E_{ci}(t)$ [GPa]
upper flange	27.0	31.63	21.37	27.0	26.53	18.56
web	29.5	33.20	22.21	29.5	28.18	19.49
bottom flange	37.7	38.63	24.78	37.7	33.44	22.34
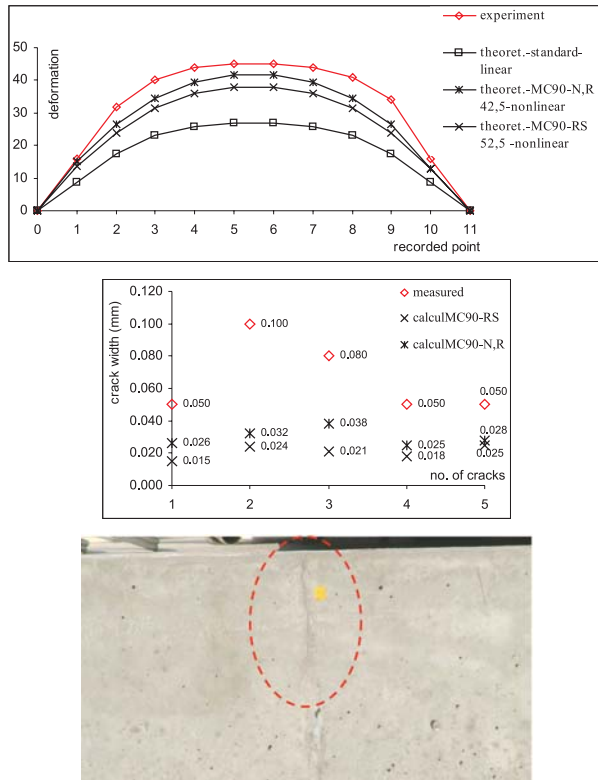
Fig. 8 Deflection and crack pattern at upper flange of girder, the real one crack at upper flange

Fig. 10 Vertical deflection vs. bending moments M in the middle span cross section

analysed using ATENA system and standard approach according to [4], the relation (3) was used too. The principle of incremental stiffness reduction based on the average cross section curvature (κ) was applied. Good coincidences between both of the theoretical values were observed. The theoretical value of critical bending moment according to EN is $M_{cr} = 1590.76$ kNm. Experimental bending moment was $M = 1701.87$ kNm when the first visible bending crack was detected. After that stage when the first crack appeared the numerical values of deflection is more conservative comparing to the experimental ones.

$$\kappa = \xi\kappa_{II} + (1 - \xi)\,\kappa_I \qquad (3)$$

The first crack of hair character with the length of 6 cm through all the bottom part of flange was developed in the distance

of around 70 cm from the middle cross section. Next bending cracks were propagated on both sides equally around the 500 mm distance. That distance was gradually decreased to 100 mm and cracks were grown to the compressed area, see Fig 10. The critical crack width of 0.2 mm for the serviceability limit stage [4] was reached between 10th - 11th load steps and the corresponding bending moment level $M = 2172,80$ kNm - 2329.60 kNm, see Fig. 11a).

The crack width (w) was calculated following the ATENA system and standard approach according to [4] and the relation (4) was used. Compared to the theoretical values of a crack width and experimental results the same course of all curves can be seen in Fig. 11b). The theoretical results according to [4] are more conservative than ATENA and the experimental ones.

$$w_k = s_{r,max} \cdot (\epsilon_{sm} - \epsilon_{cm})\,,$$

$$\text{where } \epsilon_{sm} - \epsilon_{cm} = \frac{\sigma_s - k_t \cdot \dfrac{f_{ct,eff}}{\rho_{p,eff}} \cdot (1 + \alpha^e \cdot \rho_{p,eff})}{E_s} \qquad (4)$$

The pattern of crack propagation on a real girder for the last load step is very similar to the numerical model sample, see Fig. 12. The values of distance between the cracks oscillate from 100 to 250 mm.

The development of the force in tendons is presented in Fig. 14. The indication in Fig. 14, "P1r" means the tendon in the
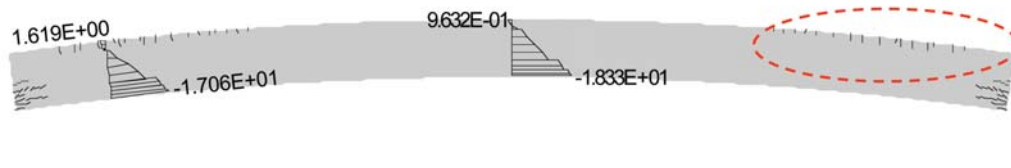

Fig. 9 Deflection, the crack pattern and normal stresses in the middle span section and section on the end of tendons separation length of the girder
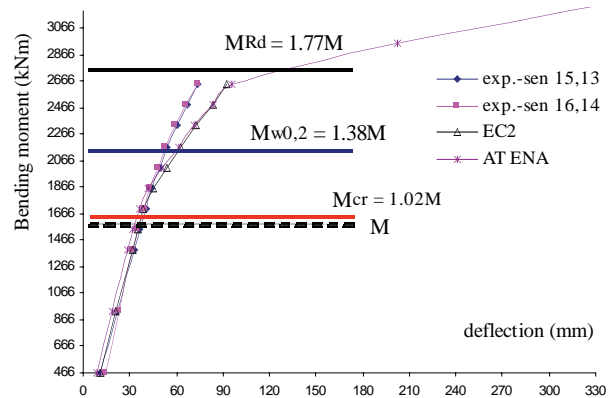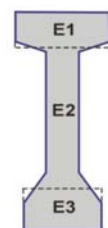
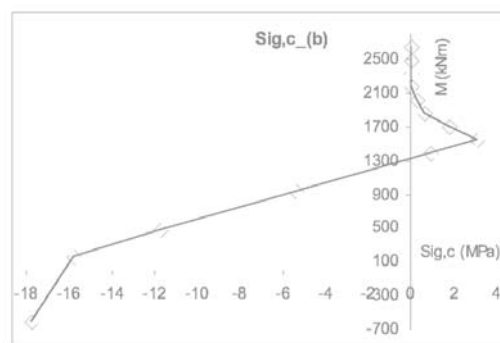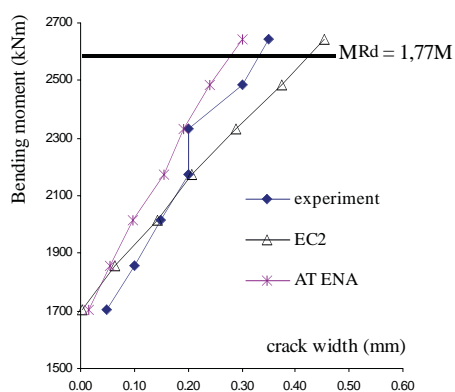*Fig. 11a) Crack propagation – experiment, ATENA – the 1l. load step*

Fig. 11b) Crack width for 7. – 13. load steps and normal stress course at bottom fibres in the middle cross section
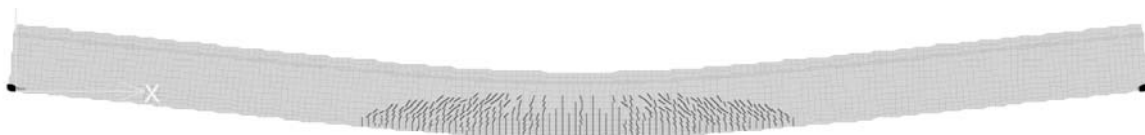

Fig. 12 Crack propagation in the real girder after load test and numerical model output - the last 15. load step
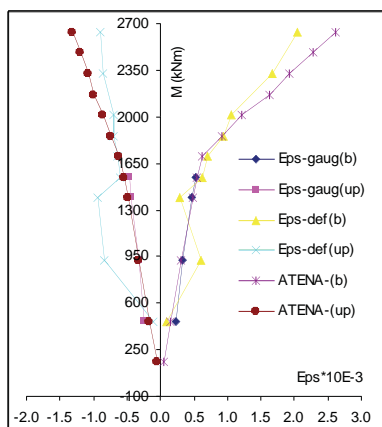

Fig. 13 The strain in edge fibres in the middle cross section – measured vs. theoretical values
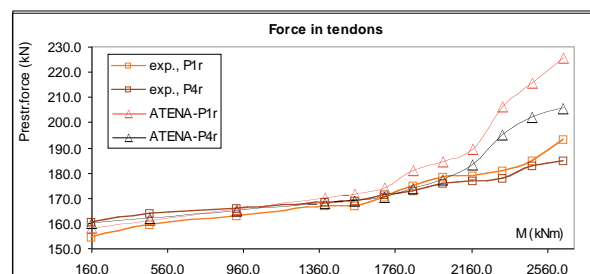

Fig. 14 Development of the force in observed tendons – measured vs. theoretical values

bottom row and "P4r" the tendon in the upper row. Proper conformity is apparent between the test and model particularly when the first crack was detected. After that point the numerical model was a little bit more conservative compared to tested values. It cor-

responds with the above mentioned results of deflection and strains in the concrete. The theoretical rupture of the tendon should become on the level of 254.7 kN.

6. Conclusions

On the basis of the experimental testing and numerical analysis results the following conclusions can be formulated:

- The theoretical assumption of prestressing force transferring was fulfilled.
- The sufficient load carrying capacity of the girder was approved for designed load and manufactured tie-beams can be reliably used in practice.
- The ATENA system can be successfully used to simulate precast prestressed structural elements on the full scale of its material behaviour. The material model SBETA and a fixed crack model are useful for numerical modelling of such problems.
- The initial camber was higher than the theoretical one but the negative influence on consequential load carrying capacity and serviceability of girder was not observed. It is necessary to use the concrete modulus of elasticity adjusted with the influence of location, the time, the temperature and the type of cement for accurate deflection determination. The recommendation relation presented in [2, 4] enable appropriate to solve that problem.
- By 6 % higher immediate prestressing losses in comparison with the theoretical values can be observed. It was caused by earlier prestressing transfer to concrete.
- The first visible hair crack was detected a little bit later than it was expected and the accurate reinforcement assured the expected crack distribution in concrete.
- The theoretical value of bending moment in the ultimate limit state $M_{Rd} = 2784.21$ kNm was exceeded over $M = 3273.60$ kNm but the element did not reach a rupture.

References

[1] STN 73 0035: *Load action of building structures,* SÚTN Bratislava 1993.
[2] STN 73 1201: *Design of concrete structures,* SÚTN Bratislava 1993.
[3] Moravcik, M.: *Report from the load test of the precast prestressed beam of I shape for building structures*, 2005, p. 1-18
[4] prEN 1992-1-1: *Design of Concrete Structures – Part 1: General rules and rules for buildings,* CEN 07/2002, Brussels.
[5] Cervenka Consulting: *ATENA Program documentation,* Theory, Prague, Oct. 2003,
[6] Commite Euro-International du Beton: *CEB-FIP Model Code 1990,* Thomas Thelford, 1991

Jaroslav Janáček *

THE TRANSPORT-PRODUCTION COORDINATION PROBLEM

Vehicle route planning process, which follows a transportation problem solution, often provides a system of cyclic routes of vehicles. This system should cover transportation demands of individual network nodes within a middle term period. Due to non-uniform demand distribution over the period, a new problem emerges in particular parts of the period. This problem consists in balancing the sub-period demands and frequencies, with which the individual routes are performed. This new problem denoted as the transport-production coordination problem is studied in this contribution.

We described the problem by mathematical programming tools and proposed a decomposition method to enable the problem decomposition to irreducible sub-problems. The individual types of the problem were studied and particular solving algorithms were designed. To complete our approach to this NP-hard problem, we developed an exchange heuristic and explored its properties. The associated computational study was performed with several series of the irreducible sub-problems, which were solved by the exchange heuristic and, simultaneously, they were solved to optimality by the universal optimization environment Mosel. The results were used for evaluation of the heuristic quality and time consumption.

1. Introduction

The transport-facility coordination problem arose when a mass transport problem was solved to ensure a fluent process of highway building. The building of a highway is accompanied by the necessity to bring a huge amount of mass as stone or clay to fill cavities at different places of the building site. At the same time, demands for taking off some amounts of material can arise. These demands are connected with excavation works at some places of the site. If the associated transportation problems are solved, then cost optimal moves of material amounts are obtained (See Fig. 1).
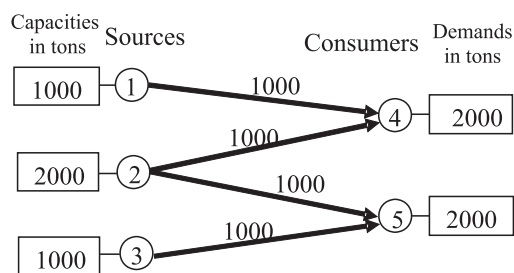

Fig. 1 Optimal flows of material

If corresponding vehicle capacities are assigned to the resulting moves, then a demand for free vehicle capacity emerges at beginning of each move and the end of move constitutes a source of free vehicle capacity. Then a problem of balancing the free and demanded vehicle capacities is to be solved. This solution results into a graph with flows of empty and loaded vehicles (See Fig. 2).
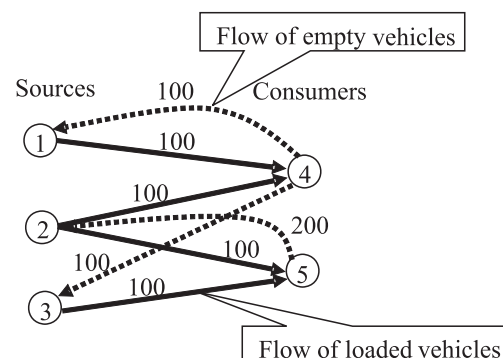

Fig. 2 Flows of vehicles having the capacity of 10 tons

These vehicle flows can be covered by numerous cyclic vehicle trips whose accomplishment usually takes several days or weeks (See Fig. 3).

After all trips are performed, all original demands for mass transport are satisfied.

The realization of above mentioned cyclic vehicle trips in the individual days brings another problem of vehicle coordination at some places, which constitute sources or consumers of the transported material. The necessity of coordination follows from the

---

* Jaroslav Janáček
Department of Transportation Networks, Faculty of Management and Informatics, University of Žilina, Slovakia, E-mail: Jaroslav.Janacek@fri.uniza.sk

fact that the material is excavated or stored at these places using assigned machines with a given productivity, which must be exploited as much as possible.
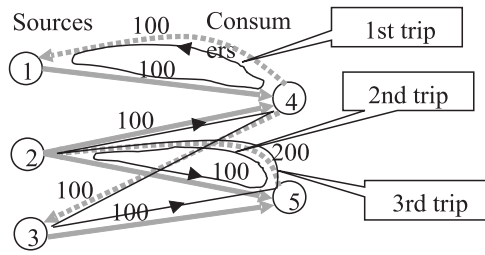

*Fig. 3 Cyclic trips of vehicles covering the flows,
when repeated hundred times*

For this purpose a transport-production coordination problem must be solved daily. As shown below, the transport-production coordination problem constitutes a serious combinatorial problem, which is NP-hard. It follows from the fact that the knapsack problem is polynomially transformable to an instance of the transport-production coordination problem. Due to the complexity of problem and necessity to solve the individual instances of the problem quickly, we perform an analysis of the problem and suggest a set of quick heuristics for solving special cases of the problem together with a decomposition algorithm.

2. The transport-production coordination problem

Given the set J of customers, where each customer $j{\in}J$ produces the demand b_j with the rate q_j of demand units per a time unit. Each customer's demand can be reduced by the amount K by one visit of a vehicle. Let the set of customers be provided with the set I of given vehicle trips and let an incidental matrix $[a_{ij}]_{i{\in}I\,j{\in}J}$ be indicated by the values one or zero of the element a_{ij} whether the trip i does or does not serve the customer j. Each performance of trip $i{\in}I$ takes a time t_i and must be performed exactly p_i times. After each trip i is performed p_i times, all customers' demands are completely satisfied. If only one vehicle performs the trip i, then the trip contributes to the satisfaction of j-th customer demand with the rate $K_i = K/t_i$.

Under assumption that $x_i{\in}\{1, ..., p_i\}$ vehicles are assigned to the trip i and they perform regularly, the trip performance will satisfy the demand with the rate $x_i\,K/t_i = x_i\,K_i$.

Let us consider a sub-set $J' \subseteq J$, for which a lack of the total demand satisfaction rate causes an additional cost. The lack u at the customer j causes the additional cost $c_j\,u$. On the other hand, a surplus of the satisfaction rate may cause an undesirable delay of the involved vehicles and this way it may influence the satisfaction rate of other customers, which is not permitted.

The objective is to determine the numbers $x_i{\in}\{1, ..., p_i\}$ $i{\in}I$ of assigned vehicles so that no total of demand satisfaction of the

customers from J' exceeds q_j and the total additional cost following the lack of satisfaction rate is minimal. It is assumed that if only one vehicle is assigned to each trip, then no satisfaction rate at any customer from J' exceeds the demand rate q_j.

3. An integer-programming model

Let us denote by $x_i{\in}\{1, ..., p_i\}$ the variables which give the numbers of vehicles assigned to the trips $i{\in}I$. Then the demand at the j-th customer is q_j. The rate of demand satisfaction is $\sum\limits_{i{\in}I} a_{ij}K_ix_i$.

The lack of demand satisfaction rate is $q_j - \sum\limits_{i{\in}I} a_{ij}K_ix_i$. The total additional cost is then $\sum\limits_{j{\in}J'} c_j[q_j - \sum\limits_{i{\in}I} a_{ij}K_ix_i] = \sum\limits_{j{\in}J'} c_j\,q_j - \sum\limits_{j{\in}J'}\sum\limits_{i{\in}I} c_j\,a_{ij}K_ix_i$.

As the first term of the total additional cost is a constant, the integer-programming model can be formulated as follows:

$$\textit{Maximize} \qquad \sum\limits_{j{\in}J'}\sum\limits_{i{\in}I} c_j\,a_{ij}K_ix_i \qquad\qquad (1)$$

$$\textit{Subject to} \qquad \sum\limits_{i{\in}I} a_{ij}K_ix_i \leq q_j \quad \text{for } j{\in}J' \qquad (2)$$

$$x_i \leq p_i \quad \text{for } i{\in}I \qquad\qquad (3)$$

$$x_i \geq 1 \quad \text{for } i{\in}I \qquad\qquad (4)$$

$$x_i \in Z^+ \quad \text{for } i{\in}I \qquad\qquad (5)$$

It is necessary to take into account that the above model is formulated for one time unit only, e.g. for one working day. It follows some further assumptions of trip durations and upper bounds of variables x_i. In the first place, we suppose that trip duration is less or equal to the time unit. In the second place, we have to take into consideration the regularity of the trip repeating. Let us imagine that the upper bound p_i of number of the assigned vehicles to a trip i equals two and that the trip takes exactly half of the time unit. In this case it makes no sense to assign two vehicles to this trip because they will contribute to the demand satisfaction in this time unit with the same unit as one vehicle even if they make their work in the half of the time unit. From this it follows that inequality $p_it_i/x_i > 1$ must hold and the constraints (3) can be replaced by the constraints $x_i \leq r_i$, where $r_i = \lfloor p_it_i \rfloor$ or $r_i = p_it_i - 1$, if p_it_i is integer.

The further rearrangement of the model follows from the fact that if each variable x_i is set to the value of one, then no rate q_j is exceeded. We can set $\underline{q}_j = q_j - \sum\limits_{i{\in}I} a_{ij}K_i$ for $j{\in}J'$. Then, the upper bound of the variables x_i can be made more precise using the following formulation $\underline{r}_i = \min\{r_i - 1, \min\lfloor \underline{q}_j/K_i \rfloor : j{\in}J', a_{ij} = 1\}\}$.

After these rearrangements, the model (1)–(5) can be reformulated this way:

$$\text{Maximize} \quad \sum_{j\in J'}\sum_{i\in I} c_j a_{ij} K_i x_i \tag{6}$$

$$\text{Subject to} \quad \sum_{i\in I} a_{ij} K_i x_i \le \underline{q}_j \quad \text{for } j\in J' \tag{7}$$

$$x_i \in [0, ..., \underline{r}_i] \quad \text{for } i\in I \tag{8}$$

4. A decomposition algorithm for the transport-production coordination problem

The problem structure is given by the sub-matrix $[a_{ij}]_{i\in I\, j\in J'}$. E.g. for the case illustrated in Fig. 3 and for $J' = [1, 2, 3]$ the incidental sub-matrix has the following form:

Incidental trip-customer matrix   Table 1

$I\backslash J'$	1	2	3
1	1		
2		1	
3		1	1

The original problem can be decomposed to smaller and simpler instances similarly as a bipartite graph with the node sets I and J' and with the edges given by an incidental matrix can be decomposed into maximal connected sub-graphs. The following labeling algorithm can do it:

0. [Initialization] Determine all the trips from I as unlabeled.
1. If each trip is labeled, then terminate. Otherwise choose an unlabeled trip. Provide the chosen trip with an unused label and insert it into a list of "labeled but unprocessed trips".
2. [Sub-problem determination] If the list of "labeled but unprocessed trips" is empty a new sub-problem has been labeled, go to the step 1, otherwise remove a trip from "labeled but unprocessed trips" and process it in the following way: Go over all incidental customers and for each of them inspect its incidental trips. If the incidental trip is unlabeled, give it the label of a removed trip and insert it into the "labeled but unprocessed trips". Repeat step 2.

5. Particular cases of the transport-production coordination problem

Even if the general transport-production coordination problem belongs to the family of NP-problems, there are some cases, which can be solved, exactly in polynomial time. We shall introduce several easily solvable cases together with the associated algorithms, which will be used to construct a general heuristic method [1] in the next section. In this section we assume that each discussed instance of the problem corresponds to a maximal connected sub-graph which means that it cannot be decomposed to smaller problems. The particular cases will be distinguished in accordance to

the sub-matrix $[a_{ij}]_{i\in I,\, j\in J'}$, where I is the set of trips and J' is the set of relevant (important) customers.

The simplest case arises if $|I| = 1$ holds, where the expression $|I|$ denotes the cardinality of the set I. For this case, where $I = \{i\}$, the sole variable x_i can be determined optimally and it can be done by the following formula: $x_i : \min \underline{r}_i, \lfloor \min\{q'_j : j\in J', a_{ij} = 1\}/K_i \rfloor\}$, where $\lfloor u \rfloor$ denotes the integer part of the number u and where q'_j is the current demand of the customer $j\in J'$. The condition $a_{ij} = 1$ can be omitted here because the assumption of connectivity caused that $a_{ij} = 1$ for each $j\in J'$. The next discussed case is distinguished from the others by the conditions $\sum_{j\in J} a_{ij} = 1$, which hold for all the trips but one. Let this only one trip be denoted by u. The unique j for $i\in I-\{u\}$, for which $a_{ij} = 1$ can be denoted as $j(i)$. Now, let us consider that x_u is fixed at some value x. If we reduce the demands q_j by the values $a_{uj} K_u\, x$ to q'_j, then the associated best values of x_i for $i\in I-\{u\}$ can be obtained as $x_i := \min \{\underline{r}_i, \lfloor \min\{q'_{j(i)}/K_i\}\rfloor\}$. Based on these preliminaries, an exact algorithm can be stated as follows:

0. Set $C^{best} := +\infty$
1. For $x_u := 0$ to $\underline{r}_u$ repeat
   set $q'_j := \underline{q}_j - a_{uj} K_u\, x_u$ for all $j\in J'$,

   set $x_i := \min \{\underline{r}_i, \lfloor \min\{q'_{j(i)}/K_i\}\rfloor\}$ for all $i\in I-\{u\}$,

   set $C := \sum_{j\in J} c_j (\underline{q}_j - \sum_{i\in I} a_{ij} K_i\, x_i)$

   if $C < C^{best}$ then set $C := C^{best}$ and $x_i^{best} := x_i$ for $i\in I$.

The complexity of this algorithm is $O(|I|\, r)$, where r is the upper bound of $\underline{r}_i$ for $i\in I$.

The third exactly solvable case is distinguished from others by the fact that the condition of a unique trip-customer assignment holds for all the trips but two. Let the two trips be denoted by u and v, and then the following steps describe the exact algorithm:

0. Set $C^{best} := +\infty$
1. For $x_u := 0$ to $\underline{r}_u$ repeat step 2.
2. Set $q'_j := \underline{q}_j - a_{uj} K_u\, x_u$ for all $j\in J'$,

   Set $x_{max} := \min\{\underline{r}_v, \lfloor \min\{q'_j : j\in J'\, a_{vj} = 1\}/K_v \rfloor\}$

   For $x_v := 0$ to x_{max} repeat

   set $q'_{j,} := \underline{q}_j - a_{uj} K_u\, x_u - a_{vj} K_v\, x_v$ for all $j\in J'$,

   set $x_i := \min \{\underline{r}_i, \lfloor \min\{q'_{j(i)}/K_i\}\rfloor\}$ for all $i\in I-\{u, v\}$,

   set $C := \sum_{j\in J} c_j (\underline{q}_j - \sum_{i\in I} a_{ij} K_i\, x_i)$

   if $C < C^{best}$ then set $C := C^{best}$ and $x_i^{best} := x_i$ for $i\in I$.

The complexity of this algorithm is $O(|I|\, r^2)$. This exact algorithm can be generalized to heuristics, which can be used in

the cases when the unique trip-customer assignment condition does not hold for more than two trips. The generalization may consist in replacing the instruction $x_i := \min \{r_i, \lfloor \min\{q'_{j(i)}/K_i\}\rfloor\}$ for all $i \in I - \{u, v\}$, by the following set of instructions, which can be performed in an arbitrary order of trips i from the set $I - \{u, v\}$:

set $x_i := \min\{r_i, \lfloor \min\{q'_j : j \in J' \ a_{vj} = 1\}/K_i\rfloor\}$,

   update $q'_j := q'_j - a_{ij}K_i x_i$ for all $j \in J'$.

This algorithm will be denoted as $H(u, v, C^{best}, x^{best})$.

6. An exchange heuristics

The algorithm $H(u, v, C^{best}, x^{best})$ described in the previous section can be used in a construction of exchange heuristics. The proposed heuristics starts with an ordered sub-set I' of all the trips I. The ordering can be done, e.g. decreasingly in accordance to the number of incidental customers. The exchange heuristics will proceed all the unordered pairs $\{u, v\}$ of the trips from I', whereas the embedded algorithm $H(u, v, C^{best}, x^{best})$ proceeds all the trips from I. Let us denote by $\leq_o$ the considered ordering of the set I', then the heuristics can be described by the following steps:

0.   Set $C^{res} := +\infty$
1.   For $u \in I'$ repeat step 2.
2.   For all $v \in I'$, $u \leq_o v$ repeat steps:
     Perform $H(u, v, C^{best}, x^{best})$.
     If $C^{best} < C^{res}$, then set $C^{res} := C^{best}$ and $x_i^{res} := x_i^{best}$ for all $i \in I$.

The complexity of this algorithm is $O(|I'|^2 \cdot |I| \cdot r^2)$, but it can be arbitrarily reduced by a restriction of the set I'.

7. Numerical experiments

In the following experiments, we have focused on investigation of the heuristic quality and time consumption. This matter was studied on six series of randomly generated instances where each series consists of ten instances. These series differ in an increasing size m of the problem which means the cardinality of the set I of trips and, as well, the cardinality of the set J' of relevant customers. The problem sizes start from ten and continue by ten to the size of sixty. The instances were generated so that no problem can be decomposed to smaller ones and that is why the decomposition heuristics was not involved into the experiments. All the problem coefficients c_j, t_i, r_i, q_j and a_{ij} were obtained this way:

a_{ij} – randomly generated zero-one matrix where each row contains $m/3$ ones and the problem is irreducible,

c_j – randomly generated real number from 10 to 80 with a uniform distribution,

t_i – randomly generated real number from 0.05 to 0.4 with a uniform distribution,

p_i – randomly generated real number from 50 to 80 with a uniform distribution,

q_j – randomly generated real from $500 + \sum_{i \in I} a_{ij}(10/t_i)$ to $800 + \sum_{i \in I} a_{ij}(10/t_i)$,

$K_i = 10/t_i$.

To perform the numerical experiments, PC Pentium 4, 2.8 GHz, 512 MB was used. To be able to evaluate the quality of the proposed heuristics, we implemented it in the development environment Delphi 7 and solved all the generated instances. Furthermore, we made use of the mathematical programming software environment Mosel [3], [4], which integrates the modeller and solver, of previous optimization packages into one comprehensive tool, which is extended by a debugging tool. This optimization software environment embedded into graphical environment Xpress-IVE is successor of the famous optimization package XPRESS [2], [5], from which it inherited the excellent optimization procedures. This solver was able to provide us with optimal solution of the problem instances. The comprehensive results of experiments are plotted in table 2, where individual columns contain average result attributes of particular series. The size m of instances from a particular series is reported in the first row of the table. The next rows of table have the following meaning:

Avg.Obj.Heur. – average of objective function values of the resulting solutions obtained by heuristics on all instances of the given series,

Avg.Obj.Xpress – average of objective function values of the optimal solutions obtained by the environment Xpress-IVE on all instances of the given series,

Avg.Obj.Diff. – average of differences of objective function values of optimal solutions obtained by the environment Xpress-IVE and resulting solutions obtained by heuristics on all instances of the given series,

Std.Obj.Diff. – standard deviation of differences of objective function values of optimal solutions obtained by the environment Xpress-IVE and resulting solutions obtained by heuristics on all instances of the given series,

Avg.Obj.Diff.% – average of differences of objective function values of optimal solutions obtained by the environment Xpress-IVE and resulting solutions obtained by heuristics given in percentage of the objective function value of optimal solutions,

Avg.Time.Heur. – average of computational times in seconds consumed by heuristics on all instances of the given series,

Std.Time.Heur. – standard deviation of computational times consumed by heuristics on all instances of the given series,

Avg.Time.Xpress. – average of computational times in seconds consumed by the environment Xpress-IVE on all instances of the given series,

Std.Time.Xpress – standard deviation of computational times consumed by the environment Xpress-IVE on all instances of the given series.

Average objective function values and computational times for the particular series

Table 2

m	10	20	30	40	50	60
Avg.Obj.Heur.	113919	240658	346992	443151	522410	625862
Avg.Obj.Xpress	115144	251109	373154	484381	596138	718652
Avg.Obj.Diff.	1225	10451	26161	41230	73727	92790
Std.Obj.Diff.	1531	6087	10707	11272	13353	15138
Avg.Obj.Diff.%	1	4	7	9	12	13
Avg.Time.Heur.	0.00	0.05	0.21	0.68	1.45	2.72
Std.Time.Heur.	0.01	0.01	0.03	0.24	0.23	0.31
Avg.Time.Xpress	0.09	0.20	0.82	5.50	48.70	236.75
Std.Time.Xpress	0.13	0.10	0.64	4.25	57.96	247.05

6. Conclusion

We introduced a new problem which originated in civil engineering practice and we called it "The Transport-Production Coordination Problem". This problem was formulated and modelled using means of integer programming and its computational complexity was studied theoretically and experimentally as well in connection with the usage of professional universal optimization environment Mosel. Our results confirmed that the problem is not easily solvable to exact optimality by a general solver due to increasing computational time (see row Avg.Time.Xpress in table 2). The designed exchange heuristics proved to be able to obtain a good solution in very short time in comparison with the general IP solver. The results of heuristics differ from the optimal ones on average by 13% when the largest studied instances of the problem were solved. Taking into consideration an uncertainty of the input data in practical situations, e.g. the time t_i of trip i performance, it can be claimed that the proposed heuristic approach is satisfactory for embedding into decision support tools for such problems.

References

[1] JANÁČEK, J.: *Optimization on Transportation Networks (in Czech)*, Žilinská univerzita, Žilina, 2002, p. 248.
[2] LAUBER, J., JABLONSKÝ, J.: *Software for Mathematical Model Building (in Czech)*, Vysoká škola ekonomická, Praha, 1993, p. 316.
[3] XPRESS-MP Manual "Getting Started", Dash Associates, Blisworth, 2005, p. 105.
[4] XPRESS-Mosel "User guide", Dash Associates, Blisworth, 2005, p. 99.
[5] XPRESS-MP Reference Manual, Dash Associates, Blisworth, 1991.

Gabor Fejes *

COMPETENCY OR DUTY – METHODS OF SELECTION IN PRACTICE

My work deals with the connection between selection methods and competencies. It seeks an answer how company managers interpret the notion of competency, how important labour selection is according to those competencies. The choice among these methods is determined by conscious or rather subjective aspects, traditions and company culture. The findings are the partial results of a current, practical research. The subject is of a significant importance, as there are hardly any researches dealing with selection and its methods. However, its practical importance is beyond doubt, since the reason for the efficiency of organizations and the only resource of permanent competitive edge is the individual. This fact requires the use of selection methods that provide the satisfaction of employees beyond company efficiency.

1. The importance of the topic

During my work as a lecturer and counsellor, which I have been doing for several years now, my scope of interest has more and more turned to the study of labour force selection. I have indulged into this field so much that I have chosen it for my PhD research and MBA thesis. The scope of the research is selection among selection methods. I aim at finding its scientific or practical, subjective or objective reasons and expedience. I believe these methods form an inseparable unity with competencies. There are, however, further difficulties with this interpretation: there is no standard definition for competency in company practice – possibly not even in technical literature. There exist different interpretations for the types and classes of competency. Without standard notions, the strategic importance of HR management can hardly be maintained. My practical research has been going on now with four multinational firms. Three firms are in the Middle-West Transdanubian Region, two of them in FMCG sector, one is a supplier for car industry. The fourth one produces informatics appliances in the agglomeration of Budapest.

Recently, HR management has been more and more in the centre of interest for researchers dealing with organizations. The importance of this field has not only grown in the world of science but in practical life since its representatives appeared in the higher management of several organizations. The reason for this, according to the latest trends in management, is that the efficiency of organizations depends on the individual. The only and most durable source of competitive advantage is the individual and his/her ability to learn and improve. The individual is capable of improving the organization consciously and embedding values which promote creative, innovative thinking, continuous change and adaptation to the environment.

These days more and more organizations employ highly qualified people. By doing so, a definite demand emerges for the efficiency of selection from HR departments. Successful selection helps the firm and makes its work easier as well as it increases motivation and satisfaction of employees. Besides, it reduces the costs, having a positive effect on the firm's economy.

2. Selection methods

According to present literature, various methods are used in both intrinsic and extrinsic selection. In my study I consider the following methods:
– application forms
– CV
– tests
– interviews
– graphology
– test work
– references
– expert examination (e. g. health certificate)
– assessment centre (AC)

3. Competency

As a result of my research and Internet browsing, here I present some descriptions of competency to prove how ambiguously this notion is used in literature.

"Competency is the ability we need in an extremely wide range of cases. It is not only the use of learned skills in new situ-

* Gabor Fejes,
Budapest Tech Regional Education and Innovation Centre Szekesfehervar, Budai road 45. 8000 Hungary, E-mail: fejesg@strategia-taktika.hu

ations but the complexity of inherent features, life experience, and other factors, intuitive mechanisms" [1].

"Competency is something by which we are able to fulfil tasks constructively in newer and newer situations in the world" [2].

"Competency resembles the features of a personality, skill, motivation or knowledge, which manifest themselves in behaviour. However, competency is above all, and includes all of them" [2].

"Competency consists of five factors:
– knowledge and ideas;
– skills and expertise;
– individual values;
– personal features;
– motivation"[2].

"Competencies are the personal features which make employees efficient and successful in a particular position or role"[2].

"Competency: skill and expertise"[3].

"Competency is a skill to fulfil a particular task or activity."

" Competency is the complexity of skills needed to do a job."

"Competency is the complexity of technical skills."

"Competency is a system of skills recognized, assessed and accepted by a particular firm." (The 4 quotations above come from the feedback from firm leaders.)

In what follows I use the notion of competency as Boyatzis defined it.

"Competency is the basic features of an individual which affect the efficiency and/or the result in compliance with the criteria."[4]

As for the types of competencies, I follow Vekerdy's typology [5]. Competency includes:

1. Skills and knowledge, which are important factors of what an individual is able to do if he/she wants. However, this knowledge does not necessarily mean that he/she does want to do it.
2. Skills and expertise which mean the possibility to realize the acquired knowledge in practice.
3. Social roles which form along individual values. The question "what an individual considers to be a value"
4. Self image, the image that the individual has about him/herself. Its important construent is reality and self-knowledge.
5. Individual features:
   • Dimensions of the senses. Reactions to the stimuli coming from the environment. The questions "what we sense" and "how we react" are especially important.
   • Cognitive skills. Features of memory, imagination and thinking.
   • Psychosocial factor: self-estimation, self-confidence, independence etc.
6. Motivation: drive for action and behaviour. Wish and desire can also be found in this area.
7. Attitude: emotional, mental and behavioural approach to things through direct or indirect experience.

Competency always includes intension for effective action. Competency used in selection is usually competency related to work and behaviour, which are the following:

– Threshold competency needed for everyone to do a particular job, but it does not make a difference between the outstanding and the average,
– Performance competency means the factors that can make a difference between the outstanding and the average.

4. Connection between selection and competency

The most important aim of selection is to help decide who can and who cannot be a member of the organization. The person whose competency fits better to the job requirements and who is more likely to prove to be good within a particular period of time can be a member of the organization.

We can decide if a person fits or not if the comparison is made in the same dimension. I believe the most suitable dimension is competency. The selection system must be based on competency because job requirements as demands for competency must be comparable, commensurable with the competency inventory of the individual. Different areas can be compared, such as learned skills, experience, dealing with connections, problem solving, decision making, taking responsibility, motivation, leadership abilities, load-ability etc. Every organization looks for individuals with the features that promote success for the organization. Selection is a key question because the organization cannot gain success without it.

Competency-based resource management and especially selection makes the opportunity for high efficiency. The introduction of the system has started but it is only in its enfancy. Traditional staff duties focused on different values, which generally decreased the individuals' self-knowledge, self-esteem and self-estimation. As opposed to this, it was a great change for Hungarian companies that they suddenly switched to be profit-centred. Value crisis of particular human features and competency does not help spread competency-based HR thinking. We must admit that the top management of Hungarian firms has hardly been interested in such problems until now. What is more, the strategic perspective has not been reflected in the selection function of HR management so far. Where efforts were made to solve the problem, they tried to do it as simply and fast as possible, slobbering or ignoring the moral and emotional process of the making values systematically.

In my opinion, its consequences are the following:
• The organization's demand for competency and the competency of employees must agree.
• The organization's demand for competency can only be defined clearly and exactly for a particular moment. A difference must be made between revealed and unrevealed demand for competency.
• Individual competency cannot be completely explored, therefore, a difference must be made between known and unknown demand for competency.
• Unrevealed and unknown demand for competency brings uncertainty into the HR system and the management of knowledge.

- Inefficiency may result not only from inadequacy but from insufficient or lacking exploration of competency demands, so admittance criteria will not be reasonable enough.
- If an individual's known demand of competency falls short of performance, the missing competency may be compensated by planned skill improvement.
- An employee can supply his/her own missing competency by self-education.

In a nutshell, we can state that accuracy, reliability, acceptability, clarity and unanimity are crucially important for a well functioning competency system. Since a longer time is needed to develop competencies, they must be ranked by firms for their future success. If it is all done, they only need to find the suitable individuals to meet these competencies. The last step in the process of successful competency-based selection is to integrate the recruited employees-to-be into the organization. By doing so, we will be able to save them for the organization and to their skills entirely for our long-term success and the preservation of our competitive power.

5. Practical experience

The findings of my research are based on a written feedback given by HR managers and structured interviews made with them. The most important findings are the following:

Human resources have a strategic importance for every company, however, it is not so obvious in the daily practice. Sentences like "Get me a good employee for tomorrow" do not reinforce the faith put in the strategic importance of HR. It is interesting that managers believe they are infallible. It can also be noticed in the case of selection officers. They feel they are wise enough to select candidates on the base of their intuitions and experience. However, if they are not objective with the methods they cannot be objective with the results either. Most of them do not know all the methods and their introduction and use are the result of personal beliefs, company culture and traditions. During the process of selection, a key factor is how problem-oriented the managers are. Today, a good candidate should be employed not only in the case of vacancy but if he/she applies! If we accept the theory that every company needs key figures, then it is appropriate to employ a candidate with the proper competency as a potential key figure by creating a position for him/her.

Experts of HR selection rarely initiate changes in their field. They generally accept the established company practice as far as technologies and methods are concerned. The reason for this is very often inflexibility, subjectivism, and resistance against changes.

An important conclusion is the inadequate use of internal selection opportunities. The reason for this is the complete lack of employees' competency inventories. Therefore, internal selection can only bring success randomly. If there is an employee who is willing to apply. Apparently, it will fall through if the employee is rejected. He/she will be a condemned person who is obviously to leave and will be dealt accordingly. I believe the other crucial problem is the inner communication channel. There are different practices for this, but it is mostly based on traditions. The opportunities of the inner company network could be used more efficiently but for this it is essential to know the expected and employees' competency. Most of the firms I examined have already defined the system of the expected competency, competency levels and classes. The direction of further development can only be to break down competency according to tasks (jobs), since besides the basic and key competencies – which are expected to be acquired by every employee – there exist functional competencies which are expected only from particular groups of employees.

As a conclusion, it can be stated that the necessity of competency-based selection has been recognized by experts. Companies have started to define and standardize the expected competencies and work out their competency model. Unfortunately, the interpretation of competency works on the level of the organization so far. No company has started to break down them down into the jobs and activities, which is the only way to proceed. Human resources are seen as a strategic factor everywhere, however, the functional units of companies do not deal with the activities of HR departments as a key factor but as a service. Subjective procedures are important beside the efforts for the enhancement of selection objectivity. The subjectivism of officers does not necessarily lead to the selection of the most efficient methods. The calculation of selection costs by HR controlling is only its infancy. Apart from raising the standards, the recognition of the importance of competency-based selection forms a firm basis of company efficiency, employees' motivation and satisfaction and the proper functioning of the company's communication process.

References

[1] UDVARDY, LAPOS, E.: *Competence, Modularity, Paradigm Change in Practice (in Hungarian)*, www.galileo.ktk.pte.hu; <http://www.galileo.ktk.pte.hu/>, 23/03/2006
[2] www.odpartner.hu <http://www.odpartner.hu/>, 23/03/2006
[3] *Dictionary of the Hungarian Language (in Hungarian)*, Akadémiai Kiadó, Budapest, 2003
[4] ELBERT, N. F., KAROLINY, M., FARKAS F., POÓR, J.: *Manual of Staff / Human Resources Management (in Hungarian)*, KJK-KERSZÖV Jogi és Üzleti Kiadó Kft., Budapest, 2002
[5] VEKERDY, I.: *Human Resources Management I. (in Hungarian)*, Szent István Egyetem, Gödöllő, 2004

COMMUNICATIONS – Scientific Letters of the University of Žilina
Writer's Guidelines

1. Submissions for publication must be unpublished and not be a multiple submission.
2. Manuscripts written **in English language** must include **abstract** also written in English. The submission should not exceed **10 pages** with figures and tables (format A4, Times Roman size 12). The **abstract** should not exceed 10 lines.
3. Submissions should be sent: **by e-mail** (as attachment in system Microsoft WORD) to one of the following addresses: *holesa@nic.utc.sk* or *vrablova@nic.utc.sk* or *polednak@fsi.utc.sk* **with a hard copy** (to be assessed by the editorial board) **or on a 3.5″ diskette** with a hard copy to the following address: Zilinska univerzita, OVaV, Univerzitná 1, SK-10 26 Zilina, Slovakia.
4. Abbreviations, which are not common, must be used in full when mentioned for the first time.
5. Figures, graphs and diagrams, if not processed by Microsoft WORD, must be sent in electronic form (as GIF, JPG, TIFF, BMP files) or drawn in contrast on white paper, one copy enclosed. Photographs for publication must be either contrastive or on a slide.
6. References are to be marked either in the text or as footnotes numbered respectively. Numbers must be in square brackets. The list of references should follow the paper (according to **ISO 690**).
7. The author's exact **mailing address of the organisation where the author works, full names, e-mail address or fax or telephone number,** must be enclosed.
8. The editorial board will assess the submission in its following session. In the case that the article is accepted for future volumes, the board submits the manuscript to the editors for review and language correction. After reviewing and incorporating the editor's remarks, the final draft (before printing) will be sent to authors for final review and adjustment.
9. The deadlines for submissions are as follows: September 30, December 31, March 31 and June 30.
10. Topic for issue 1/2008: Security engineering.

POKYNY PRE AUTOROV PRÍSPEVKOV DO ČASOPISU
KOMUNIKÁCIE – vedecké listy Žilinskej univerzity

1. Redakcia prijíma iba príspevky doteraz nepublikované alebo inde nezaslané na uverejnenie.
2. Rukopis musí byť **v jazyku anglickom**. Príspevok by nemal prekročiť **10 strán** vrátane obrázkov a tabuliek (formát A4, písmo Times Roman 12 bodové). K článku dodá autor **resumé** v rozsahu maximálne 10 riadkov (v anglickom jazyku).
3. Príspevok prosíme poslať: **e-mailom**, ako prílohu spracovanú v aplikácii Microsoft WORD, na adresu: *holesa@nic.utc.sk* alebo *polednak@fsi.utc.sk* príp. *vrablova@nic.utc.sk* (alebo doručiť na diskete 3,5″) **a jeden výtlačok** článku na adresu Žilinská univerzita, OVaV, Univerzitná1, 010 26 Žilina.
4. Skratky, ktoré nie sú bežné, je nutné pri ich prvom použití rozpísať v plnom znení.
5. Obrázky, grafy a schémy, pokiaľ nie sú spracované v Microsoft WORD, je potrebné doručiť buď v digitálnej forme (ako GIF, JPG, TIFF, BMP súbory), prípadne nakresliť kontrastne na bielom papieri a predložiť v jednom exemplári. Pri požiadavke na uverejnenie fotografie priložiť ako podklad kontrastnú fotografiu alebo diapozitív.
6. Odvolania na literatúru sa označujú v texte alebo v poznámkach pod čiarou príslušným poradovým číslom v hranatej zátvorke. **Zoznam použitej literatúry** je uvedený za príspevkom. Citovanie literatúry musí byť **podľa STN 01 0197 (ISO 690)** „Bibliografické odkazy".
7. K rukopisu treba pripojiť **plné meno a priezvisko autora a adresu inštitúcie v ktorej pracuje, e-mail adresu** alebo číslo telefónu event. faxu.
8. Príspevok posúdi redakčná rada na svojom najbližšom zasadnutí a v prípade jeho zaradenia do niektorého z budúcich čísiel podrobí rukopis recenziám a jazykovej korektúre. Pred tlačou bude poslaný autorovi na definitívnu kontrolu.
9. Termíny na dodanie príspevkov do čísiel v roku sú: 30. september, 31. december, 31. marec a 30. jún.
10. Nosná téma pre č. 1/2008: Bezpečnostné inžinierstvo.